

ASKAP J005512.2–255834: A Luminous, Long-Lived Radio Transient at $z = 0.1$ – an Orphan Afterglow or an off-nuclear TDE from an IMBH?

ASHNA GULATI ^{1,2,3} TARA MURPHY ^{1,2} DAVID L. KAPLAN ^{4,2} DOUGAL DOBIE ^{1,2} CHARLOTTE WARD ⁵
GEMMA ANDERSON ^{3,1} MANISHA CALEB ^{1,2} POONAM CHANDRA ⁶ JEFF COOKE ^{7,2} BARNALI DAS ⁸
ADAM DELLER ^{7,2} ADELLE GOODWIN ⁹ KELLY GOURDJ ^{3,2} GIANCARLO GHIRLANDA ^{10,11} EMIL LENC ³
ANAIS MÖLLER ^{7,2} JAMES K. LEUNG ^{12,13,14} STELLA KOCH OCKER ^{15,16} JOSHUA PRITCHARD ³
CLAUDIO RICCI ^{17,18} ELAINE M. SADLER ^{1,2,3} OM SHARAN SALAFIA ^{10,11} KAVYA SHAJI ^{1,2,3}
ROBERTO SORIA ^{19,1} MARK SUHR,⁷ ARTEM TUNTISOV,²⁰ AND ZITENG WANG ²¹

¹*Sydney Institute for Astronomy, School of Physics, The University of Sydney, NSW 2006, Australia*

²*ARC Centre of Excellence for Gravitational Wave Discovery (OzGrav), Australia*

³*Australia Telescope National Facility, CSIRO, Space and Astronomy, PO Box 76, Epping, NSW 1710, Australia*

⁴*Department of Physics, University of Wisconsin-Milwaukee, P.O. Box 413, Milwaukee, WI 53201, USA*

⁵*Department of Astronomy & Astrophysics, 525 Davey Lab, 251 Pollock Road, The Pennsylvania State University, University Park, PA 16802, USA*

⁶*National Radio Astronomy Observatory, 520 Edgemont Rd, Charlottesville, VA 22903, USA*

⁷*Centre for Astrophysics and Supercomputing, Swinburne University of Technology, Hawthorn, VIC 3122, Australia*

⁸*Australia Telescope National Facility, CSIRO, Space and Astronomy, P.O. Box 1130, Bentley WA 6102, Australia*

⁹*International Centre for Radio Astronomy Research, Curtin University, Bentley, WA, Australia*

¹⁰*INAF - Osservatorio Astronomico di Brera, via E. Bianchi 46, I-23807 Merate (LC), Italy*

¹¹*INFN - Sezione di Milano-Bicocca, Piazza della Scienza 3, 20126 Milano (MI), Italy*

¹²*David A. Dunlap Department of Astronomy and Astrophysics, University of Toronto, 50 St. George Street, Toronto, ON M5S 3H4, Canada*

¹³*Dunlap Institute for Astronomy and Astrophysics, University of Toronto, 50 St. George Street, Toronto, ON M5S 3H4, Canada*

¹⁴*Racah Institute of Physics, The Hebrew University of Jerusalem, Jerusalem 91904, Israel*

¹⁵*Cahill Centre for Astronomy and Astrophysics, California Institute of Technology, Pasadena, CA 91125 USA*

¹⁶*Observatories of the Carnegie Institution for Science, Pasadena, CA 91101 USA*

¹⁷*Department of Astronomy, University of Geneva, ch. d'Ecogia 16, 1290, Versoix, Switzerland*

¹⁸*Instituto de Estudios Astrofísicos, Facultad de Ingeniería y Ciencias, Universidad Diego Portales, Av. Ejército Libertador 441, Santiago, Chile*

¹⁹*INAF - Osservatorio Astrofisico di Torino, Strada Osservatorio 20, I-10025 Pino Torinese, Italy*

²⁰*Manly Astrophysics, 15/41-42 East Esplanade, Manly 2095, Australia*

²¹*International Centre for Radio Astronomy Research, Curtin University, Bentley, Western Australia, Australia*

ABSTRACT

We report the discovery of a slowly evolving, extragalactic radio transient, ASKAP J005512.2–255834 (hereafter ASKAP J0055–2558), identified using the Australian SKA Pathfinder in a search for orphan afterglows associated with archival gravitational wave events. Although discovered in this context, there is no evidence that the transient is associated with any known gravitational wave event. Nonetheless, this source exhibits a 20-fold increase in flux density over < 250 days, and it remains in a declining, detectable state more than 1000 days after the initial detection. Follow-up observations from 0.3 to 9 GHz reveal an evolving spectrum consistent with synchrotron emission. ASKAP J0055–2558 is spatially coincident with a low-mass, star-forming galaxy at redshift $z = 0.116$ ($d_L = 543$ Mpc), placing its peak radio luminosity at $\nu L_\nu \sim 10^{39}$ erg s^{−1}. Analysis of its radio light curve, inferred blastwave velocity, energetics, host galaxy properties and the absence of counterparts at other wavelengths suggest that ASKAP J0055–2558 is most consistent with either the late-time phase of an orphan long gamma-ray burst afterglow or a tidal disruption event involving an intermediate-mass

black hole spatially offset from the galaxy nucleus. The radio discovery of either of these phenomena is extremely rare, with only a few or no confirmed examples to date.

Keywords: High energy astrophysics(739) — Radio transient sources(2008) — Transient sources(1851) — Gamma-ray bursts(629) — Tidal disruption(1696)

1. INTRODUCTION

The study of explosive transients at radio wavelengths has expanded significantly in recent years, driven by large surveys using instruments such as the Australian SKA Pathfinder (ASKAP; Johnston et al. 2007; Hotan et al. 2021) and the Karl G. Jansky Very Large Array (VLA; Perley et al. 2011). Until recently, the discovery of explosive transients such as gamma-ray bursts (GRBs), supernovae (SNe), and tidal disruption events (TDEs) has largely relied on high-energy telescopes such as Swift and Fermi Gamma-ray Burst Monitor (GBM), and optical survey facilities such as the Zwicky Transient Facility (ZTF) (Gehrels et al. 2004; Meegan et al. 2009; Bellm et al. 2019). While these will remain essential for studying prompt emission and identifying the transient type, they can miss events that are either dust obscured (Mattila et al. 2012) or beamed away from the observer (Rhoads 2003; Frail et al. 2001). Radio observations are well-suited to detecting shock-driven emission produced as relativistic or sub-relativistic outflows (Chevalier 1982; Mészáros & Rees 1997a) interact with the surrounding medium, even in cases where the event is viewed off-axis (Ghirlanda et al. 2015). This makes radio wavelengths a critical tool for discovering transients and measuring rates for asymmetric transients with reduced selection bias.

Earlier radio surveys were constrained by limited sensitivity and cadence, making them ineffective at detecting extragalactic transients (e.g. Levinson et al. 2002; Gal-Yam et al. 2006; Croft et al. 2010; Bell et al. 2011; Bannister et al. 2011; Rowlinson et al. 2016; Murphy et al. 2017). Instead, some transient searches focused on deep and targeted radio follow-up of nearby, face on spiral galaxies, with some yielding detections of long-lived synchrotron transients that remain unclassified (e.g. Muxlow et al. 2010; Joseph et al. 2011; Perley et al. 2017; de Vries et al. 2019; Tingay et al. 2020; Anderson et al. 2019). Recent wide-field surveys, such as the Variables and Slow Transients Survey (VAST; Murphy et al. 2021), the Rapid ASKAP Continuum Survey (RACS; McConnell et al. 2020) and the Very Large Array Sky Survey (VLASS; Lacy et al. 2020) have significantly enhanced our ability to detect a range of synchrotron transient classes at low frequencies such as orphan afterglows (Leung et al. 2023), off-axis TDEs (Dykaar et al.

2024), changing-look AGN (CL-AGN; Birmingham & Ward 2025), and rebrightening supernovae (Rose et al. 2024).

In this paper, we present ASKAP J005512.2–255834 (hereafter ASKAP J0055–2558), identified as a luminous, slowly evolving radio transient, in a search for orphan afterglows from archival gravitational wave events (see Gulati et al. 2025, for details). In Section 2, we describe the discovery of the transient. Section 3 details the multiwavelength observation campaign. In Section 4, we describe its basic properties. Section 5 focuses on the analysis of the candidate host galaxy. In Section 6, we summarise the key observational properties of the transient and attempt its classification by comparison with known classes of astrophysical transients. In Section 7, we evaluate the plausibility of interpreting this event as either an orphan afterglow or an off-nuclear TDE. Finally, we draw our conclusions in Section 8. Throughout this work, we assume a flat Λ CDM cosmology with $H_0 = 69.6 \text{ km s}^{-1} \text{ Mpc}^{-1}$, $\Omega_M = 0.286$, and $\Omega_\Lambda = 0.714$ (Hinshaw et al. 2013).

2. DISCOVERY

We identified ASKAP J0055–2558 in archival ASKAP data during a search for off-axis afterglows in the GW190814 localisation region. The search was conducted to a survey sensitivity $F_{\nu, \text{lim}}$, range of 0.15 – 1.5 mJy (most constraining limit from a dedicated ASKAP project AS111 and least constraining from RACS), over an effective area of 22 deg^2 corresponding to the 90% localisation region of GW190814 (more comprehensive search details given in Gulati et al. 2025). The source is absent in earlier epochs and first appears on 2022 February 4 at 3 GHz, at least $\sim 20\times$ brighter than the last non-detection limit 250 days prior at 0.9 GHz (see 0.9 GHz panel of Fig.1). In subsequent observations, its flux density declines steadily for > 1000 days. Although found within the GW190814 localisation region, the transient is unrelated as its potential host’s redshift (see Section 5) places it outside the gravitational-wave distance range, implying a chance sky coincidence.

Motivated by this discovery and evolution, we searched for multi-wavelength counterparts. We cross-matched the coordinates of ASKAP J0055–2558 with

the Transient Name Server¹ and found no association within 1′. Likewise, no known active galactic nuclei (AGN) or quasars were identified along the line of sight within 5′ using the Million Quasars (Milliquas) catalogue (Flesch 2023). We also found no matches in archival X-ray catalogues hosted by NASA² within 15″ of the source.

We queried the GRBWeb catalogue by Paul Coppin³ (Coppin et al. 2020) for GRBs occurring before our earliest radio detection (2022 February 4) whose localisation regions overlap the position of ASKAP J0055–2558. We identified 54 such GRBs over the past ~ 30 years. Given the reported localisation areas and the average all-sky GRB detection rate, the chance-coincidence probability for any single burst to overlap our position exceeds 50%; none therefore constitutes a compelling counterpart (see Appendix B for details). We also used SWIFTBAT_python⁴, and found that the source position was in the BAT field of view $\sim 65\%$ of the time (for a 1000 s cadence search) during the two years preceding our first radio detection. No counterpart is seen immediately before the radio discovery, although gaps in coverage leave open the possibility that a prompt event was missed.

ASKAP J0055–2558 lies 4.1″ from the galaxy 2dFGRS TGS143Z140. If associated with this galaxy (Section 6.3), the peak specific luminosity would be $\sim 10^{30} \text{ erg s}^{-1} \text{ Hz}^{-1}$, making it more luminous and longer lived than all known supernovae (Bietenholz et al. 2021).

3. OBSERVATIONS AND DATA PROCESSING

To characterise ASKAP J0055–2558 we conducted a comprehensive multi-wavelength observing campaign. In this Section, we describe the observational setup and reduction pipelines used for each facility.

3.1. Radio Observations

Following our discovery with ASKAP, we conducted targeted follow-up with the Australia Telescope Compact Array (ATCA), upgraded Giant Metrewave Radio Telescope (uGMRT), MeerKAT and Parkes. All radio data used in this work are tabulated in Appendix A and shown in Fig. 1, including the early 0.9 GHz ASKAP non-detections. Our best source position, derived from ATCA and GMRT observations, is (R.A._{J2000}, Decl._{J2000}) = 00:55:12.21, $-25:58:34.9$, with an uncertainty of 0.1″.

¹ <https://www.wis-tns.org>

² <https://heasarc.gsfc.nasa.gov/cgi-bin/W3Browse/w3browse.pl>

³ https://user-web.icecube.wisc.edu/~grbweb_public/index.html

⁴ https://github.com/lanl/swiftbat_python

3.1.1. ASKAP

ASKAP J0055–2558 was detected in the VAST survey (Murphy et al. 2021), which observes at 888 MHz with a roughly bimonthly cadence. Typical 12–15 min integrations reached $\sim 0.3 \text{ mJy rms}$.

Short-timescale (minutes) variability and polarisation provide powerful diagnostics of scintillation or coherent bursts (whereas weakly polarised emission favours synchrotron). To test these possibilities, we also analysed the 943 MHz ASKAP observations on 2024-01-02 with DSTOOLS⁵ (Pritchard 2025). After subtracting field sources with WSCLEAN, we formed full-Stokes time–frequency (dynamic) spectra at the source by averaging calibrated visibilities over all antenna pairs, produced 50 s–binned light curves, and computed modulation indices.

3.1.2. ATCA

We observed ASKAP J0055–2558 with ATCA for nine epochs between May 4, 2023, and March 20, 2025 (Project code C3363; PI: T. Murphy), measuring the flux density at a range of frequencies to determine its evolution. All our observations used 2048 MHz-wide bands centred on 2.1, 5.5, and 9.0 GHz. For the L-band ATCA observations, we also produced sub-band images: the 2048-MHz band was split into four 512-MHz sub-bands centred at 1.332, 1.844, 2.100, and 2.356 GHz, and each sub-band was imaged independently. In addition to the independently imaged sub-bands, we also present the flux density at 2.1 GHz, which corresponds to the full 2048-MHz band. We considered a source detected if its measured flux exceeded five times the local image rms (5σ); measurements below this threshold were treated as non-detections and reported as upper limits. We reduced the visibility data using standard routines in MIRIAD (Sault et al. 1995). We used a combination of manual and automatic radio frequency interference (RFI) flagging before calibration. We used PKS B1934–63 to determine the bandpass response and calibrate the flux density scale for all epochs and frequency bands. We used PKS 0023–26 to calibrate the gains for all frequency bands. After calibration, we inverted the visibilities using a robust weighting of 0.5 and then used the CLEAN algorithm (Clark 1980) with 3000 iterations to the target source field. We also searched 2100 MHz ATCA images on 2023-08-27 for short-timescale variability and polarised emission as described in Section 3.1.1.

3.1.3. uGMRT

⁵ <https://github.com/askap-vast/dstools>

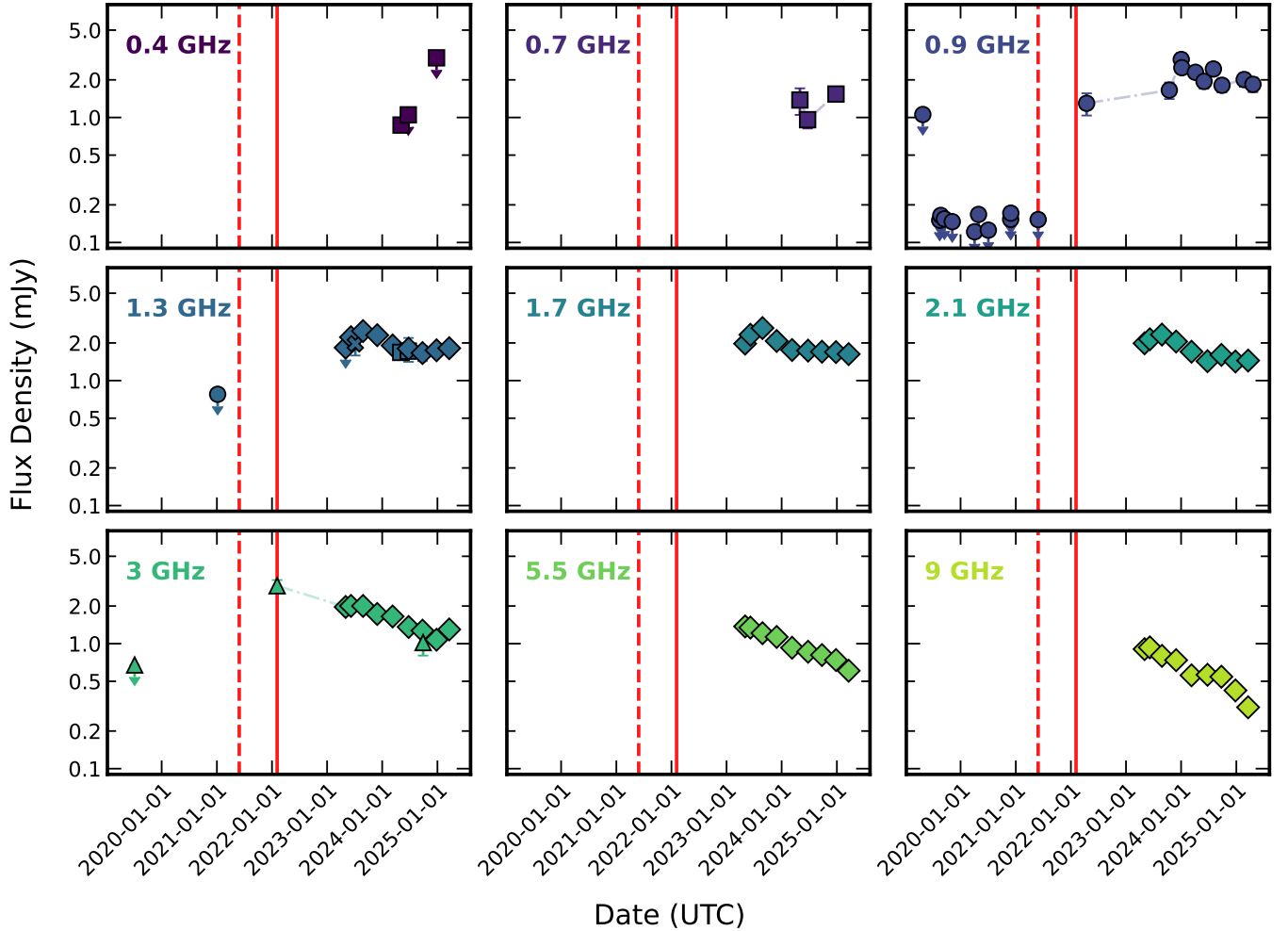


Figure 1. Radio light curves of ASKAP J0055–2558. The data span frequencies from 0.4 to 9 GHz, obtained with ASKAP (“○”), ATCA (“◇”), GMRT (“□”), VLA (“△”) and MeerKAT (“×”). Different frequency bands are represented by distinct colours. 5σ upper limits are indicated by downward arrows. The dashed red vertical line marks the last non-detection prior to the onset of detections, while the solid red vertical line marks the first radio detection.

We conducted observations with the uGMRT in 2024 May, June and December (Project code 46.054). All our observations used 400 MHz-wide bands centred on 0.67 and 1.27 GHz, and 200 MHz-wide bands centred on 0.4 GHz. We reduced the visibility data using the Common Astronomy Software Applications (CASA) package (McMullin et al. 2007). We used a combination of manual and automatic RFI flagging before calibration. 3C48 was used as primary and bandpass calibrator (flux set by Perley & Butler (2017) scale), while 0025–260 was used for gain calibration. Imaging used w-projection convolution to correct wide-field non-coplanar baselines (Cornwell et al. 2008) and Briggs robust=0 weighting, yielding higher angular resolution than natural weighting at the cost of slightly increased noise. At uGMRT low frequencies, ionospheric delays induce phase errors (Masqué et al. 2019), mitigated via self-calibration—iteratively

solving on compact, bright sources and re-imaging to refine the model (Pearson & Readhead 1984). We ran four phase-only self-cal cycles (solution intervals 4, 2, 1, and 0.5 min) followed by four amplitude-and-phase cycles (8, 4, 2, and 1 min) on the target visibilities. The phase calibrator set below the horizon after the initial scans for band 5, resulting in significant phase errors in the 26 December 2024 observation. Consequently, this data has been excluded from the analysis.

3.1.4. MeerKAT

We observed with the MeerKAT array (Jonas & MeerKAT Team 2016) in L-band (856–1712 MHz) on 2023 July 7, using the c856M4k mode with ~ 770 MHz of usable bandwidth and 8 s integrations. Full-polarisation data from the on-source beam were recorded (but not searched in real time) with the PTUSE backend of the MeerTime pulsar timing project (Bailes et al. 2020),

in search mode with $38.28 \mu\text{s}$ sampling and stored in `psrfits` format. We carried out periodicity searches with `pulsar_miner`⁶ (Ridolfi et al. 2021), a wrapper for PRESTO (Ransom 2011), dividing the data into 5 min segments. We searched dispersion measures up to 50 pc cm^{-3} , twice the maximum Galactic DM along this sightline predicted by the YMW16 Galactic electron-density model (Yao et al. 2017), and periods from 1 ms to 10 s, including Fourier-domain acceleration searches with $z_{\text{max}} = \pm 200$. No convincing pulsar-like candidates were detected with $S/N > 8$.

3.1.5. Parkes

We monitored ASKAP J0055–2558 for short-duration bursts with the Ultra-Wideband Low (UWL) receiver on Murriyang, the 64 m Parkes telescope, covering 704–4032 MHz continuously (Hobbs et al. 2020). A 1 hr observation on 2023 November 18 was conducted in single-polarisation pulsar search mode, with 250 kHz spectral resolution (13312 channels), $64 \mu\text{s}$ sampling, and data recorded in 2-bit `psrfits` search format (Hotan et al. 2004). We searched for bursts using a subbanded pipeline (Kumar et al. 2022) that integrates HEIMDALL (Barsdell 2012) and FETCH (Agarwal et al. 2020). The search covered $0\text{--}1000 \text{ pc cm}^{-3}$ dispersion measures (step 0.1) and boxcar widths up to 2 min, dividing the band into overlapping subbands (64–3328 MHz) to avoid edge losses. All FETCH candidates were visually inspected, and no events with $S/N > 7$ were found.

3.2. Optical/IR Observations

We obtained optical and near-infrared imaging with Magellan and Keck telescopes, and spectroscopy with Keck and the ANU 2.3-m telescope, to characterise the candidate host galaxy morphology and constrain any excess emission at the transient position.

3.2.1. Magellan Imaging

We observed ASKAP J0055–2558 with the Low Dispersion Survey Spectrograph (LDSS-3) on the 6.5-m Magellan Clay Telescope at Las Campanas Observatory on 2024 November 26 (e.g., Osip et al. 2008). Eighteen 300 s images were taken using the Sloan g' filter, for a total exposure of 1.5 hr, under $\approx 0.7''$ seeing conditions. Images were flat-fielded, sky-subtracted, and combined using a custom data reduction pipeline based in part on `ccdproc` (Craig et al. 2017), and cosmic rays were removed with the Laplacian edge detection algorithm

implemented in `astroscrappy` (van Dokkum 2001; McCully et al. 2018). Astrometric and photometric calibration were performed using standard data reduction pipelines, including `SExtractor` (Bertin & Arnouts 1996) for aperture photometry calibrated to the Pan-STARRS1 system (Tonry et al. 2012; Chambers et al. 2016).

3.2.2. ANU 2.3m WiFeS IFU spectroscopy

On 2023 July 12, we obtained spectra around the position of the radio source with the ANU 2.3m telescope at Siding Spring Observatory (Mathewson et al. 2013). We used the Wide Field Spectrograph (WiFeS; Dopita et al. 2007), which provides a $25'' \times 38''$ field of view, enabling integral field unit (IFU) spectroscopy of both the radio source position and the candidate host galaxy in a single pointing. We obtained $R = 3000$ resolution spectra using the R3000 and B3000 gratings, for the red and blue arms of the spectrograph and the RT560 dichroic covering a wavelength range of 3500–9000 Å. To obtain a better signal-to-noise ratio, we use the Nod & Shuffle (N&S) mode. Following the configuration used in Möller et al. (2025), we observed three N&S 1200 s exposures (600 s on target, 600 s on sky). The ANU 2.3m IFU cube only detected the main component of the potential host galaxy.

3.2.3. Keck KCWI/KCRM IFU spectroscopy

On 2023 August 17, we observed the candidate host galaxy and surrounding region with the Keck Cosmic Web Imager (KCWI; blue arm) and the Keck Cosmic Reionisation Mapper (KCRM; upgraded red arm) on the 10 m Keck-2 telescope, as an alternate target during poor weather for an unrelated program (W377; PI Deller). We obtained 2×290 s exposures with KCWI and 2×300 s exposures with KCRM. We used the BL and RL gratings for KCWI and KCRM, respectively, and the medium slicer for both instruments, providing a $16.5'' \times 20.4''$ field of view. We calibrated and reduced the data using standard `PypeIt` (Prochaska et al. 2020) routines and formed spectral cubes for each dataset covering wavelengths 3420–5590 Å using KCWI and 6502–10360 Å using KCRM. We extracted the spectra of the galaxy nucleus as well as the surrounding bright components using `QFitsView` and analysed the reduced data with the `LIME` package (Fernández et al. 2024).

3.2.4. Keck MOSFIRE

Near-infrared J-band ($1.2 \mu\text{m}$) imaging for ASKAP J0055–2558 on 2024 September 14 was acquired using the Multi-Object Spectrometer For InfraRed Exploration (MOSFIRE; McLean et al. 2010,

⁶ https://github.com/alex88ridolfi/PULSAR_MINER

2012) mounted on the 10m Keck 1 telescope. We obtained 200×10 s images for a total of 2000s using a “box5” dithering pattern under moderate seeing conditions (average ~ 0.8 arcsec seeing FWHM measured from the stacked image). The data were reduced and median stacked using IRAF (Tody 1986) and SWARP (Bertin et al. 2012), and sources were detected using SExtractor (Bertin & Arnouts 1996).

3.3. X-ray Observations

3.3.1. SWIFT

We observed ASKAPJ0055–2558 with the X-ray Telescope (XRT; Burrows et al. 2005) on board *Swift* on 2024 August 8 (916 days post first radio-detection) for 3.6 ks (ObsID 00016752001; PI: Gulati). We processed the data with XRTPIPELINE, following standard guidelines (e.g., Evans et al. 2009). We detect zero counts in the 0.2–12, 0.2–2, or 2–12 keV images which gives us an upper count rate limit of 6.4×10^{-4} cts $^{-1}$ in any band, corresponding to 90% upper limits on the Galactic-absorbed flux of 2.9×10^{-14} , 1.1×10^{-14} , and 1.8×10^{-14} erg cm $^{-2}$ s $^{-1}$. Fluxes were computed with PIMMS⁷ assuming a power-law spectrum with photon index $\Gamma = 1.7$ and Galactic line-of-sight absorption $N_{\text{H}} = 2 \times 10^{20}$ cm $^{-2}$, appropriate given the transient’s location outside the main body of the potential host galaxy⁸. This choice is motivated by late-time, optically thin synchrotron emission (for $p \sim 2.2$ – 2.4 , $\Gamma \approx (p + 1)/2 \sim 1.6$ – 1.7 ; Granot & Sari 2002) and is consistent with typical *Swift*/XRT afterglow spectra (Evans et al. 2009). To illustrate sensitivity to the assumed spectrum, adopting Γ in the range 1.5–2.1 changes the flux limits in the 0.2–12 keV band by $\lesssim 20\%$ for the same N_{H} ; we therefore regard our non-detection and derived constraints as robust.

4. TRANSIENT PROPERTIES

In this section, we present the observational constraints from our multi-wavelength campaign and the radio characterisation of ASKAP J0055–2558. Firstly, we summarise the non-detections that rule out several common source classes.

The source has no infrared counterpart in NIR J-band to 23 mag (Section 5.2.1), inconsistent with a typical background AGN, no optical transients reported at this location. Despite persistent radio emission, near-simultaneous X-ray follow-up yields no detection (Section 3.3.1); with 90% upper limits on the Galactic-

absorbed flux reaching the few nJy level. L-band searches with MeerKAT and Parkes UWL reveal no pulsed emission, excluding Galactic pulsars and γ -ray binaries. From the 5.5 GHz ATCA epoch on 2023 June 8, we constrain circular polarisation to $V/I < 5.6\%$ (5σ ; $S_V = 0.08$ mJy, $S_I = 1.39$ mJy) and find no significant signal in Stokes Q , U , or V . These limits rule out emission dominated by strongly circularly polarised coherent processes (e.g. pulsars or flare-stars) and are consistent with unpolarised synchrotron emission. An extreme scattering event is also unlikely as even though large plasma lenses can, in principle, yield $> 20\times$ magnification, the associated fractional bandwidth is typically narrow unless a contrived lens is invoked (e.g. Tuntsov et al. 2016); while a broadband de-magnification followed by a brief enhancement could mimic early non-detections and a trailing horn (Fiedler et al. 1987; Bannister et al. 2016), the observed years-long, broadband decline, strong at 5.5 and 9 GHz with little variation below 2 GHz, rules out an ESE origin.

In the following subsections, we present the radio spectral, temporal evolution, and variability analyses.

4.1. Radio variability

We searched for variability on timescales of minutes to months. There was no minute-scale variability within the 15-min scans (with modulation indices 0.10 ± 0.10 (ATCA) and 0.3 ± 0.3 (ASKAP)). The expected timescale of diffractive interstellar scintillation is 6.8 and 18.9 min, respectively; hence, this can be ruled out for ASKAP J0055–2558. On longer timescales, however, we do detect variability at 0.9 GHz (ASKAP) consistent with refractive ISS (RISS), which yields only a loose size limit, $\theta_s \lesssim 0.5''$. Because this is not constraining, we instead predict the RISS contribution and fold it into our flux uncertainties.

Assuming ASKAP J0055–2558 is a compact synchrotron source, we expect RISS to modulate its flux density. We used the NE2001 Galactic electron-density model (Cordes & Lazio 2002) to evaluate the line-of-sight scattering measure at the source Galactic coordinates. Adopting the relations in Walker (1998) to convert the scattering measure to a transition frequency, we obtain $\nu_0 = 7.46$ GHz, i.e. the frequency separating the strong and weak scattering regimes. Following Walker (1998) for extragalactic sources, we compute the scattering-disk angular size θ_r , which sets the angular scale below which a source remains in the strong-scintillation regime at a given observing frequency (Table 1).

We estimate the intrinsic source size via a preliminary equipartition analysis (Section 6.2, RISS errors not in-

⁷ <https://heasarc.gsfc.nasa.gov/docs/software/tools/pimms.html>

⁸ Calculated with the NASA HEASARC N_{H} tool: <https://heasarc.gsfc.nasa.gov/cgi-bin/Tools/w3nh/w3nh.pl>

Table 1. Estimated RISS Parameters for ASKAP J0055–2558

ν	m_p	θ_{F0}	θ_r	m
(GHz)		(μas)	(μas)	
0.4	0.19	2076	1296346	0.19
0.7	0.26	790	144024	0.26
0.9	0.30	455	47720	0.30
1.3	0.37	202	9434	0.37
1.7	0.43	112	2899	0.43
2.1	0.49	70	1138	0.49
2.3	0.51	58	772	0.51/0.30
3.0	0.60	32	237	0.60/0.09
5.5	0.84	8	16	0.04/0.005
9.0	0.76	3	2	0.005/0.001

NOTE—Parameters include the point-source modulation index (m_p), Fresnel-zone size (θ_{F0}), scattering-disk size (θ_r), and the final modulation index (m) after accounting for source size. For $\nu \geq 3$ GHz, two m values correspond to $\theta_s = 230$ and $1247 \mu\text{as}$, respectively. Values are based on NE2001 and are used to compute additional flux uncertainties from RISS.

cluded, see Appendix A Fig. 10 top panel for fitted spectral parameters). For all assumed geometries other than the 5° angle geometry ($\theta_s = 1247 \mu\text{as}$), the mean source size θ_s is smaller than θ_r for $\nu \lesssim 2.3$ GHz, whereas at 5.5 GHz the mean θ_s exceeds θ_r in every geometry. Accordingly, we report modulation indices for two representative sizes: $230 \mu\text{as}$ (less-collimated geometries) and $1247 \mu\text{as}$ (the 5° cone). The RISS modulation index m from Walker (1998) is

$$m = \begin{cases} \left(\frac{\nu}{\nu_0}\right)^{17/30}, & \theta_s \leq \theta_r, \\ \left(\frac{\nu}{\nu_0}\right)^{17/30} \left(\frac{\theta_r}{\theta_s}\right)^{7/6}, & \theta_s > \theta_r, \end{cases} \quad (1)$$

where

$$\theta_r = \theta_{F0} \left(\frac{\nu}{\nu_0}\right)^{-11/5}, \quad (2)$$

and θ_{F0} is the angular size of the first Fresnel zone.

Before spectral fitting, we add a RISS term in quadrature to each flux-density uncertainty, equal to $m(\nu, \theta_s) \times S_\nu$. This contributes 19% at 0.4 GHz, 51% at 2.3 GHz, and $\sim 1\%$ at 9 GHz (weak regime). Because the 5° geometry yields smaller m at $\nu \geq 3$ GHz, we conservatively adopt the larger uncertainties from the less-collimated case for all spectral fits. All RISS contributions used in the modelling are reported in Table 3.

4.2. Radio Spectral Evolution

ASKAP J0055–2558 exhibits a peaked radio spectrum in our broadband radio data. Such spectra can arise from two generic mechanisms: (i) synchrotron self-absorption (SSA), in which the low-frequency turnover is intrinsic to a compact, recently activated (age $\lesssim 10^5$ yr) jet, lobe, or blast wave (Chevalier 1998; O’Dea & Baum 1997; Owsianik & Conway 1998); and (ii) free-free absorption (FFA), in which emission is attenuated by dense ionized plasma along the line of sight (Weiler et al. 2002)—either homogeneous or inhomogeneous (e.g. in Compact Steep Spectrum, CSS, and Gigahertz Peaked Spectrum, GPS, sources; van Breugel et al. 1984). Slower outflows (e.g. SN ejecta or cocoons) can also show SSA/FFA, and both processes may operate simultaneously (as seen in radio SNe). In epochs with adequate low-frequency coverage, we therefore fit the optically thick index as a free parameter, following Ross et al. (2022) (RISS errors not included), to distinguish among SSA, homogeneous FFA, and inhomogeneous FFA. Only SSA and inhomogeneous FFA reproduce the observed rising, optically thick spectrum of ASKAP J0055–2558 below the turnover (mean α_1 of 1.2 ± 0.4); homogeneous FFA yields an exponential cutoff inconsistent with the data.

While our low-frequency coverage is not sufficient to fully disentangle SSA from FFA, a GPS/CSS interpretation is specifically disfavored due to the absence of an IR/optical counterpart at the radio position (unusual for GPS/CSS), a steep post-peak temporal decline that is faster than typical GPS/CSS evolution (Oriente 2016; Ross et al. 2022), and a low chance alignment probability with the potential host galaxy (Section 5). With homogeneous FFA excluded by the spectral shape, and given that our low-frequency coverage cannot separately constrain any inhomogeneous FFA contribution, we adopt an SSA-only baseline model for a compact, recently activated jet associated with the host galaxy.

Assuming an SSA origin, we performed a preliminary fit to each epoch’s spectrum, including scintillation uncertainties, using a smoothly broken power-law (SBPL) model expressed as:

$$S(\nu) = A \left[\left(\frac{\nu}{\nu_b}\right)^{-s\alpha_1} + \left(\frac{\nu}{\nu_b}\right)^{-s\alpha_2} \right]^{-1/s} \quad (3)$$

Where $S(\nu)$ is the flux density at frequency ν , ν_b is the break (or peak) frequency, A is a normalization constant (corresponding to the peak flux density), α_1 and α_2 are the spectral indices below and above the break, respectively, and s is a smoothness parameter. We fixed $s = 1$ to ensure a gradual transition between spectral

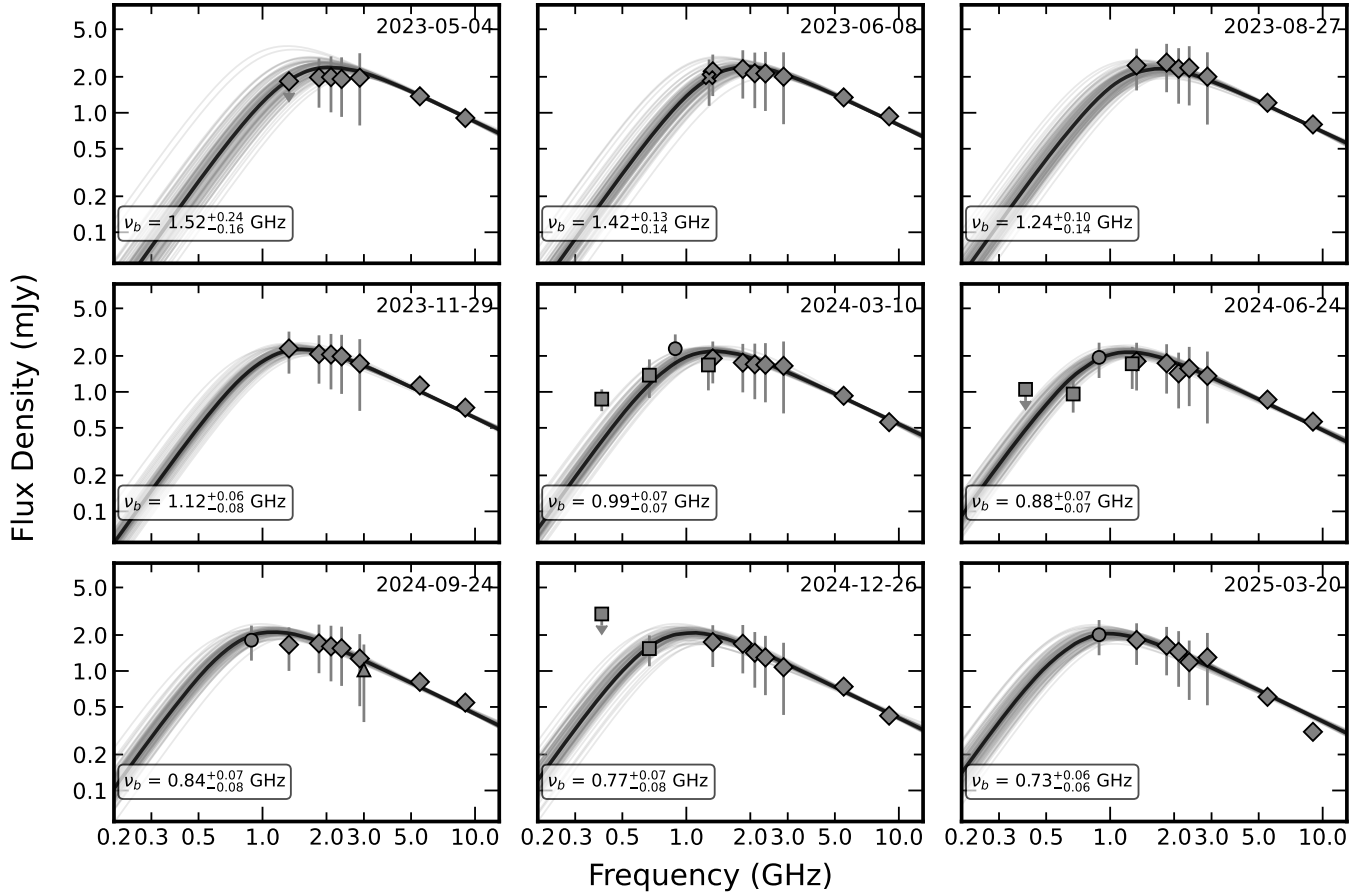


Figure 2. Radio spectral evolution of ASKAP J0055–2558 over nine ATCA epochs from 2023 to 2025. The errors on datapoints include both measurement and Interstellar Scintillation (ISS) errors. Dark solid curves show the best-fitting time-evolving SBPL model obtained from a joint fit to all epochs, with the peak at each epoch set by the self-absorption break; faint thin curves show 50 random draws from the MCMC posterior.

regimes. This choice is physically motivated, as the aggregate optically thin spectral index $\alpha \simeq -0.9$ (for frequencies > 2 GHz) implies an electron index $p \simeq 2.7$. Using the empirical relations $s = 1.47 - 0.21 p$ (ISM) and $s = 1.25 - 0.18 p$ (wind) from Granot & Sari (2002), we obtain $s \approx 0.7-0.9$, that is, an order-unity smoothness consistent with our adopted value of $s = 1$. Following Granot & Sari (2002); Mooley et al. (2022), we fixed the value of $\alpha_1 = 5/2$ consistent with the optically-thick spectral index of a self-absorbed synchrotron spectra i.e. $\nu_m < \nu_a$, where ν_m is the characteristic frequency of electrons at the minimum Lorentz factor and ν_a is the synchrotron self-absorption frequency below which the emission is optically thick. We implemented the model in Python, and spectral fitting was performed using the `emcee` package (Foreman-Mackey et al. 2013), an affine-invariant Markov Chain Monte Carlo (MCMC) ensemble sampler.

The fitted peak flux density and frequency are either constant or declining and the optically thin index re-

mains at $\alpha_2 \approx -0.9$ (see Appendix A Fig. 10 middle panel). Apart from the three GMRT epochs with low-frequency coverage, most epochs are sparsely sampled below the spectral peak, leaving peak parameters poorly constrained or even unconstrained for epochs 2023-05-04 and 2023-08-27. This is compounded by large flux uncertainties near the peak, where interstellar scintillation is strong (Section 4.1). To mitigate these issues, we fit all epochs jointly with weak, uniform priors and shared parameters. This time-dependent fit (including ISS error inflation; Section 4.1) constrains the evolution of peak frequency and amplitude. The spectrum is modelled as a smoothly broken power law with fixed optically thick index α_1 , global (epoch-independent) α_2 and smoothness s , break frequency and amplitude evolving with time as a power law (index positive, negative, or zero).

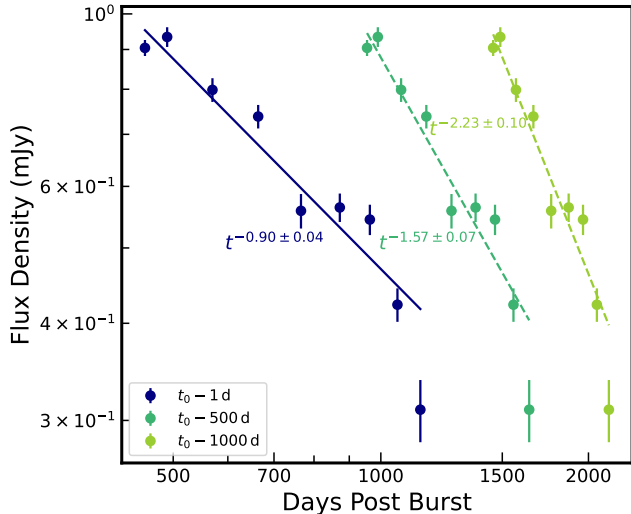


Figure 3. The 9 GHz light curve of ASKAP J0055–2558, where the temporal index is derived by shifting the reference epoch of the first radio detection ($t_o = 2022\text{-}02\text{-}04$) by +1, +500, and +1000 days. The blue, teal, and green lines show the corresponding power-law fits.

Specifically,

$$F(\nu, t) = A(t) \left[\left(\frac{\nu}{\nu_b(t)} \right)^{-s\alpha_1} + \left(\frac{\nu}{\nu_b(t)} \right)^{-s\alpha_2} \right]^{-\frac{1}{s}},$$

$$\nu_b(t) = \nu_{b,0} \left(\frac{t}{t_0} \right)^m, \quad A(t) = A_0 \left(\frac{t}{t_0} \right)^b \quad (4)$$

The amplitude $A(t)$ evolves as a single power law in time with slope b , and is normalised such that $A(t_0) = A_0$ at the reference epoch t_0 . The break frequency $\nu_b(t)$ evolves as a power law with index m from the reference value $\nu_{b,0}$. Since limited sub-GHz coverage leaves α_1 weakly constrained, we fix $\alpha_1 = 5/2$ (SSA-like) and $s = 1$ (spectral low-energy slope and smoothness), while fitting the parameters $\{A_0, \nu_{b,0}, m, b, \alpha_2\}$. The priors were allowed to vary uniformly within the following ranges: $A_0 \in [0, 1000]$ mJy; $\nu_{b,0} \in [0.1, 100]$ GHz; $m \in [-5, 5]$; $b \in [-5, 5]$; $\alpha_2 \in [-5, 0]$.

The observed and modelled spectra are shown in Fig. 2 (see Appendix A Fig. 10 bottom panel for fitted spectral parameters). The optically thin spectral index from the combined fit is $\alpha_2 = -0.86 \pm 0.04$, implying an electron energy distribution with a power-law index of $p = 2.72 \pm 0.08$, consistent with synchrotron emission (Granot & Sari 2002). From the joint fit to all epochs, we find a reference break frequency of $\nu_{b,0} = 0.97^{+0.07}_{-0.07}$ GHz with temporal evolution $m = -0.80^{+0.22}_{-0.21}$ (i.e., $\nu_b \propto t^m$). The amplitude slope is $b = -0.18^{+0.18}_{-0.19}$. Extrapolating our fit to higher optical and X-ray frequencies for the epochs

with near-simultaneous observations, we find that the upper limits are consistent with the non-detections.

We also fit the datapoints at 9 GHz with power law $F_\nu \propto t^b$ (see Fig. 3), to estimate the transient’s temporal evolution. Since the time of explosion is not known, we try fiducial values of 1, 500 and 1000 days for the age of the transient at the time of first radio detection at epoch 2022-02-04 and we find $F_{9\text{GHz}} \propto t^{-0.9 \pm 0.04}$, $F_{9\text{GHz}} \propto t^{-1.57 \pm 0.07}$ and $F_{9\text{GHz}} \propto t^{-2.23 \pm 0.10}$ respectively. The final radio data point deviates from the single power-law fit; this could be a measurement artefact, or genuine late-time steepening, also seen in orphan the afterglow candidates FIRST J141918.9+394036 (Mooley et al. 2022), and jetted TDE Swift J1644+57 (Eftekhari et al. 2018). Temporal evolution is shallower for lower frequencies, which should be expected depending on where the observation frequency lies with respect to the characteristic synchrotron peak frequency (Granot & Sari 2002).

5. POTENTIAL HOST GALAXY

ASKAP J0055–2558 is offset $4.1''$ from the galaxy 2dFGRS TGS143Z140 (see Fig. 4), which has a confirmed spectroscopic redshift of $z = 0.116$ (Colless et al. 2001). Using the angular diameter distance of 436 Mpc, this corresponds to a projected physical offset of approximately 8.7 kpc. The probability of a chance alignment between ASKAP J0055–2558 and 2dFGRS TGS143Z140 is only 1.87% (computed using the formalism of Bloom et al. 2002, see Appendix B.2), supporting a likely association. The galaxy is clearly detected in the DESI Legacy Surveys *DR10* (Dey et al. 2019), with catalogued z , i , r , and g magnitudes of 19.27, 19.33, 19.58, and 20.01 mag, respectively. It is also UV-luminous, identified as GALEXASC J005512.43–255832.9, with far-UV and near-UV magnitudes of 21.53 and 21.06 mag (DR6; Martin et al. 2005).

5.1. Spectroscopy

We extracted the galaxy spectrum from the ANU 2.3 m spectral cube, revealing $H\alpha$ and oxygen emission lines. Using the software MARZ (Hinton et al. 2016), we found that the spectrum is consistent with a galaxy at redshift 0.116. Using the more sensitive Keck spectra, the fitted redshifts of all optical components near the transient are consistent, indicating that they all form part of the same host galaxy. The spectral parameters fitted for the galaxy core are listed in Appendix B Table 5. The galaxy exhibits prominent emission lines, including [O II], [O III], $H\beta$, and $H\alpha$ (see Fig. 4 and Appendix B), consistent with active star formation and relatively low dust extinction along

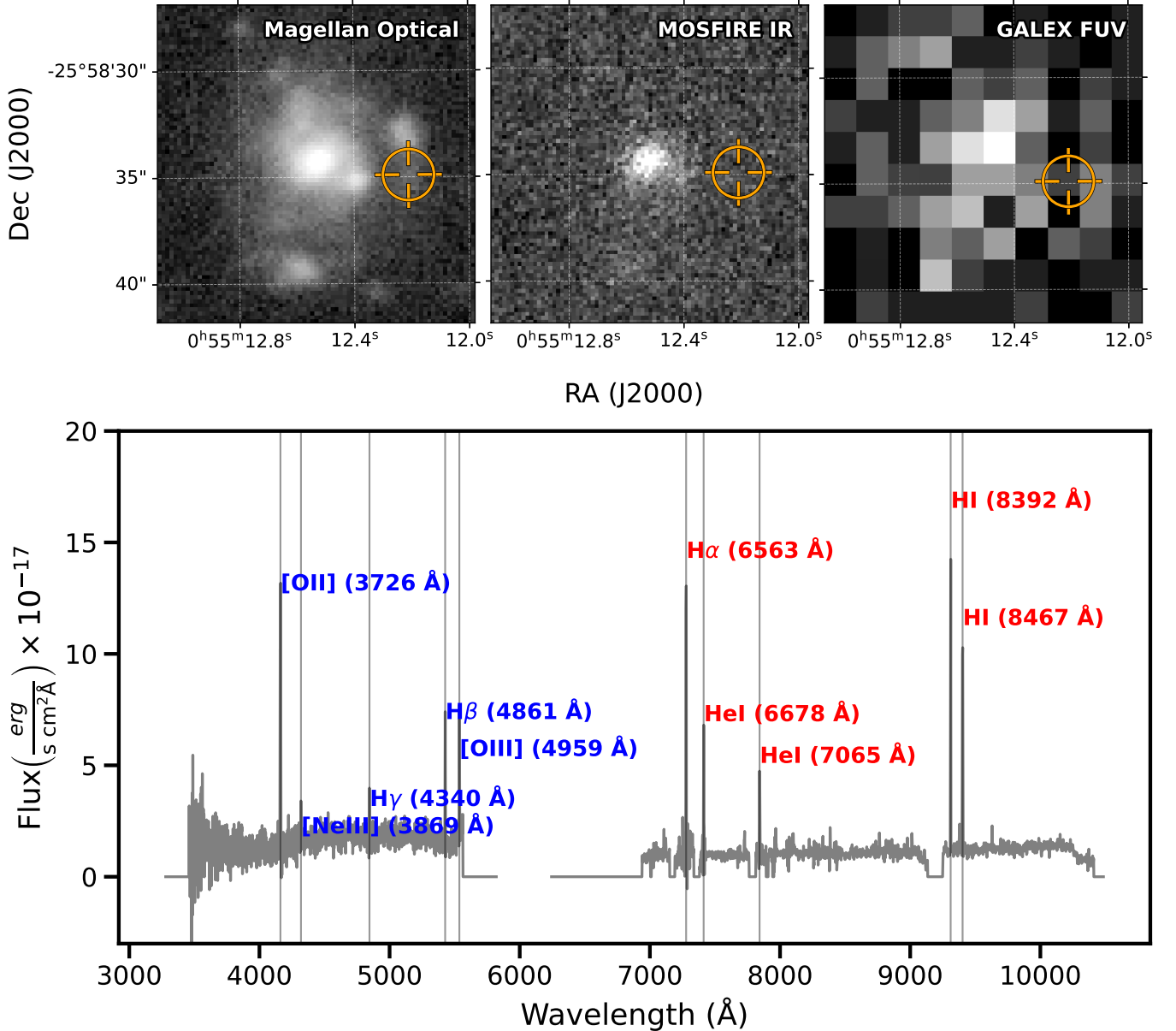


Figure 4. Top: Magellan (5σ AB limiting magnitude 28.0 in g' -band), MOSFIRE (23.5 in J-band), and GALEX FUV (22.6) images of the transient position overlaid by the aggregate source position derived from ATCA and GMRT observations (the circle around the position corresponds to the aggregate PSF with a radius of 1.2 arcsec). Bottom: Spectra obtained with Keck KCWI and KCRM for the galaxy nucleus, with emission lines fitted using the LIME package. The signal-to-noise ratio, as defined by Rola & Pelat (1994) for each of the fitted lines, is above 5σ . The fitting results are given in the Appendix B Fig. 11.

the line of sight (Kennicutt 1998; Calzetti et al. 2000). The presence of high-excitation lines such as [Ne III], as well as hydrogen and helium recombination features, suggests intense ionising radiation, potentially from vigorous star-forming activity or a low-luminosity AGN (Kewley & Dopita 2002; Baldwin et al. 1981). In star-forming environments, these emission lines trace ionised gas in H II regions and serve as important diagnostics of the physical conditions, including temperature, den-

sity, and chemical abundance patterns (Osterbrock & Ferland 2006).

We derived key physical parameters using a combination of broadband photometry and optical spectroscopy (see Appendix B.3 for details). These parameters are summarised in Table 2. Based on the total stellar mass of $1.55 \times 10^9 M_{\odot}$, the galaxy falls within the low-mass galaxy regime ($\lesssim 10^9 M_{\odot}$) and is consistent with typical star-forming, disk-dominated systems (Kauffmann et al. 2003). The relatively low mass, combined with the

Table 2. Physical Parameters of the Host Galaxy Core

Quantity	Value
Stellar Mass (M_{\odot})	$1.55^{+0.42}_{-0.30} \times 10^9$
SFR ($M_{\odot} \text{ yr}^{-1}$)	$4.16^{+4.95}_{-1.52}$
sSFR (Gyr^{-1})	$0.39^{+0.34}_{-0.17}$
Metallicity (Z_{\odot})	$0.58^{+0.42}_{-0.24}$
Extinction Magnitude	1.16
Balmer Decrement	4.00
Ionisation Ratio	0.92

NOTE—Physical parameters were derived using extinction laws for star-forming (Calzetti et al. 2000) galaxies. Core properties include stellar mass, gas mass, total mass, star formation rate (SFR), specific SFR (sSFR), metallicity, extinction magnitude, Balmer decrement and ionisation ratio.

derived star formation rate ($4.16 M_{\odot} \text{ yr}^{-1}$), indicates an active star-forming galaxy. Star formation rates derived using the Calzetti attenuation law from extinction-corrected $H\alpha$ and UV luminosities are lower, at 0.40 and $2.24 M_{\odot} \text{ yr}^{-1}$, respectively.⁹ We find a Balmer decrement of 4.00, significantly higher than the intrinsic value of 2.86 (Osterbrock 1989), suggesting the presence of dust extinction likely associated with recent or ongoing star formation.

The dust extinction corrected $[\text{O III}]/[\text{O II}]$ ratio ($\lesssim 1$) points to a moderately low ionization environment, characteristic of evolved H II regions rather than the hard radiation fields typical of AGN (Kewley & Dopita 2002; Kewley et al. 2006; Feuillet et al. 2024). Furthermore, key Baldwin–Phillips–Terlevich (BPT; Baldwin et al. 1981) diagnostic ratios are $[\text{N II}]/H\alpha \lesssim 0.03$ (using 3σ limit on N II) and $[\text{O III}]/H\beta = 3.46$, consistent with the galaxy lying well within the star-forming region of the BPT diagram, characteristic of low-metallicity H II regions ionized by young, massive stars, with no indication of AGN or composite excitation. At the position of the transient, the KCWI spectrum reveals emission features, including $[\text{O II}]$ (3726 Å), $H\beta$ and $[\text{Ne III}]$ and the KCRM spectrum reveals emission features, including $H\alpha$ and $[\text{He I}]$ (7065 Å) (see Appendix B Fig. 13). At

⁹ The discrepancy between these values and the higher SED-based star formation rate is expected, as different indicators probe star formation over distinct timescales and are subject to varying uncertainties in dust attenuation corrections (see Kennicutt & Evans 2012)). SED fitting provides a time-averaged estimate of the star formation rate (Conroy 2013).

the transient position, the Balmer decrement ($H\alpha/H\beta$) is 4.34, significantly higher than the intrinsic value of 2.86 as well as the galaxy core, indicating a dusty region likely associated with star-formation. Although the key Baldwin–Phillips–Terlevich (BPT; Baldwin et al. 1981) diagnostic ratios— $[\text{N II}]/H\alpha$ and $[\text{O III}]/H\beta$ —cannot be measured directly, upper limits derived from the continuum noise indicate that the source does not lie within the AGN regime. Furthermore, all detected emission lines have Gaussian dispersions of $\sigma < 1 \text{ \AA}$, corresponding to narrow intrinsic velocities ($\sigma_v = c\sigma_{\lambda}/\lambda$; $\text{FWHM} = 2.355\sigma_v$) of $\text{FWHM} \lesssim 100 \text{ km s}^{-1}$ for $H\alpha$, $H\beta$, and $\text{O II } \lambda 3726$. These low widths are consistent with photoionized gas in H II regions or nuclear star clusters and are far below the several-hundred to thousand km s^{-1} lines typical of AGN.

Taken together, the spatial coincidence, low chance alignment probability, spectroscopic diagnostics, and derived physical parameters strongly support the interpretation that 2dFGRS TGS143Z140 is the likely host galaxy of ASKAP J0055–2558 and strongly disfavour a background AGN as a plausible explanation.

5.2. Imaging

5.2.1. IR

No infrared counterpart was detected in the stacked image above the 5-sigma infrared detection threshold of $m(J) = 23.3$ in AB magnitudes. The stacked image is presented in Fig. 4.

5.2.2. Optical

The deep Magellan imaging of the galaxy reveals a complex post-merger system with multiple extended components. Keck spectroscopy confirms that all of these structures lie at the same redshift, with the outer clumps consistent with H II regions. The galaxy exhibits prominent tidal tails, indicative of a recent interaction or merger. This interpretation is further supported by spatially resolved velocity maps, which show a smooth and continuous emission-line velocity gradient along the tidal features (see Fig. 14 in Appendix B). No kinematically distinct component is detected at the location of the transient, indicating that the gas in this region is dynamically connected to the host galaxy and its tidal debris rather than associated with a background system. The radio transient is located at the end of a tidal tail, coincident with a slight enhancement in emission.

To assess emission excess at the transient location, we modelled the Magellan data using the *Scarlet* scene modelling software¹⁰ (Melchior et al. 2018). We con-

¹⁰ <https://pmelchior.github.io/scarlet/>

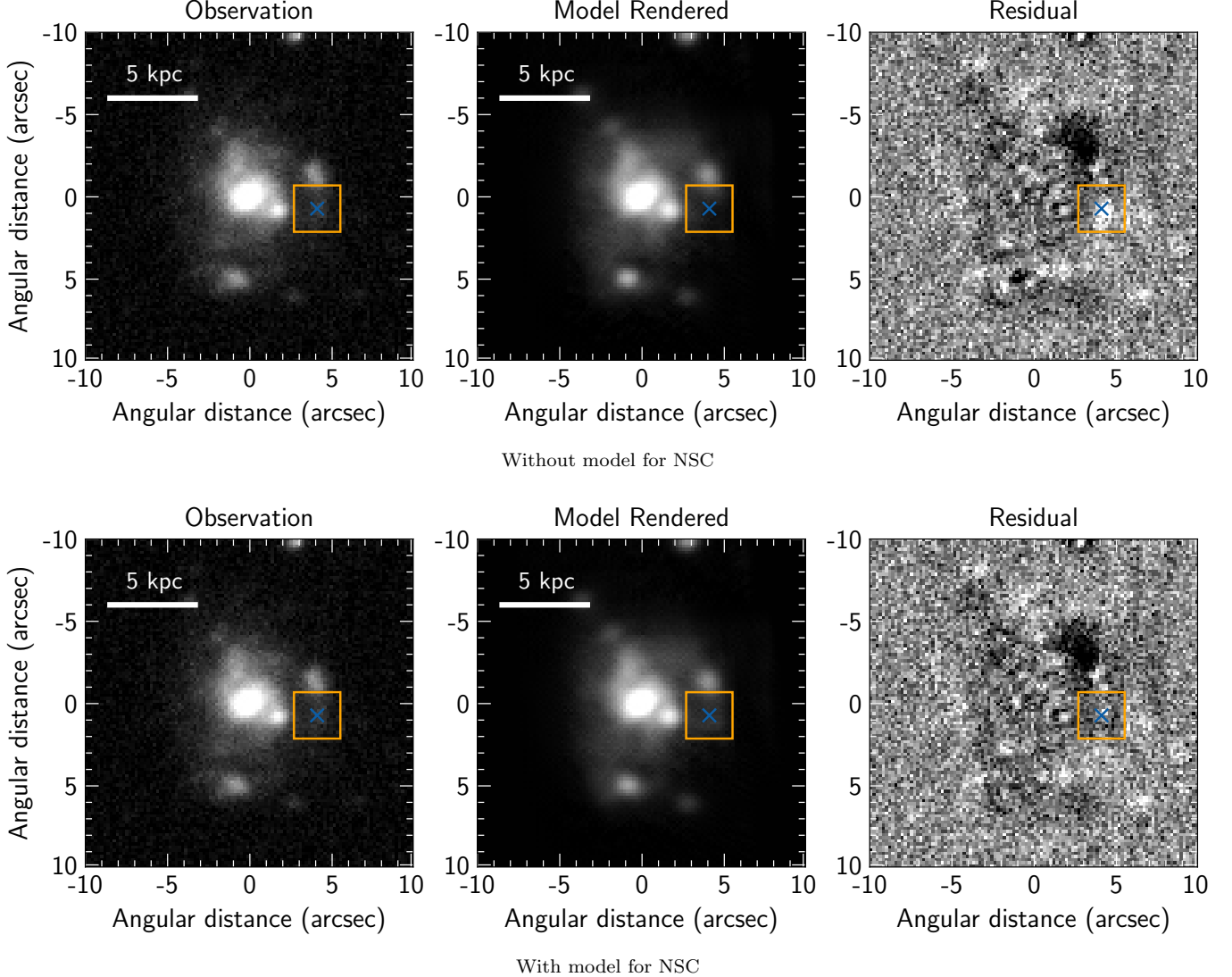


Figure 5. *Scarlet* scene model from Magellan imaging. Each source was modelled as a monotonically decreasing profile. We show the Magellan image (left), model rendered to match the Magellan imaging (centre), and the residual (right). Above, we show the model, observation and residuals for the case where no source is modelled at the position of the radio transient. Below, we show the case where a source is modelled at the radio transient position. We show the ATCA position centre with a blue cross, and an orange box where an additional extended source was fit to account for galaxy emission in the region of the transient.

structured the PSF model by weighted-mean stacking cutouts of all $> 10\sigma$ stars in the image. On a $20''$ by $20''$ cutout centred on the host galaxy, we used Source Extractor (Bertin & Arnouts 1996) to detect all sources above 2.5σ . We modelled each source as a non-parametric, monotonically decreasing (but not radially symmetric) extended source and ran *Scarlet* to convergence. The best-fit model, together with the observations and residuals, is shown in Fig. 5. A clear flux excess relative to the *Scarlet* model of the host galaxy is evident at the position of the radio transient. To place an upper limit on the magnitude of this excess, we refit

the model including an additional extended source component at the transient location (Fig. 5). The best-fit AB magnitude and 5σ uncertainty of the excess emission is $m_g = 24.1 \pm 0.7$. This enabled us to estimate the flux of local galaxy emission in the region of the transient. We also used the pixel variance of the residuals in a 30×30 pixel cutout at the source location to determine that the 5σ limiting magnitude based on the background variance was 28.0 (AB magnitudes).

6. TRANSIENT CLASSIFICATION AND MODELLING

In this section, we estimate the physical parameters of ASKAP J0055–2558 and compare with other transient classes to help its classification.

6.1. Spectral Luminosity and Lightcurve Evolution

In Fig. 6, we compare the luminosity evolution of ASKAP J0055–2558 for three possible start dates with that of other synchrotron transients. If ASKAP J0055–2558 is indeed associated with the galaxy 2dFGRS TGS143Z140 ($z = 0.116$), its high luminosity is unprecedented among known supernovae (Bietenholz et al. 2021) and thermal TDEs¹¹ (Goodwin et al. 2022, 2023). Additionally, the transient exhibits a slow decline between ~ 400 –1000 days post first radio-detection. This long-lived, gradual evolution contrasts with the behaviour of FBOTs, which typically fade much more rapidly, often at rates of $\gtrsim t^{-3}$ and complete their entire evolution in < 1000 days (Margutti et al. 2019; Coppejans et al. 2020; Ho et al. 2020a).

Its luminosity evolution appears to resemble the late-time emission from a jetted TDE like SWIFT J164449.3+573451 (Eftekhari et al. 2018), or a long-GRB (l-GRB). Alternatively, luminosity may also be consistent with delayed TDEs, where flares occur long after the initial optical burst as seen in AT2018hyz (Cendes et al. 2022; Sfaradi et al. 2024). In terms of longevity, ASKAP J0055–2558 is consistent with off-axis GRB afterglows, such as that of GW170817 (Katira et al. 2025), and with TDE events that have entered their late-time Newtonian phase, such as AT2019azh (Burn et al. 2025) and AT 2022cmc (Rhodes et al. 2025). However, the lack of early-time coverage complicates efforts to determine whether this was an on-axis or off-axis event. At late times, distinguishing between the two is challenging, as both exhibit similar evolution once the jet decelerates, widens, and becomes Newtonian (Huang et al. 2002; Lamb et al. 2018).

Taken together, the luminosity evolution is inconsistent with supernovae, thermal TDEs, FBOTs, and even lower-luminosity sources such as X-ray binaries (Geldzahler et al. 1983; Spencer 1996) and radio bubbles (Berghea et al. 2020; Urquhart et al. 2019). Instead, it aligns more closely with the late-time behaviour of a l-GRB or a jetted/delayed TDE.

6.2. Equipartition Analysis

¹¹ We define “thermal” TDEs as events that exhibit an early, single radio flare associated with the initial accretion phase, and “delayed” TDEs as those in which the radio emission either shows a second, later flare or appears only months to years after disruption.

To constrain the physical parameters of the synchrotron-emitting region, we adopt the synchrotron self-absorption model developed by Barniol Duran et al. (2013). This model, which assumes an instantaneous energy injection event, relates observed spectral properties (peak flux density F_p and peak frequency ν_p) to physical parameters based on the assumption of equipartition between the energy densities of relativistic electrons and magnetic fields. The parameters minimal energy radius (R_{eq}) and the total minimal energy (E_{eq}) are calculated using the relativistic solutions presented in Equations 27 and 28 from Barniol Duran et al. (2013). Crucially, in the absence of a measured ν_m (the synchrotron frequency of the minimal Lorentz factor electrons), we assume $\eta = 1$, corresponding to the simplified case where the synchrotron self-absorption frequency ν_a is greater than or equal to ν_m ($\nu_a \geq \nu_m$).

Since the bulk Lorentz Factor (Γ) of the outflow is not directly observed, we adopt the theoretical value derived from the shock acceleration model outlined in Barniol Duran et al. (2013). The model relates the minimal electron Lorentz factor, γ_m , to the source Lorentz Factor Γ via $\gamma_m = \chi_e(\Gamma - 1)$, where χ_e depends on the electron power-law index p and the fraction of the shock energy imparted to the electrons, ϵ_e :

$$\chi_e = \left(\frac{p-2}{p-1} \right) \epsilon_e \left(\frac{m_p}{m_e} \right)$$

By assuming a fixed value for the electron energy fraction, $\epsilon_e = 0.1$, and setting $\gamma_m = 2$, we derive a fixed, theoretical value for the bulk Lorentz factor Γ for the source, which is then used as a parameter in the calculation of R_{eq} and E_{eq} via the Barniol Duran et al. (2013) equations.

The geometric factors, f_A (area factor) and f_V (volume factor), are applied based on the assumed geometry. For spherical geometry, $f_A = 1.0$ and $f_V = 4/3$ (Barniol Duran et al. 2013). For conical geometry, the area factor f_A is set based on the half-opening angle θ_j . For narrow angles ($\theta_j \leq 10^\circ$), we implement the relativistic jet convention where $f_A = f_V = \Gamma\theta_j^2$. For wider angles, we use the geometric expression $f_A = 1 - \cos\theta_j$ and fix the volume filling factor at $f_V = 1.0$, following the standard unit-volume convention in non-relativistic equipartition models (Alexander et al. 2016; Goodwin et al. 2024). For opening angles (Θ) of 5° , 15° , and 30° , this yields $f_A = f_V = 0.0019$, $f_A = f_V = 0.017$, and $f_A = 0.034$ with $f_V = 1.0$, respectively.

Following the calculation of R_{eq} and E_{eq} , the magnetic field (B), electron number (N_e) and ambient density (n_e) are calculated directly from the equipartition relations. The outflow velocity (β_{ej}) is then determined

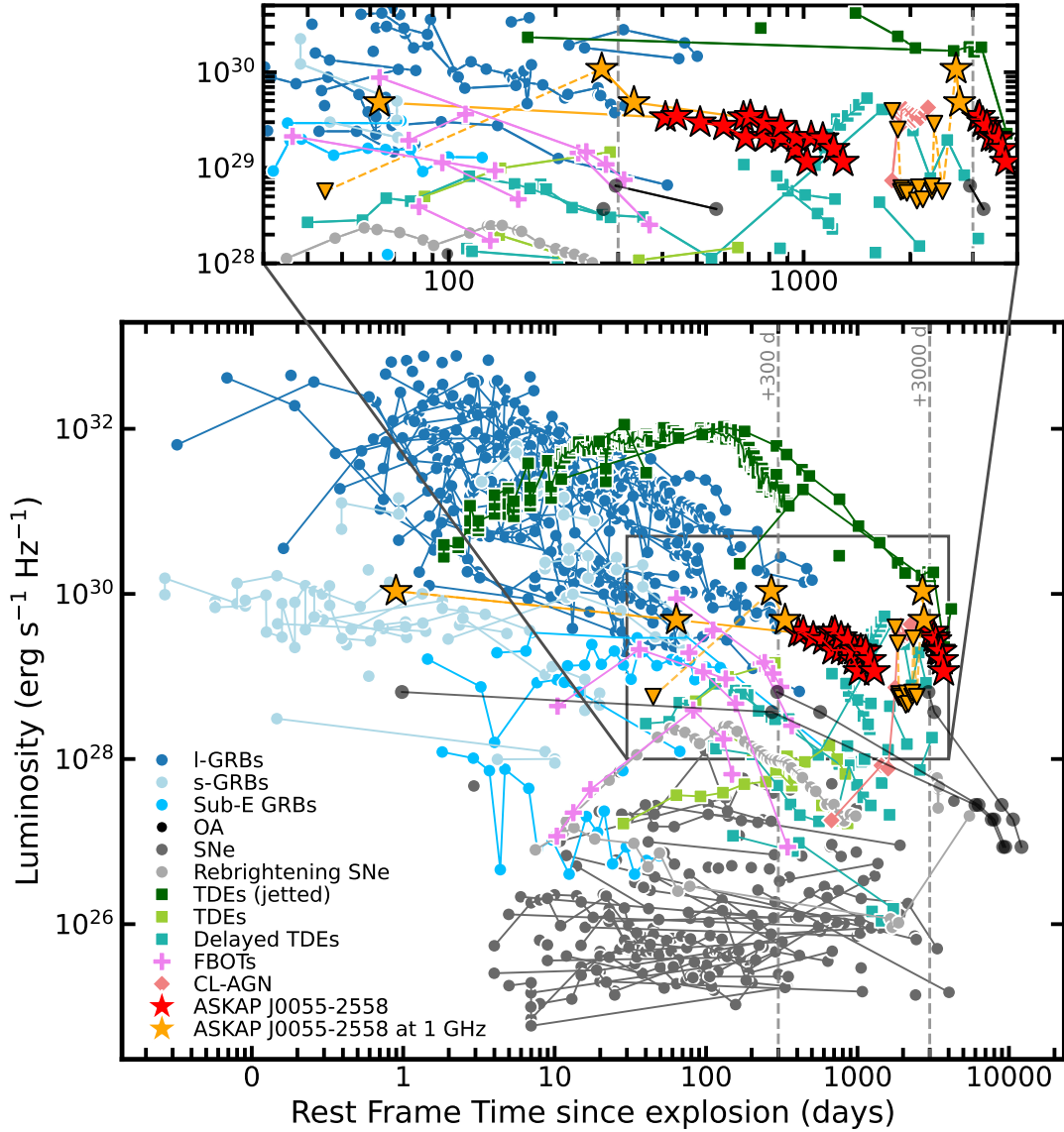


Figure 6. 8–10 GHz light curve of ASKAP J0055–2558 (red stars) shown in comparison with other classes of explosive transients: gamma-ray bursts (long-GRBs; blue circles), short-GRBs (light-blue circles), sub-energetic GRBs (deep sky blue circles), supernovae (SNe; dark gray circles), rebrightening SNe (light gray circles), tidal disruption events (TDEs; light-green squares), relativistic TDEs (dark-green squares), delayed TDEs (light seagreen squares), fast blue optical transients (FBOTs; pink pluses), and changing-look AGN (coral diamonds). Luminosities are plotted relative to 2022 Feb 3 (one day before first detection), though the true explosion date may precede this; we therefore show ASKAP J0055–2558 with additional shifted reference times of 300 and 3000 days prior to detection. Orange datapoints represent the early-time low frequency radio emission of ASKAP J0055–2558 at 1 GHz. 5-sigma limits are shown using downward triangles. No limits are shown for observations assuming launch was a day before first radio detection. Jetted TDE AT2022cmc’s datapoints are plotted at 15.5 GHz (Rhodes et al. 2025). The source’s luminosity is comparable to late-time GRBs and TDEs, and exceeds that of SNe and thermal TDEs. For context, another orphan radio afterglow candidate is shown in black circles, time-shifted similarly to ASKAP J0055–2558. To recreate this plot, please use code https://github.com/ashnagulati/Transient_Comparison_Plots.git [DATASET]. References: Chandra & Frail (2012); Alexander et al. (2016, 2017); Andreoni et al. (2022); Berger et al. (2001b,a, 2000, 2003); Bietenholz et al. (2021); Bright et al. (2022); Brown et al. (2017); Cendes et al. (2022, 2021, 2024); Cenko et al. (2011, 2006, 2012); Chandra et al. (2008, 2010); Chrimes et al. (2024); Coppejans et al. (2020); Djorgovski et al. (2001); Eftekhari et al. (2018); Frail et al. (2005, 2006, 2000, 1999); Galama et al. (2000, 2003); Goodwin et al. (2023, 2025); Greiner et al. (2013); Harrison et al. (2001, 1999); Ho et al. (2019, 2020); Horesh et al. (2021b,a, 2015); Laskar et al. (2023, 2016, 2018); Fong et al. (2014); Laskar et al. (2022); Lamb et al. (2019); Fong et al. (2021); Anderson et al. (2024); Soderberg et al. (2006b); Levan et al. (2024); Berger et al. (2005); Fong et al. (2021); Anderson et al. (2025); Law et al. (2018); Leung et al. (2021); Margutti et al. (2019, 2013); Mattila et al. (2018); Meyer et al. (2025); Moin et al. (2013); Mooley et al. (2022); O’Connor et al. (2023); Pasham et al. (2015); Perley et al. (2014, 2008); Rhodes et al. (2024); Rol et al. (2007); Rose et al. (2024); Schroeder et al. (2025, 2024); Sfaradi et al. (2024); Soderberg et al. (2004a,b, 2006); Stein et al. (2021); Taylor et al. (1998); van der Horst et al. (2008); Zauderer et al. (2013); Alexander et al. (2017); Chrimes et al. (2024); Kulkarni et al. (1998); Frail et al. (1997); Hajela et al. (2025); Hancock et al. (2012); Anderson et al. (2023); Perley et al. (2008); Price et al. (2002); van der Horst et al. (2008)

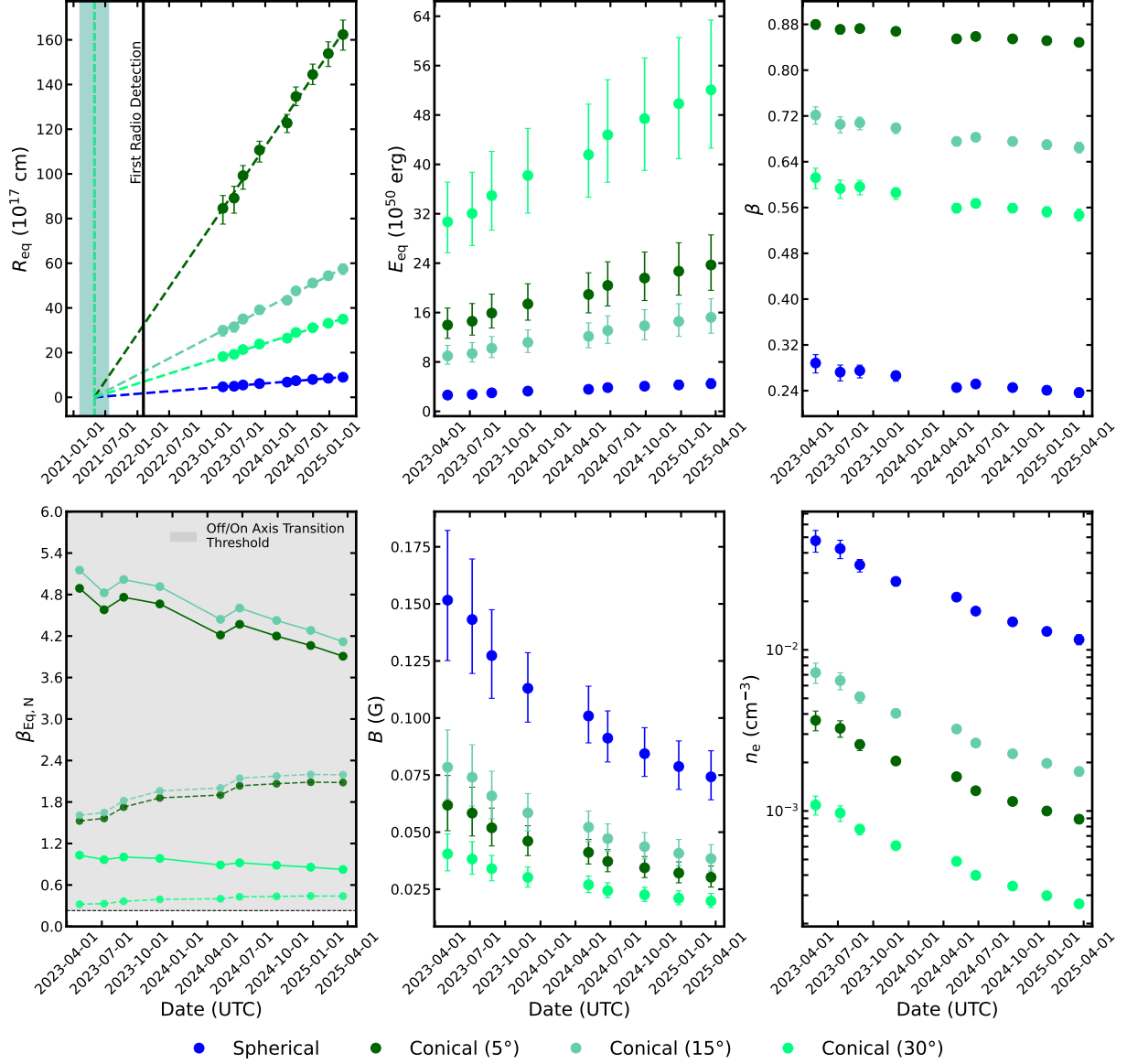


Figure 7. Outflow properties of ASKAP J0055–2558 inferred from equipartition modelling of its radio spectra from epoch 2023-08-27 to 2025-03-20. Results assuming spherical geometry are shown in blue, and conical geometry in shades of green. Shown are the outflow radius (R), energy (E), velocity (β), equipartition velocity ($\beta_{\text{eq},N}$), magnetic field strength (B) and ambient electron density (n_e). E and R are derived under equipartition and are uncorrected for deviations from it. In the upper left panel, dashed lines show linear fits to R for each geometry. The first radio detection is marked by a solid black line; dashed vertical lines (colour-coded by geometry) indicate the estimated outflow launch date (when $R = 0$). In the lower left panel, Equipartition-based Newtonian velocity ($\beta_{\text{eq},N}$) versus epoch of observation. Since $\beta_{\text{eq},N} \propto t^{-1}$, dashed lines show the evolution assuming an outflow launch 1000 days prior to detection. The grey shaded region marks the on/off-axis threshold; values above 0.23 suggest the outflow may have originated as a relativistic jet that has since decelerated into the Newtonian regime.

kinetically. This velocity represents the actual speed of the blastwave’s shock front at the time of observation t . In this case, t has been calculated relative to the first radio detection. This β_{ej} is calculated by solving the expression that relates the instantaneous radius R_{eq} and the observed time:

$$\frac{R_{\text{eq}}(1+z)}{ct} = \frac{\beta_{\text{ej}}}{1-\beta_{\text{ej}}}$$

The parameters are summarised in Fig. 7 and in Appendix B Table 6. Since the burst (or explosion) date is unknown but must precede the first radio detection, it should be noted that only the velocity ($\beta \propto t^{-1}$) varies explicitly with time, and we have illustrated how this variation would appear. We also calculated the relative velocity for each geometry and epoch, and we find that while there are large errors on these numbers,

they are consistent with the velocity values extrapolated using the time of first radio detection as the launch date. Furthermore, astrophysical sources may deviate from equipartition, hence, we applied corrections assuming plausible ranges for electron, $\epsilon_e \in \{0.1, 0.0005\}$, and magnetic energy fractions, $\epsilon_B \in \{0.1, 0.01, 0.001\}$ (Horesh et al. 2013; Alexander et al. 2016; Ryan et al. 2020; Cendes et al. 2021; Goodwin et al. 2022) and the following equations.

$$\epsilon = \left(\frac{\epsilon_B}{\epsilon_e} \right) \left(\frac{11}{6} \right) \quad (5)$$

$$R = R_{\text{eq}} \cdot \epsilon^{1/17} \quad (6)$$

$$E = E_{\text{eq}} \cdot \left[\frac{11}{17} \cdot \epsilon^{-6/17} + \frac{6}{17} \cdot \epsilon^{11/17} \right] \quad (7)$$

In the following sections, we compare these parameters to other transient classes.

6.2.1. Energy-velocity

The inferred outflow velocity from the equipartition analysis in Section 6.2, β , spans 0.2–0.9, with higher values for conical geometries, placing ASKAP J0055–2558 in the mildly relativistic regime. These estimates, anchored to the first radio detection, represent upper limits, as the outflow launch likely preceded the first radio detection. The corresponding equipartition-corrected energy ranges from 10^{50} to 10^{53} erg. We find that the inferred outflow velocity shows clear mild deceleration in the spherical model, while the conical models are consistent with only weak deceleration and nearly constant expansion speed. The observed decreasing velocity follows expectations for jetted TDEs (e.g., Swift J1644+57; Eftekhari et al. 2018) and GRBs (e.g., GRB 030329; Van Der Horst 2008). In all geometries, the equipartition energy increases monotonically with time, indicative of ongoing energy injection such as slower ejecta catching up with the forward shock, which appears to taper off and approach a plateau at the latest epochs. This flattening occurs when the outflow has swept up an external mass comparable to its own and begins to decelerate, causing the radio emission to fade as the kinetic energy stabilises (Barniol Duran et al. 2015).

In Fig. 8, we place ASKAP J0055–2558 in energy-velocity space alongside various synchrotron transient classes. Its kinetic energy and velocity significantly exceed those of ordinary core-collapse supernovae ($E_k \sim 10^{51}$ erg; $\beta \ll 1$), but remain below those of typical, on-axis GRBs. It lies within the mildly relativistic, high-energy regime characteristic of the late-time evolution of jetted TDEs and l-GRBs, delayed TDEs and FBOTs.

The mildly relativistic velocities and high kinetic energy suggest ASKAP J0055–2558 to be the late-time phase of an engine-driven transient, such as the one found by Law et al. (2018), claimed to be an off-axis orphan afterglow event.

The distribution of kinetic energy as a function of outflow velocity ($E_{\text{eq}} - \Gamma\beta^k$) exhibits a steeply declining slope of roughly -2.5 to -3.7, indicating that the fastest-moving material carries comparatively little energy, found also in the Newtonian afterglow of GW170817 (Balasubramanian et al. 2022; Katira et al. 2025) and on-axis jetted TDE SWIFT J1644+57 (Eftekhari et al. 2018). However, inferred velocity depends inversely on the assumed launch time. Adopting a delay of 300–1000 days prior to first radio detection shifts the outflow towards a comparatively less relativistic regime ($\Gamma\beta < 1$; indicated by the dashed lines in Fig. 8), where the relationship transitions towards a positive slope with increasing delay, consistent with the Sedov–Taylor scaling $E \propto v^2$. This supports a scenario where the outflow has significantly decelerated and is in the deep Newtonian regime. Either of those scenarios would still place ASKAP J0055–2558 in the non-relativistic phase of a TDE or GRB.

6.3. Host Galaxy and Local Environment

The host galaxy of this transient is a low-mass, moderately star-forming, and dusty system, characterised by prominent H II regions. Galaxies with similar properties are known to host a range of energetic transients, including supernovae, GRBs, and FBOTs (Bhandari et al. 2020; Coppejans et al. 2020). The transient lies at a projected distance of ~ 8.7 kpc from the galaxy’s core, larger than typical offsets for long GRBs, but it is coincident with a star-forming region in the galaxy’s outskirts. Given that long GRBs are preferentially associated with sites of active star formation, and that the host shows a complex morphology with extended H II regions, an orphan GRB afterglow remains a plausible explanation despite the relatively large offset.

Deep Magellan imaging also reveals an additional flux excess spatially coincident with the transient position within the positional uncertainty. While this excess lies above the radio-to-optical extrapolation of the optically thin synchrotron spectrum, it could be associated with the transient if the optical emission is dominated by thermal radiation from accretion-powered reprocessing or outflows (Metzger & Stone 2016; Roth et al. 2016), rather than by a jet afterglow. Alternatively, the excess emission at the transient position may originate from a globular or nuclear star cluster with an inferred absolute magnitude of $M_g \approx -14.71$ (uncorrected for extinc-

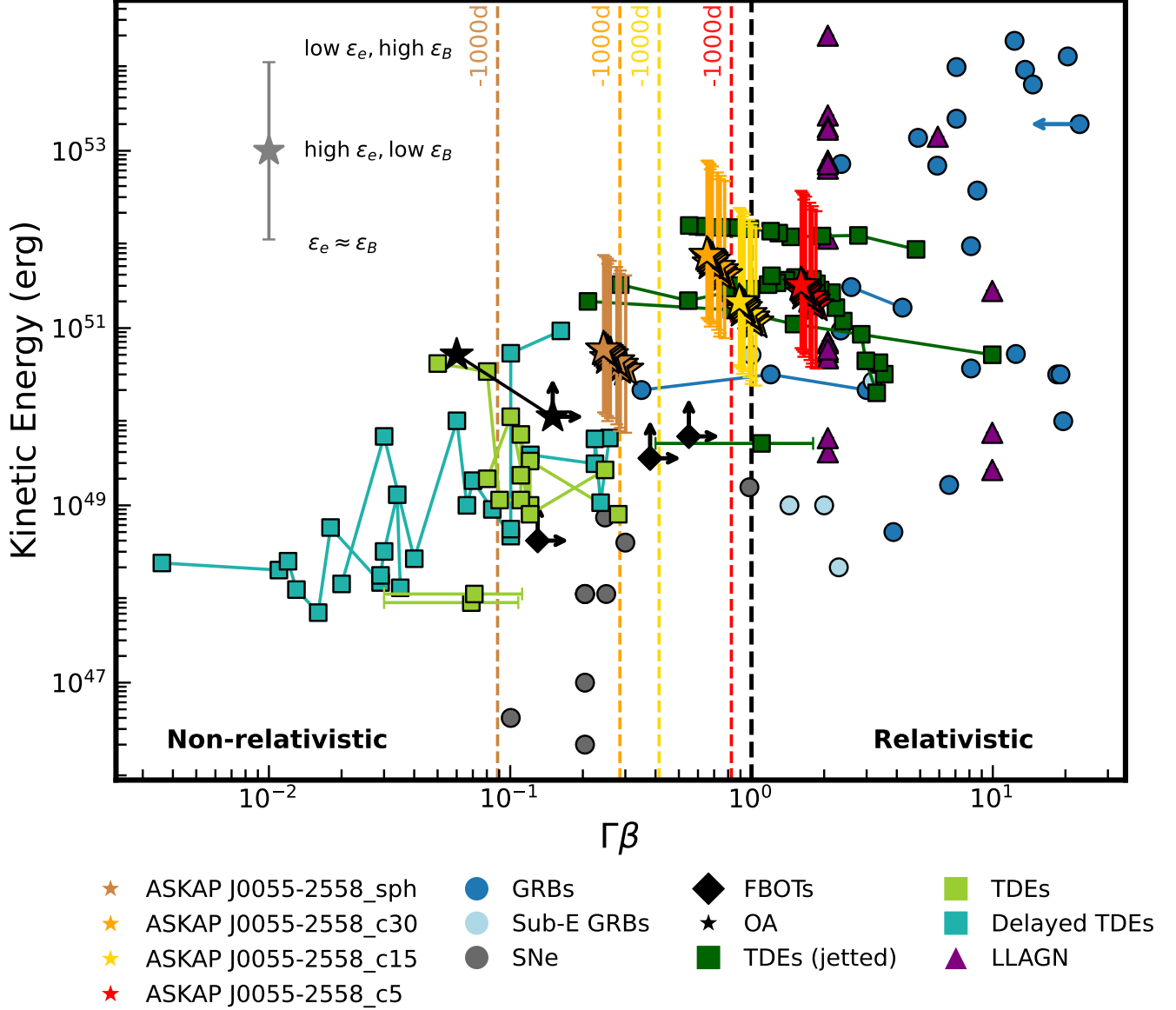


Figure 8. Intrinsic (beaming-corrected) kinetic energy (E_K) versus outflow speed ($\Gamma\beta$), where $\Gamma = (1 - \beta^2)^{-1/2}$ is the bulk Lorentz factor and $\beta = v/c$ is the velocity, computed with time referenced to the first radio detection on 2022 Feb 4. ASKAP J0055–2558 is shown assuming different conical geometries: red stars (5°), yellow (15°), orange (30°), and brown (spherical). Stars (from right to left) mark nine observer-frame epochs. For comparison, other explosive transients are included: GRBs (blue circles), sub-energetic GRBs (light-blue), SNe (dark grey), TDEs (light-green squares), relativistic TDEs (dark-green), delayed TDEs (light sea-green), FBOTs (black diamonds), LLAGN (purple triangles), and a radio orphan afterglow candidate (black stars). All values are derived from radio observations; for LLAGN, constant jet power over 10 years is assumed. The error bars on energy values for ASKAP J0055–2558 reflect the range of corrections for deviations from equipartition, based on combinations of ϵ_e and ϵ_B . As the explosion time is uncertain and $\beta \propto t^{-1}$, velocities are scaled assuming an explosion 1000 days before first detection; dashed lines indicate this assumed shift. To recreate this plot, please use code https://github.com/ashnagulati/Transient_Comparison_Plots.git. References: Soderberg et al. (2008, 2010, 2005); Kamble et al. (2013); Chakraborti et al. (2015); Soderberg et al. (2006a); Berger et al. (2002); Salas et al. (2013); Soderberg et al. (2005, 2012); Suzuki et al. (2019); Soderberg et al. (2006); Margutti et al. (2013); Kulkarni et al. (1998); Berger et al. (2003); Panaitescu & Kumar (2001); Yost et al. (2003); Berger et al. (2000); Soderberg et al. (2006b); Fox et al. (2005); Berger et al. (2005); Cenko et al. (2010); Frail et al. (2006); Chandra et al. (2008); Cenko et al. (2011); Laskar et al. (2013, 2014); Frail et al. (2005); van der Horst et al. (2008); Eftekhari et al. (2018); Mattila et al. (2018); Cenko et al. (2012); Alexander et al. (2016); Goodwin et al. (2023, 2022); Alexander et al. (2017); Cendes et al. (2022); Goodwin et al. (2025a); Hajela et al. (2025); Ho et al. (2019); Coppejans et al. (2020); Ho et al. (2020a); Ma et al. (2014); Mooley et al. (2022); Rhodes et al. (2025)

tion), potentially hosting a massive black hole (MBH). This estimate should be regarded as an upper limit, as the detected emission could alternatively arise from a clumpy tidal feature associated with the primary host galaxy.

Using the measured flux of this excess and assuming it arises from a star cluster, we estimate the stellar mass under three different age hypotheses. From this measured g -band magnitude, we derived stellar masses by combining rest-frame g -band luminosity with mass-to-light ratios from EzGal¹² SSP models (Chabrier IMF, solar metallicity), yielding $M_\star \sim 3 \times 10^6$, 4×10^7 , and $3 \times 10^8 M_\odot$ for ages of 10 Myr, 1 Gyr, and 10 Gyr, respectively (the 10 Myr value corresponds to the youngest valid SSP grid point). At the low-mass end ($M_\star \sim 3 \times 10^6 M_\odot$, young), the system would resemble a “super star cluster” in a starburst galaxy such as M82 (McCraday & Graham 2007; Portegies Zwart et al. 2010). At the high-mass end ($M_\star \sim 10^8 M_\odot$, old), it approaches the regime of the most massive ultra-compact dwarfs (UCDs; Hilker et al. 2007; Chilingarian et al. 2011; Mieske et al. 2008; Liu et al. 2015), while the overall mass range overlaps with that of nuclear star clusters (Walcher et al. 2005). For context, extreme Virgo UCDs such as M59-UCD3, with a luminosity comparable to our candidate, and M60-UCD1 both host central black holes of a few $\times 10^6 M_\odot$ (Seth et al. 2014; Liu et al. 2015; Ahn et al. 2018).

To estimate the central black-hole mass in this potential star cluster, we apply the star cluster scaling relation of Graham (2020) to the young and intermediate-age cases, obtaining $M_{\text{bh}} \sim 4.8 \times 10^4 M_\odot$ (10 Myr) and $\sim 3.8 \times 10^7 M_\odot$ (1 Gyr). For the old case ($M_{\text{nc}} \sim 3.4 \times 10^8 M_\odot$), the relation would imply $M_{\text{bh}} \sim 1.2 \times 10^{10} M_\odot$, unphysically exceeding the cluster mass by a factor of ~ 30 , so we consider it inapplicable. The high luminosity and stellar mass disfavour a classical globular cluster and instead point to a nuclear star cluster, consistent with environments expected to host 10^4 – $10^7 M_\odot$ black holes and supporting the interpretation of a TDE.

6.4. Ambient Electron Density-Radius

In Fig. 9, we place ASKAPJ0055–2558 in electron-density–radius space alongside known TDEs. For this comparison, we adopt black hole masses of 10^4 – $10^7 M_\odot$ (Section 6.3), with the intermediate-mass range showing the best consistency with the observed trend. The inferred $\log(n_e)$ – $\log(R_{\text{eq}})$ trends across all assumed geometries indicate a decreasing density profile, with

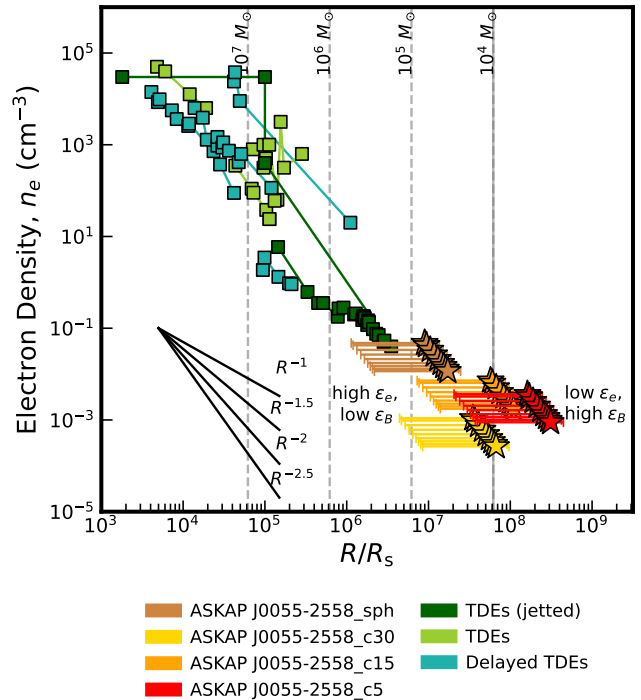


Figure 9. Variation of ambient density with distance from the black hole for TDEs compared to ASKAP J0055–2558. Distances are scaled to Schwarzschild radii. ASKAP J0055–2558 is shown assuming different conical geometries: red stars (5°), yellow (15°), orange (30°), and brown (spherical). The radii are corrected for deviations from equipartition, with uncertainties reflecting the range of ϵ_e and ϵ_B combinations. The grey dashed vertical lines show distance scalings for our source assuming black holes of masses between 10^4 and $10^7 M_\odot$ as derived in Section 6.3. References: Stein et al. (2021); Cendes et al. (2021); Alexander et al. (2016); Eftekhari et al. (2018); Mattila et al. (2018); Alexander et al. (2017); Goodwin et al. (2022, 2023, 2024); Hajela et al. (2025); Cendes et al. (2022)

power-law slopes of ~ -2.2 . This trend is consistent with that observed in the TDE population (Fig. 9), in core-collapse supernovae (e.g., Chevalier 1982; Chandra et al. 2012), and in GRBs expanding into a stellar-wind environment (Panaitescu & Kumar 2000; Chevalier & Li 2000). Similar behaviour is seen in GRB 171205A, where the afterglow remains consistent with a wind-like medium even beyond 1000 days post-burst, showing no evidence for a transition to a constant-density regime (Leung et al. 2021; Maity & Chandra 2021).

Notably, the circumnuclear medium (CNM) surrounding ASKAP J0055–2558 appears significantly less dense than that typically associated with thermal TDEs, FBOTs (e.g., Margutti et al. 2019; Coppejans et al. 2020), and supernovae (Fransson et al. 1996; Soderberg et al. 2006a; Chandra et al. 2012). The relatively low

¹² <https://github.com/cmancone/easyGalaxy>

density inferred for ASKAP J0055–2558 is more consistent with GRB environments (Panaitescu & Kumar 2002; Laskar et al. 2013) or with the sparse surroundings which may be expected near an IMBH in a globular cluster (for eg., Freire et al. 2001). This low density could explain the transient’s slow evolution. As shown by Lu & Bonnerot (2020), transients in denser environments tend to evolve faster and appear brighter due to stronger interaction between the outflow and the surrounding material. Overall, the observed density scaling across different geometries supports a scenario in which a jet is propagating into a low-density, steeply declining coherent circumburst medium.

7. ORPHAN AFTERGLOW OR OFF-NUCLEAR IMBH TDE: PHYSICAL PLAUSIBILITY

In this section, we evaluate whether the transient classification inferred from our comparative analysis is physically plausible. Specifically, we assess whether the observed properties can be explained by synchrotron emission from shock-accelerated electrons.

GRBs are followed by long-lived, multi-wavelength afterglows produced as the relativistic blast wave decelerates in the surrounding medium, causing the Lorentz factor (Γ) to drop and the beaming angle to widen as $\Omega(t) \propto 1/\Gamma(t)^2$ (Mészáros & Rees 1997b). Even without a detected prompt GRB, the afterglow can become visible once the jet decelerates and spreads laterally, producing so-called orphan afterglows (Dermer et al. 1999). These arise either because the GRB was outside the detector’s field of view or because the jet was initially misaligned with the observer ($\theta_{\text{view}} > \theta_j$; Rhoads 2003; Salafia & Ghirlanda 2022). While many optical (Cenko et al. 2015; Ho et al. 2020b) and a few radio candidates have been reported (Leung et al. 2023), only one convincing case has been identified in the radio (Law et al. 2018; Marcote et al. 2019; Mooley et al. 2022).

TDEs occur when a star is disrupted by a black hole’s tidal forces (Hills 1975; Rees 1988), typically in galaxy nuclei hosting supermassive black holes (SMBHs; $M_{\text{BH}} > 10^6 M_{\odot}$; Alexander et al. 2020). Radio studies reveal two main classes: non-relativistic, thermal events (Goodwin et al. 2022) and relativistic, non-thermal, jetted events (Eftekhari et al. 2018). A rarer subclass involves IMBHs, seen in dwarf-galaxy nuclei (Angus et al. 2022) or in off-nuclear environments such as galaxy clusters (Lin et al. 2018). Although IMBH-associated TDEs have not yet been detected at radio wavelengths, several recent discoveries include radio afterglows from off-nuclear candidates (Zhang et al. 2025; Jin et al. 2025; Li et al. 2025; Eyles-Ferris et al. 2025; Goodwin et al. 2025b; Levan et al. 2025; Sfaradi et al. 2025), high-

lighting that off-nuclear events can indeed produce detectable radio emission.

Studies of orphan afterglow candidates in the last few decades, such as J060938-333508 (Bannister et al. 2011) and ASKAP J175036.1-181454 (Leung et al. 2023), demonstrate long-lived, luminous synchrotron emission with peaked or evolving spectra and off-nuclear host associations, key features also observed in ASKAP J0055-2558. These events, together with well-studied analogues such as the orphan afterglow candidate FIRST J141918.9+394036 (Law et al. 2018) and the off-nuclear TDE AT 2024tvd (Sfaradi et al. 2025), highlight an emerging population of radio transients likely powered by relativistic outflows occurring at significant offsets from their host galaxy centres. The persistence of their radio emission over years, combined with the absence of contemporaneous high-energy counterparts, collectively suggests that ASKAP J0055-2558 is part of an emerging class of extragalactic, synchrotron-powered transients such as orphan afterglows or off-nuclear TDEs.

7.1. Spectral and Temporal Index Consistency: Closure Relations

We compare the derived spectral and temporal indices for ASKAP J0055–2558 with the standard closure relations for synchrotron afterglows in the Newtonian (wide-angle geometries) and relativistic (narrow-angle geometries) phase (Gao et al. 2013; Granot & Sari 2002). Based on the electron density–radius scaling, a wind-like environment is favoured. In such a medium, with spectral ordering $\nu_m < \nu_a < \nu_c$ and assuming the observed band lies in the optically thin segment between ν_a and ν_c , the closure relations for (a) the Newtonian regime predict temporal and spectral indices of $\alpha = (7p - 5)/6$ and $\beta = (p - 1)/2$, respectively, and (b) for the relativistic regime predict $\alpha = (3p - 1)/4$ and $\beta = (p - 1)/2$, where $F_{\nu} \propto \nu^{-\beta} t^{-\alpha}$. From the optically thin spectral index derived in Section 4.2, we estimate an average electron energy distribution index of $p = 2.72 \pm 0.08$. Substituting this into the closure relation yields (a) $\alpha = 2.34 \pm 0.09$ in the Newtonian regime and (b) $\alpha = 1.79 \pm 0.06$ in the relativistic regime, which is consistent with the observed light curve decay rate assuming the explosion occurred approximately 1000 days before the first radio detection for wide-angle geometries and approximately 500 days for narrow-angle geometries (see Fig. 3). Alternatively, if the emission is already in the Deep Newtonian regime, the temporal decay would be $\sim t^{-1}$, consistent with a launch date approximately 100 days prior to radio detection (Sironi & Giannios 2013). However, a late launch of ~ 100 days prior is in

tension with the expansion velocity inferred from our equipartition analysis and can be ruled out.

7.2. *The Late-time Radio Lightcurve and Spectrum*

The peaked spectrum of ASKAPJ0055–2558 is well fit by the assumed synchrotron self-absorption (SSA) with the ordering $\nu_m < \nu_a < \nu_c$ (Granot & Sari 2002). This ordering remains consistent for over 500 days of follow-up multifrequency observations similar to the long-lived evolution observed in GRB970508 (Frail et al. 2000) and GRB171205A (Maity & Chandra 2021). The minimum cooling frequency, ν_c , inferred from equipartition parameters in a Newtonian/relativistic wind model lies in the X-ray band, consistent with its placement above the peak frequency. Our joint SBPL fits yield a temporal evolution of ν_a with an index of $-0.80^{+0.22}_{-0.21}$. This value is broadly consistent with the theoretical expectation of -1.24 ± 0.01 for a Newtonian, wind-like circumburst medium in the case of a wide-angle jet, given by $-(7p+6)/3(p+4)$. It is also consistent, within uncertainties, with the theoretical expectation of -1.05 ± 0.01 for a relativistic, wind-like circumburst medium in the case of a narrow jet, given by $-3(p+2)/2(p+4)$. Both expectations correspond to an electron power-law index of $p = 2.72 \pm 0.08$ and assume the spectral ordering $\nu_m < \nu_a < \nu_c$ (Frail et al. 2000; Gao et al. 2013; Maity & Chandra 2021; Granot & Sari 2002).

At 9 GHz the decline is clearly evident, with the flux decreasing by a factor of ~ 3 over 600 days. At 0.9 GHz (see Fig. 1), the decay is much slower and remains poorly constrained due to substantial scatter, though the overall trend is again consistent with a factor of ~ 1.5 decline over 600 days. The scatter can be naturally explained by refractive interstellar scintillation, since the inferred source size is much smaller than the scattering disk at this frequency (see Section 4.1).

7.3. *Constraints on the Outflow Launch Time*

Using the radii derived from our equipartition analysis and assuming a constant outflow velocity, a linear back-extrapolation of the late-time expansion implies that the outflow was launched approximately 281 ± 81 days before the first radio detection i.e. 2021-04-28, corresponding to the epoch when $R_{\text{eq}} \rightarrow 0$ (Fig. 7). While this estimate is model-dependent and relies on extrapolating the evolution backward from late times (our monitoring begins ~ 500 days after the first detection), it provides a physically motivated fiducial launch epoch.

Independent constraints are obtained from standard synchrotron closure relations, which permit launch times in the range of ~ 500 – 1000 days prior to the first radio detection. This broad range is further restricted by deep

pre-discovery 0.9 GHz non-detections between 2019 and 2021 at ~ 0.15 mJy. Between the final non-detection on 2021-05-29 (< 0.15 mJy) and the first detection on 2022-04-15 (1.30 mJy) at 0.9 GHz, the source brightened by a factor of $\gtrsim 8.7$ in $\lesssim 321$ days, which represents an upper limit on the rise rate. We parameterise the rise as a power law, $F_\nu \propto (t - t_0)^\alpha$. To constrain α , we construct simple power-law light curves that are required to pass through both the non-detection limit and the first detection, while varying the assumed launch time ($t_0 = 1, 10, 50, 100, 200,$ and 500 days prior to the non-detection). As the launch time is placed progressively earlier, the interval between the non-detection and detection constitutes a smaller fraction of the total time since launch, requiring increasingly steep power-law indices to reproduce the observed flux increase while remaining below the pre-discovery limits. Hence, if the outflow was launched shortly before the 2021-05-29 non-detection, relatively modest rise indices are sufficient (e.g. $\alpha \gtrsim 0.6$ for a launch 10 days earlier, or $\alpha \gtrsim 1.0$ for 50 days earlier). In contrast, launches hundreds of days earlier require much steeper rises, with $\alpha \gtrsim 1.5$ for 100 days, $\alpha \gtrsim 2.1$ for 200 days, and $\alpha \gtrsim 4.0$ for 500 days prior to the non-detection. If the outflow were launched after the last non-detection, assuming the same flux limit the latest possible launch time consistent with the first radio detection would be 70 days earlier, requiring a maximum rise slope of $\alpha \lesssim 0.5$.

As shown in Fig. 6, an on-axis relativistic blast-wave launched $\gtrsim 250$ days prior to the first detection should have produced detectable radio emission during the non-detection period. For a standard on-axis GRB or TDE afterglow, launch times $\lesssim 250$ days before the first radio detection would give a slow radio rise which is inconsistent with the rapid rise and decay expected for on-axis jets. Furthermore, if it was launched $\lesssim 250$ days before first radio detection, it should have been fading at a decay rate of $\lesssim 1.24$ which is inconsistent with the predicted decays rate using the applicable closure relations for $p = 2.72$. No GRB localisations overlapped the source position during the 250-day period prior to the first radio detection, therefore, an on-axis GRB interpretation is further discouraged.

In contrast, off-axis relativistic outflows and delayed TDE scenarios naturally accommodate both the observed steep radio rise rate for an earlier launch date and the lack of early-time radio emission. In an off-axis jet scenario, the brightening is primarily driven by the decreasing Lorentz factor, gradually bringing the emission into the observer’s line of sight. This geometric effect can produce a characteristically steep rise $\alpha > 2$ (Margutti et al. 2018), which would be physically un-

usual for an on-axis source at such late times but is a hallmark of off-axis evolution. We therefore conclude that while the precise launch epoch remains model dependent, the data favour an outflow launched a few $\gtrsim 250$ days prior to the first radio detection and disfavour scenarios involving an on-axis relativistic jet.

7.4. Off-axis relativistic jet-like outflow

Matsumoto & Piran (2023) extended the equipartition framework to off-axis relativistic jets, wherein the jet initially moves outside our line of sight and later becomes visible as it decelerates and transitions into the Newtonian regime. At the point of this transition, when the jet becomes non-relativistic, the different branches of the equipartition solution converge to a unique solution that satisfies the condition for Newtonian velocity, given by $\beta_{\text{Eq,N}}$,

$$\begin{aligned} \beta_{\text{Eq,N}} \approx 0.73 & \left[\left(\frac{F_p}{\text{mJy}} \right)^{8/17} \left(\frac{d_L}{10^{28} \text{ cm}} \right)^{16/17} \eta^{35/51} \right. \\ & \times \left(\frac{\nu_p}{10 \text{ GHz}} \right)^{-1} (1+z)^{-8/17} \left(\frac{t}{100 \text{ d}} \right)^{-1} \left. \right] \\ & \times f_A^{-7/17} f_V^{-1/17} > 0.23 \end{aligned} \quad (8)$$

Where all parameters are defined in Section 6.2. Below 0.23, the relativistic and Newtonian branches split, and the transition should only happen when $\beta_{\text{Eq,N}}$ is above this value. For ASKAP J0055–2558 the inferred $\beta_{\text{Eq,N}}$ exceeds the threshold of 0.23 under all assumed collimated geometries, whether time is measured from the first radio detection or shifted 1000 days earlier to approximate the outflow launch (see Fig. 7). This suggests the source may be transitioning from a collimated off-axis relativistic jet to the Newtonian regime, supporting the applicability of the off-axis jet scenario to this event.

8. CONCLUSION

Based on all the observational data and analysis of ASKAP J0055–2558 we draw the following conclusions.

1. ASKAP J0055–2558 is a long-lived, radio transient that exhibited a steep rise in brightness by a factor of at least 20 over 250 days. It has remained detectable in the radio for over 1000 days since its initial discovery.
2. ASKAP J0055–2558 is very likely ($> 98\%$ confidence) associated with the low-mass, star-forming galaxy 2dFGRS TGS143Z140 at a redshift of $z = 0.116$ with prominent HII regions, and lies

~ 8.7 kpc from the galaxy core in an outer star-forming complex. Deep imaging reveals a potential compact stellar system coincident with the transient position, with a stellar mass of $M_\star \sim 10^6\text{--}10^8 M_\odot$ and a possible central black hole of $M_{\text{bh}} \sim 10^4\text{--}10^7 M_\odot$. Such an environment is consistent with sites that host GRBs, FBOTs, and off-nuclear IMBH or low-mass SMBH TDEs, supporting both an orphan GRB and a jetted or delayed TDE scenario. If associated to this galaxy, ASKAP J0055–2558 has a peak radio luminosity of $\sim 10^{29} \text{ erg s}^{-1} \text{ Hz}^{-1}$.

3. The inferred blast wave velocity, β , lies in the range 0.2–0.9, placing the transient in the mildly relativistic regime (assuming an explosion date of a day before first radio detection). This holds even if the explosion occurred up to 1000 days before the first radio detection, particularly for more collimated geometries. The corresponding blast wave energy spans $10^{50}\text{--}10^{53}$ erg, depending on the assumed microphysical parameters. This combination of high energy and mildly relativistic velocities places ASKAP J0055–2558 in a sparsely populated region of energy–velocity phase space, consistent with the late-time phase of a long GRB afterglow or a delayed or jetted TDE, depending on the outflow geometry.
4. The electron density evolution with radius, $n_e \propto (R_{\text{eq}}/R_s)^{-2.2}$, is consistent with TDEs and with GRBs propagating through a wind-like medium. This scaling supports a scenario in which a jet expands into a low-density, steeply declining circumburst environment, hence, again consistent with a l-GRB afterglow scenario. The inferred densities ($\sim 10^{-4}\text{--}10^{-1} \text{ cm}^{-3}$) are consistent with GRB environments or possibly with the sparse surroundings of IMBHs in globular clusters.
5. The late-time radio light curve and spectra exhibit behaviour consistent with that seen in TDEs and GRBs observed at similarly late epochs. The spectral peak frequency evolves slowly, consistent with either a Newtonian or a relativistic outflow propagating through a wind-like medium. The inferred ν_c based on the equipartition parameters stays in the X-ray regime, consistent with a $\nu_m, \nu_a < \nu_c$ regime. The 0.9 GHz light curve continues to exhibit variability during its decay, persisting even 1000 days after the first radio detection. This variability is consistent with the source size remaining smaller than the scattering disk at low frequencies.

6. Equipartition-based back-extrapolation, synchrotron closure relations, radio non-detections, and rise-time constraints together indicate that the outflow was launched $\gtrsim 250$ days prior to the first radio detection. These considerations disfavour an on-axis event and instead favour an interpretation in which ASKAP J0055–2558 represents late-time emission from either an orphan GRB afterglow or an off-axis or delayed TDE. An off-axis geometry is also supported by the inferred Newtonian velocity, $\beta_{\text{eq,N}} > 0.23$, across a range of jet and ejecta configurations.

In conclusion, the properties of ASKAP J0055–2558 are most consistent with the late-time detection of an orphan l-GRB afterglow or an off-nuclear TDE involving an IMBH. If ASKAP J0055–2558 is indeed an orphan afterglow detected in the radio, it would represent only the second such discovery to date (Law et al. 2018; Marcote et al. 2019; Mooley et al. 2022), and arguably the most compelling candidate of its kind. Alternatively, if it is an off-nuclear TDE associated with an IMBH, it would mark the first such event discovered exclusively via radio observations.

At such late times, when the jet has entered its Newtonian phase, distinguishing between progenitor classes becomes intrinsically difficult. In our case, the UV-bright host complicated the isolation of any long-lived accretion-disk emission expected from a TDE (Gezari 2021), whereas in a UV-quiet host, such a signal (or its absence) would offer a clearer diagnostic. Early X-ray observations could have been decisive: off-axis GRB afterglows are typically faint in X-rays at early times, while jetted TDEs can produce luminous, long-lived X-ray emission (Zauderer et al. 2011; Levan et al. 2011). Similarly, uninterrupted optical photometric monitoring would have constrained the rise time, helping better panchromatic modelling, but there was a 200 day gap in ZTF monitoring coincident with the last radio non-detection (2021-01-15 - 2021-08-09) and the first radio detection (2021-12-2 - 2022-08-12). A prompt optical spectrum of the transient would have provided an additional, independent diagnostic through line features or continuum shape (Sfaradi et al. 2025). Future discoveries of this kind will benefit most from rapid multi-wavelength follow-up, particularly early X-ray/UV coverage, dense radio monitoring, and timely optical spectroscopy to break the orphan-afterglow versus off-nuclear TDE degeneracy.

9. ACKNOWLEDGEMENTS

We are grateful to the reviewer for their insightful and helpful comments, which have strengthened

the manuscript. We thank Marcus Lower for helping with the Parkes UWL observations and Themiya Nanayakara for a discussion on optical analysis techniques. AG is supported by the Australian Government Research Training Program Scholarship. This research was conducted with support from the Australian Research Council Centre of Excellence for Gravitational Wave Discovery (OzGrav), project number CE230100016. AM is supported by the ARC Discovery Early Research Award (DE230100055). This scientific work uses data obtained from Inyarrimanha Ilgari Bundara / the CSIRO’s Murchison Radio-astronomy Observatory. We acknowledge the Wajarri Yamaji People as the Traditional Owners and native title holders of the Observatory site. CSIRO’s ASKAP radio telescope is part of the [Australia Telescope National Facility](#). Operation of ASKAP is funded by the Australian Government with support from the National Collaborative Research Infrastructure Strategy. ASKAP uses the resources of the Pawsey Supercomputing Research Centre. Establishment of ASKAP, Inyarrimanha Ilgari Bundara, the CSIRO Murchison Radio-astronomy Observatory and the Pawsey Supercomputing Research Centre are initiatives of the Australian Government, with support from the Government of Western Australia and the Science and Industry Endowment Fund. We acknowledge the Gomeri people as the traditional owners of the Australia Telescope Compact Array (ATCA) observatory site. The ATCA is part of the Australia Telescope National Facility, which is funded by the Australian Government for operation as a National Facility managed by CSIRO. Jeff Cooke acknowledges funding from the Australian Research Council Discovery Project DP200102102. This work is (partly) based on data obtained through Swinburne. Keck program 2024B-W377; Keck Observatory is a private 501(c)3 non-profit organisation operated as a scientific partnership among the California Institute of Technology, the University of California, and the National Aeronautics and Space Administration. The Observatory was made possible by the generous financial support of the W. M. Keck Foundation. The authors wish to recognise and acknowledge the very significant cultural role and reverence that the summit of Maunakea has always had within the Native Hawaiian community. We are most fortunate to have the opportunity to conduct observations from this mountain. AI tools (ChatGPT-4) were used for language editing and clarity. AG takes full responsibility for the content.

Software: VAST Tools (Stewart et al. 2023), MIRIAD (Sault et al. 1995), CASA (McMullin et al. 2007), XRTPipeline (Evans et al. 2009), Scarlet (Melchior

et al. 2018), LIME (Fernández et al. 2024), IRAF (Tody 1986), SExtractor (Bertin & Arnouts 1996), SWARP (Bertin et al. 2002), MARZ(Hinton et al. 2016)

APPENDIX

A. RADIO OBSERVATIONAL DATA AND FITS

Table 3. The radio data used in this work. All upper limits are 5σ and errors are 1σ .

Epoch	Frequency (GHz)	Flux Density (mJy)	Flux Density Error (mJy)	ISS Error (mJy)	RMS (mJy)	Telescope, Survey, Project
2019-04-26	0.887	<1.06	-	-	0.21	ASKAP, RACS
2019-07-06	3.0	<0.68	-	-	0.14	VLA, VLASS
2019-08-16	0.943	<0.15	-	-	0.03	ASKAP, AS111
2019-08-23	0.943	<0.16	-	-	0.03	ASKAP, AS111
2019-09-16	0.943	<0.15	-	-	0.03	ASKAP, AS111
2019-11-07	0.943	<0.15	-	-	0.03	ASKAP, AS111
2020-04-03	0.943	<0.12	-	-	0.02	ASKAP, AS111
2020-04-29	0.943	<0.17	-	-	0.03	ASKAP, AS111
2020-07-03	0.943	<0.13	-	-	0.03	ASKAP, AS111
2020-11-28	0.943	<0.15	-	-	0.03	ASKAP, AS111
2020-11-29	0.943	<0.17	-	-	0.03	ASKAP, AS111
2021-01-06	1.3675	<0.78	-	-	0.16	ASKAP, RACS
2021-05-29	0.943	<0.15	-	-	0.03	ASKAP, AS111
2022-02-04	3.0	2.91	0.29	1.73	0.14	VLA, VLASS
2022-04-15	0.887	1.30	0.23	0.39	0.13	ASKAP, RACS
2023-05-04	1.332	<1.83	-	-	0.37	ATCA, C3363
2023-05-04	1.844	1.97	0.15	0.85	0.08	ATCA, C3363
2023-05-04	2.1	1.99	0.11	0.97	0.08	ATCA, C3363
2023-05-04	2.356	1.92	0.11	0.98	0.07	ATCA, C3363
2023-05-04	2.868	1.97	0.12	1.17	0.09	ATCA, C3363
2023-05-04	5.5	1.37	0.02	0.06	0.02	ATCA, C3363
2023-05-04	9.0	0.90	0.02	0.01	0.01	ATCA, C3363
2023-06-08	1.332	2.22	0.13	0.83	0.12	ATCA, C3363
2023-06-08	1.844	2.33	0.07	1.01	0.06	ATCA, C3363
2023-06-08	2.1	2.14	0.06	1.04	0.07	ATCA, C3363
2023-06-08	2.356	2.13	0.06	1.10	0.04	ATCA, C3363
2023-06-08	2.868	2.00	0.10	1.20	0.07	ATCA, C3363
2023-06-08	5.5	1.34	0.02	0.06	0.02	ATCA, C3363
2023-06-08	9.0	0.93	0.02	0.01	0.02	ATCA, C3363
2023-07-07	1.28	1.97	0.03	0.73	0.38	MeerKat
2023-08-27	1.332	2.49	0.14	0.92	0.17	ATCA, C3363
2023-08-27	1.844	2.63	0.10	1.14	0.08	ATCA, C3363
2023-08-27	2.1	2.33	0.05	1.14	0.08	ATCA, C3363
2023-08-27	2.356	2.38	0.10	1.22	0.08	ATCA, C3363
2023-08-27	2.868	2.00	0.13	1.19	0.09	ATCA, C3363
2023-08-27	5.5	1.21	0.03	0.06	0.02	ATCA, C3363
2023-08-27	9.0	0.80	0.02	0.01	0.02	ATCA, C3363
2023-10-15	0.887	1.66	0.17	0.50	0.18	ASKAP, VAST

2023-11-29	1.332	2.31	0.18	0.86	0.13	ATCA, C3363
2023-11-29	1.844	2.07	0.07	0.90	0.06	ATCA, C3363
2023-11-29	2.1	2.05	0.05	1.00	0.04	ATCA, C3363
2023-11-29	2.356	1.98	0.06	1.02	0.04	ATCA, C3363
2023-11-29	2.868	1.73	0.07	1.03	0.05	ATCA, C3363
2023-11-29	5.5	1.13	0.02	0.05	0.02	ATCA, C3363
2023-11-29	9.0	0.74	0.02	0.01	0.01	ATCA, C3363
2024-01-02	0.943	2.91	0.27	0.88	0.23	ASKAP, RACS
2024-01-06	0.943	2.50	0.13	0.75	0.17	ASKAP, RACS
2024-03-10	1.332	1.91	0.12	0.71	0.13	ATCA, C3363
2024-03-10	1.844	1.76	0.07	0.76	0.07	ATCA, C3363
2024-03-10	2.1	1.70	0.04	0.83	0.06	ATCA, C3363
2024-03-10	2.356	1.69	0.06	0.87	0.05	ATCA, C3363
2024-03-10	2.868	1.65	0.08	0.99	0.06	ATCA, C3363
2024-03-10	5.5	0.93	0.03	0.04	0.02	ATCA, C3363
2024-03-10	9.0	0.56	0.02	0.00	0.02	ATCA, C3363
2024-04-05	0.887	2.30	0.15	0.69	0.16	ASKAP, VAST
2024-05-01	0.67	1.38	0.29	0.36	0.16	GMRT, 46_054
2024-05-03	1.27	1.68	0.13	0.62	0.13	GMRT, 46_054
2024-05-05	0.4	0.87	0.05	0.17	0.05	GMRT, 46_054
2024-06-01	0.887	1.94	0.16	0.59	0.19	ASKAP, , VAST
2024-06-22	1.27	1.72	0.10	0.64	0.14	GMRT, 46_054
2024-06-21	0.67	0.96	0.06	0.25	0.13	GMRT, 46_054
2024-06-22	0.4	<1.05	-	-	0.21	GMRT, 46_054
2024-06-24	1.332	1.80	0.33	0.67	0.21	ATCA, C3363
2024-06-24	1.844	1.74	0.14	0.75	0.09	ATCA, C3363
2024-06-24	2.1	1.43	0.06	0.70	0.06	ATCA, C3363
2024-06-24	2.356	1.57	0.07	0.81	0.04	ATCA, C3363
2024-06-24	2.868	1.36	0.07	0.81	0.05	ATCA, C3363
2024-06-24	5.5	0.86	0.02	0.04	0.02	ATCA, C3363
2024-06-24	9.0	0.56	0.02	0.00	0.01	ATCA, C3363
2024-08-02	0.887	2.44	0.15	0.74	0.17	ASKAP, VAST
2024-09-24	1.332	1.66	0.18	0.62	0.14	ATCA, C3363
2024-09-24	1.844	1.70	0.09	0.74	0.06	ATCA, C3363
2024-09-24	2.1	1.61	0.05	0.78	0.06	ATCA, C3363
2024-09-24	2.356	1.55	0.06	0.80	0.04	ATCA, C3363
2024-09-24	2.868	1.27	0.07	0.76	0.05	ATCA, C3363
2024-09-24	5.5	0.81	0.03	0.04	0.02	ATCA, C3363
2024-09-24	9.0	0.54	0.02	0.00	0.01	ATCA, C3363
2024-09-28	0.887	1.81	0.14	0.55	0.17	ASKAP, VAST
2024-09-28	3.0	1.02	0.15	0.61	0.15	VLA, VLASS
2024-12-26	0.4	<3.00	-	-	0.60	GMRT, 46_054
2024-12-26	0.67	1.54	0.17	0.40	0.08	GMRT, 46_054
2024-12-26	1.332	1.75	0.12	0.65	0.10	ATCA, C3363
2024-12-26	1.844	1.69	0.06	0.73	0.05	ATCA, C3363
2024-12-26	2.1	1.42	0.04	0.69	0.06	ATCA, C3363
2024-12-26	2.356	1.30	0.06	0.67	0.04	ATCA, C3363
2024-12-26	2.868	1.08	0.07	0.64	0.05	ATCA, C3363
2024-12-26	5.5	0.74	0.02	0.03	0.01	ATCA, C3363
2024-12-26	9.0	0.42	0.02	0.00	0.01	ATCA, C3363

2025-02-22	0.887	2.01	0.18	0.61	0.18	ASKAP, VAST
2025-03-20	1.332	1.82	0.11	0.67	0.11	ATCA, C3363
2025-03-20	1.844	1.63	0.06	0.70	0.05	ATCA, C3363
2025-03-20	2.1	1.45	0.04	0.71	0.06	ATCA, C3363
2025-03-20	2.356	1.19	0.06	0.61	0.04	ATCA, C3363
2025-03-20	2.868	1.30	0.09	0.78	0.06	ATCA, C3363
2025-03-20	5.5	0.61	0.03	0.03	0.02	ATCA, C3363
2025-03-20	9.0	0.31	0.02	0.00	0.02	ATCA, C3363
2025-04-21	0.887	1.84	0.17	0.56	0.18	ASKAP, VAST

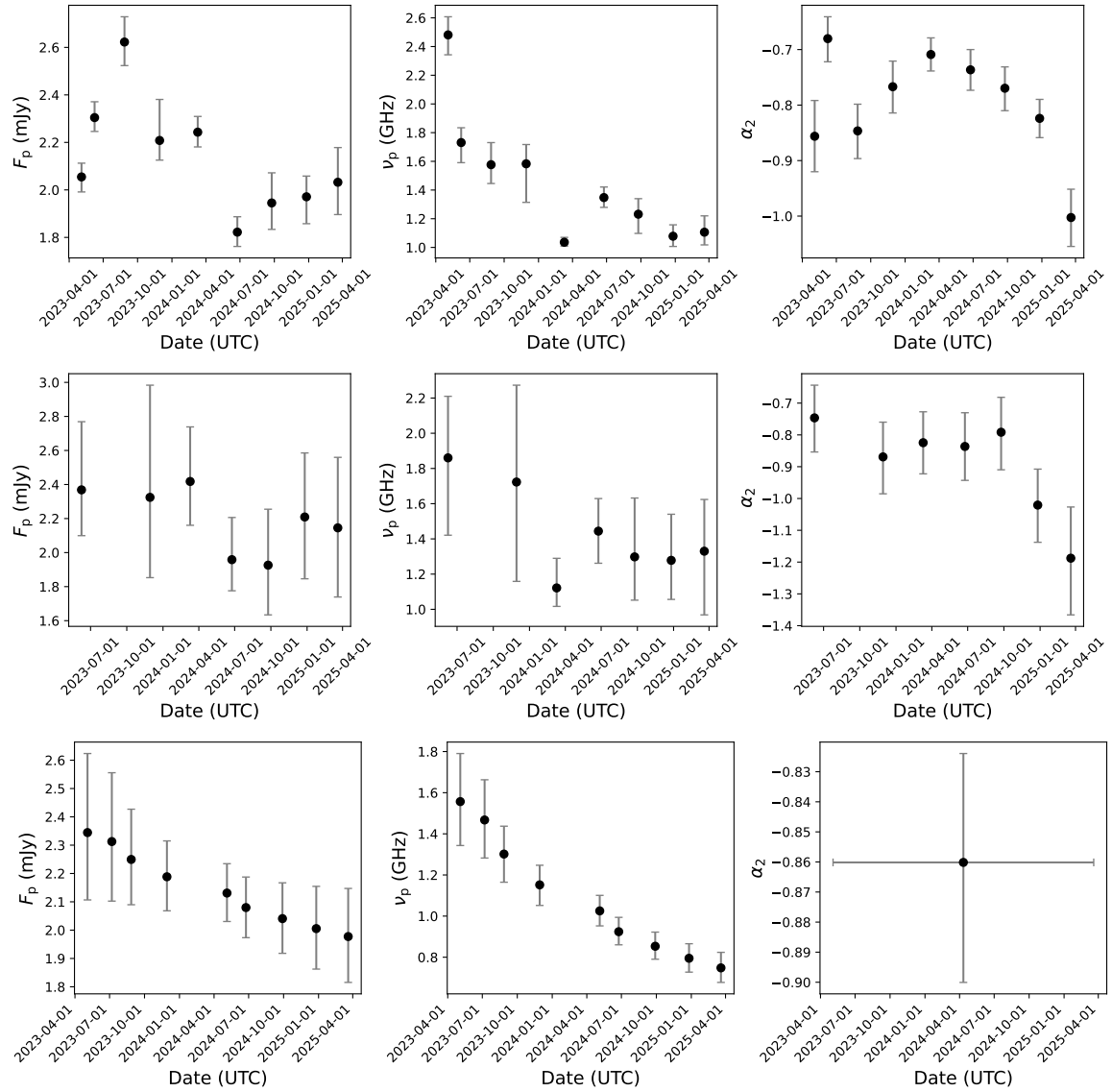


Figure 10. Temporal evolution of the SBPL spectral fit parameters for ASKAP J0055–2558 across nine radio epochs. The top panel shows the results of the initial fits without including interstellar scintillation (ISS) and without a joint fit. The middle panel shows the results with ISS included and with individual epoch SBPL fits applied. The bottom panel shows the results with ISS included and with a joint fit applied. For the joint fit, the peak flux and frequency were derived for each epoch from the global fit. In each panel, the parameters are displayed as a function of observation date: peak flux density (F_p , right), peak frequency (ν_p , middle), and optically thin spectral index (α_2 , left). Error bars represent 1σ uncertainties from the MCMC fitting.

Table 4. Best-Fit SBPL Parameters for ASKAP J0055–2558 Radio Spectra

Observation Date (UTC)	F_p (mJy)	ν_p (GHz)	α_2	p
2023-05-04	$2.34^{+0.28}_{-0.24}$	$1.56^{+0.23}_{-0.21}$		
2023-07-07	$2.31^{+0.24}_{-0.21}$	$1.47^{+0.20}_{-0.19}$		
2023-08-27	$2.25^{+0.18}_{-0.16}$	$1.30^{+0.14}_{-0.14}$		
2023-11-29	$2.19^{+0.13}_{-0.12}$	$1.15^{+0.10}_{-0.10}$		
2024-05-05	$2.13^{+0.10}_{-0.10}$	$1.03^{+0.08}_{-0.07}$	$-0.86^{+0.04}_{-0.04}$	$2.72^{+0.07}_{-0.04}$
2024-06-24	$2.08^{+0.11}_{-0.11}$	$0.92^{+0.07}_{-0.06}$		
2024-09-28	$2.04^{+0.13}_{-0.12}$	$0.85^{+0.07}_{-0.06}$		
2024-12-26	$2.01^{+0.15}_{-0.14}$	$0.79^{+0.07}_{-0.07}$		
2025-03-20	$1.98^{+0.17}_{-0.16}$	$0.75^{+0.08}_{-0.07}$		

NOTE—Best-fit parameters from the joint fit smoothly broken power-law (SBPL) model applied to the radio spectra of ASKAP J0055–2558 across nine epochs simultaneously. Listed parameters are the derived peak flux density (F_p), peak frequency (ν_p), high-frequency spectral index (α_2), and electron power-law index (p). The joint fit yields $\chi^2_{\text{red}} = 0.89$ with ~ 74 degrees of freedom. Uncertainties are 1σ credible intervals from MCMC fitting.

B. EXTENDED MULTIWAVELENGTH ANALYSIS

B.1. GRB Chance-coincidence estimation

To test whether spatially coincident GRBs could be genuine counterparts, we estimated chance-alignment probabilities via Monte Carlo simulations. Using the first radio detection (2022 February 4 UTC) as the reference date, we considered GRBs within time windows of Y years prior and generated $N = 300 \times Y$ synthetic bursts uniformly distributed over the sky to match the observed GRB rate. Repeating this 500 times per window, we calculated the mean hit fraction f_{hit} (probability of chance coincidence). For $Y = 5$ yr (2 GRBs) $f_{\text{hit}} \approx 1.1\%$, for $Y = 10$ yr (3 GRBs) $\approx 2.5\%$, for $Y = 20$ yr (12 GRBs) $\approx 23.8\%$, and for $Y = 30$ yr (54 GRBs) $\approx 55.5\%$. Thus, chance-coincidence probabilities are low for $\lesssim 10$ yr windows but become substantial over ~ 30 yr.

B.2. Host Galaxy Chance Coincidence Estimation

To estimate the chance alignment of the galaxy offset from ASKAP J0055–2558 we used the method described in Bloom et al. (2002) and the code from `astropath` (Aggarwal et al. 2021). For each galaxy of apparent magnitude r_{mag} , the number density of field galaxies on the sky, n_{den} , is estimated from the empirical relation of Bloom et al. (2002) available in `astropath`. The effective search radius is conservatively defined as

$$\theta_{\text{eff}} = \sqrt{4\sigma_R^2 + 4r_{1/2}^2 + \text{sep}^2}, \quad (\text{B1})$$

where σ_R is the 1σ localisation error of the transient, $r_{1/2}$ is the galaxy half-light radius, and sep is the measured angular offset between the transient and the galaxy centre. The expected number of unrelated galaxies within the search area is $\bar{N} = \pi \theta_{\text{eff}}^2 n_{\text{den}}$ and the corresponding probability of a chance alignment is

$$P_{\text{chance}} = 1 - e^{-\bar{N}}. \quad (\text{B2})$$

All these calculations are directly run within `astropath`, which assumes galaxies follow a Poisson distribution on the sky. The returned values are P_{chance} , representing the probability that a galaxy of magnitude $\leq r_{\text{mag}}$ would fall within

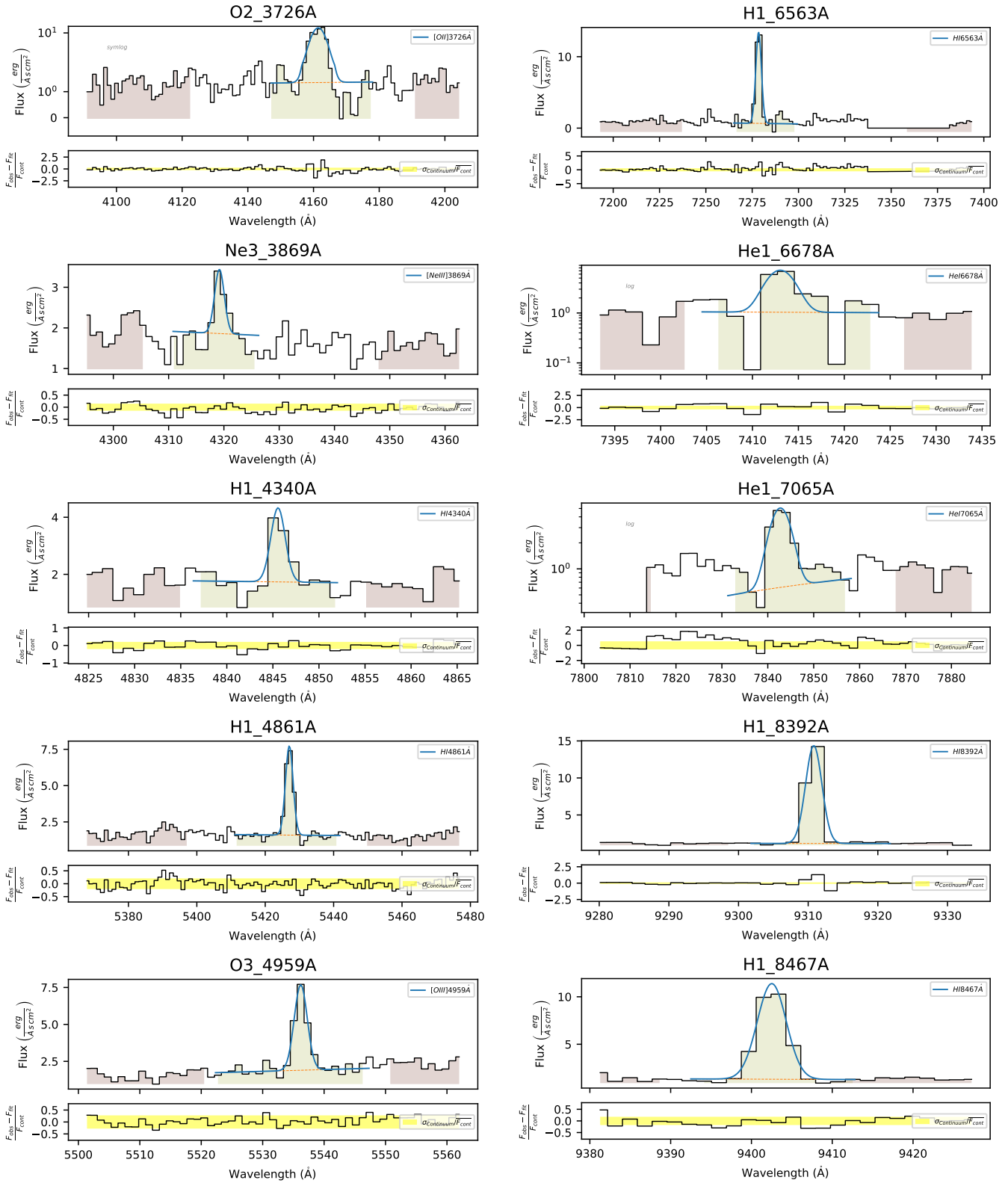


Figure 11. Spectral fitting results obtained using the LIME package for the galaxy core, showing the best-fit model (blue solid line) overlaid on the observed spectrum. The continuum (bottom panels) and emission-line (top panels) components are indicated separately.

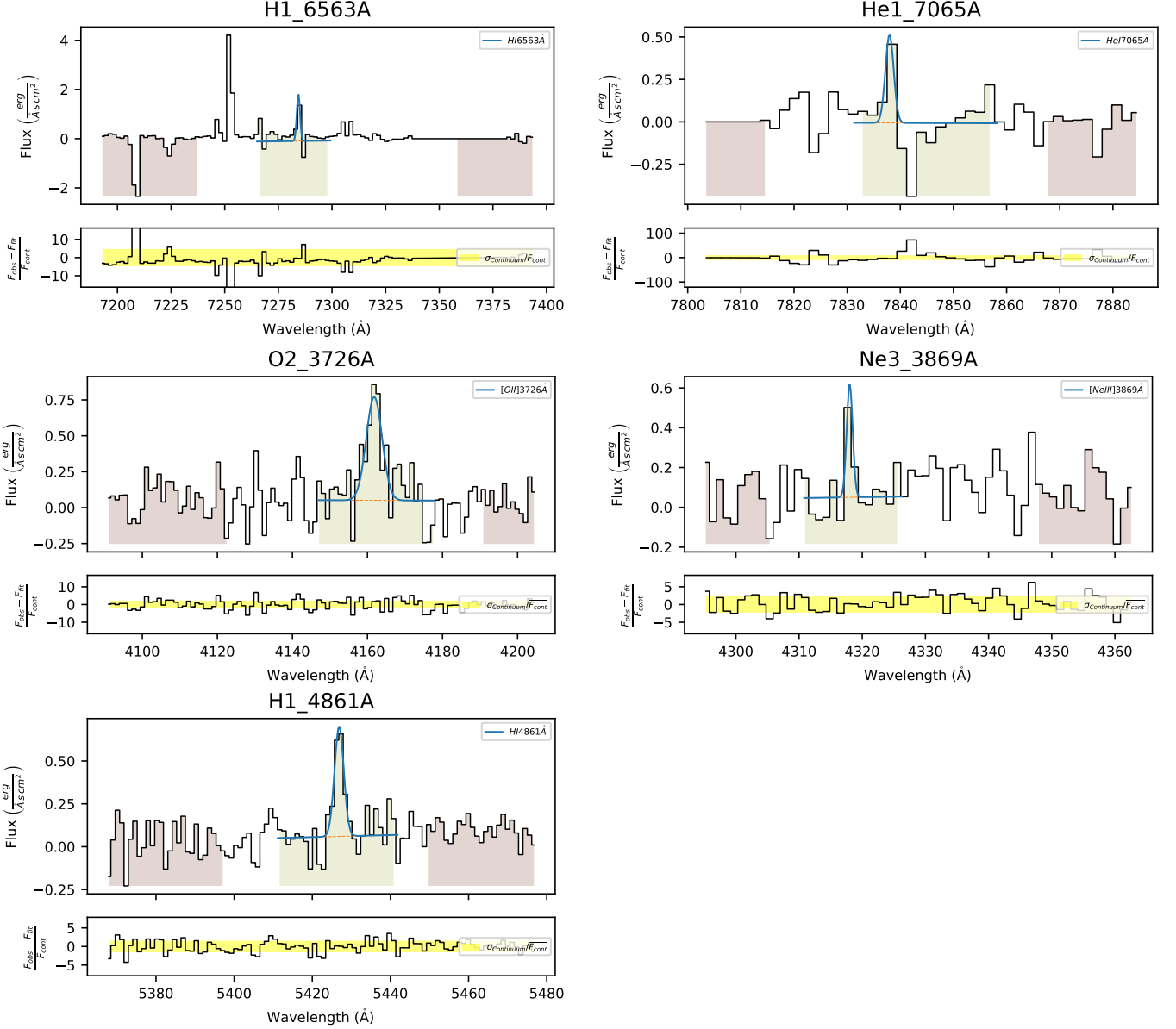


Figure 12. Spectral fitting results obtained using the LIME package at the transient position, showing the best-fit model (blue solid line) overlaid on the observed spectrum. The continuum (bottom panels) and emission-line (top panels) components are indicated separately.

the observed offset by chance. This probability of chance coincidence for our transient in relation to the potential host galaxy has been quoted in Section 5.

B.3. Host Galaxy Physical Parameters Calculations

The host galaxy is clearly detected in the DESI Legacy Imaging Surveys in the g , r , and i optical bands and in the near-infrared J band from Keck imaging. We therefore derived its stellar population properties by fitting stellar population synthesis (SPS) templates to the available broadband photometry. The fitting was performed with the **Bagpipes** code (Carnall et al. 2018), which models galaxy spectral energy distributions (SEDs) using parametric star-formation histories and a Bayesian framework. The input photometry included GALEX FUV and NUV fluxes together with the DESI g , r , i , z and Keck J measurements. From the resulting posterior distributions, we extracted the galaxy’s stellar mass, star-formation rate, and metallicity parameters quoted in Section 5.

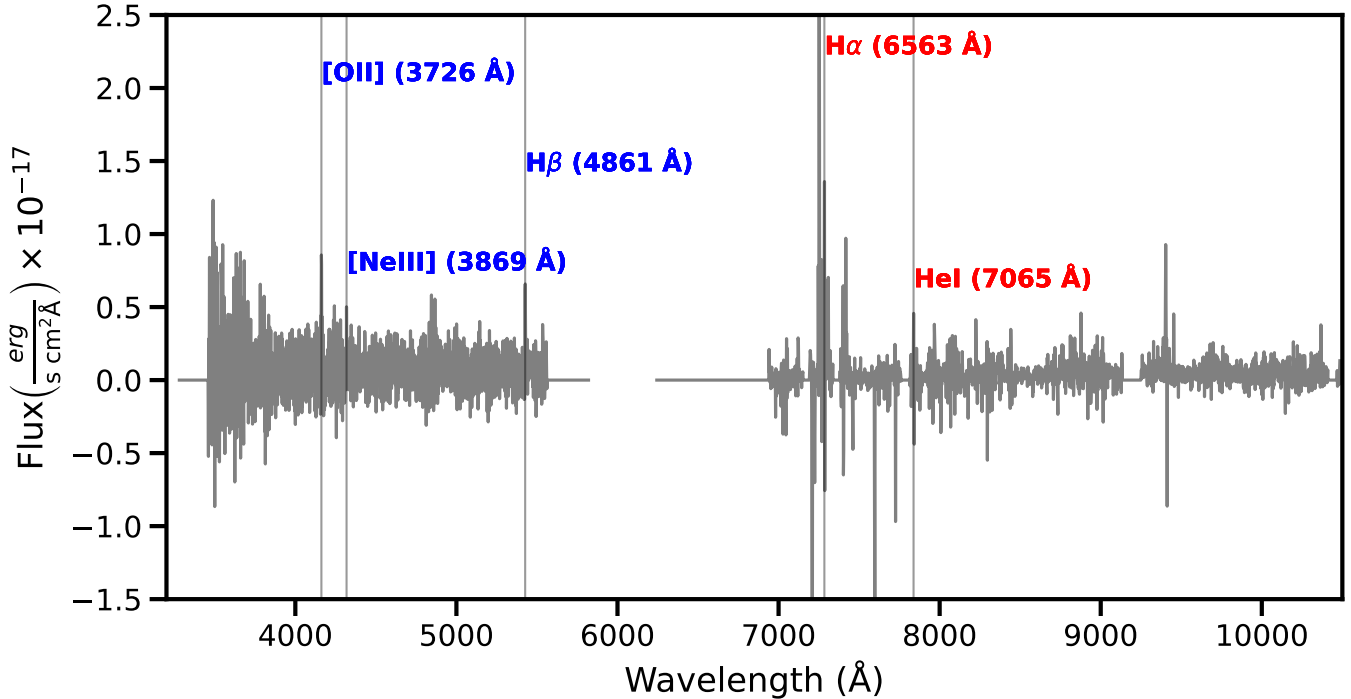


Figure 13. Spectra obtained with Keck KCWI and KCRM at the transient position, with emission lines fitted using the LIME package. The signal-to-noise ratio, as defined by [Rola & Pelat \(1994\)](#) for each of the fitted lines, is above 5σ . The fitting results are given in the [Appendix B Fig. 12](#).

From the observed Balmer decrement ($H\alpha/H\beta = 4.00$ vs. the intrinsic 2.86; [Osterbrock 1989](#)), we derive color excesses of $E(B - V) = 0.27$ (Calzetti law; [Calzetti et al. 2000](#)) corresponding to $A_V \approx 1.1$ mag. Line fluxes are then corrected for dust attenuation using the wavelength-dependent reddening law ([Calzetti et al. 1994](#); [Calzetti 1997](#)). The $[O\text{III}]/[O\text{II}]$ ratio is a widely used probe of ionization conditions, where the total $[O\text{III}]$ flux is inferred from the 4959 Å line assuming the theoretical 5007/4959 ratio of 2.98 ([Dimitrijević et al. 2007](#)). The $[O\text{II}] \lambda 3727$ doublet traces singly ionised oxygen (O^+), arising in lower-ionisation zones, and thus provides a complementary measure to the higher-ionisation $[O\text{III}]$ lines. For the main galaxy, dust-corrected fluxes give $[O\text{III}]/[O\text{II}]$ ratios of 0.92 (Calzetti law consistent with a moderately ionised interstellar medium).

Table 5. Gaussian Fit Parameters for Emission Lines.

Line	Rest Wavelength (Å)	Center (Å)	Amplitude (10^{-17} erg s $^{-1}$ cm $^{-2}$ Å $^{-1}$)	Gaussian Width (Å)	Integrated Flux (10^{-17} erg s $^{-1}$ cm $^{-2}$)	Reduced χ^2	DOF
Galaxy Nucleus							
H α (6563 Å)	6563.0	7278.46 \pm 0.08	12.75 \pm 0.63	1.51 \pm 0.09	59.51 \pm 2.98	2.60	63
He I (6678 Å)	6678.0	7413.02 \pm 0.17	6.16 \pm 0.71	1.37 \pm 0.19	23.77 \pm 2.30	2.63	21
He I (7065 Å)	7065.0	7842.75 \pm 0.15	4.46 \pm 0.29	2.01 \pm 0.15	25.44 \pm 2.23	1.08	31
H I (8392 Å)	8392.0	9310.72 \pm 0.46	13.23 \pm 0.59	1.17 \pm 0.07	40.46 \pm 0.84	9.96	28
H I (8467 Å)	8467.0	9402.52 \pm 0.05	10.08 \pm 0.24	1.79 \pm 0.05	41.90 \pm 1.48	1.21	23
O II (3726 Å)	3726.0	4161.44 \pm 0.10	11.49 \pm 0.49	2.11 \pm 0.10	52.64 \pm 2.20	4.31	70
Ne III (3869 Å)	3869.0	4319.19 \pm 0.21	1.58 \pm 0.35	0.88 \pm 0.23	-0.16 \pm 1.20	1.35	38
H γ (4340 Å)	4340.0	4845.56 \pm 0.14	2.60 \pm 0.52	0.78 \pm 0.20	3.23 \pm 1.51	1.15	34
H β (4861 Å)	4861.0	5427.03 \pm 0.06	6.14 \pm 0.28	1.12 \pm 0.06	14.90 \pm 1.92	0.87	79
O III (4959 Å)	4959.0	5536.20 \pm 0.09	5.79 \pm 0.44	1.06 \pm 0.09	17.20 \pm 2.67	0.78	51
Transient Position							
H α (6563 Å)	6563.0	7284.34 \pm 2.36	1.90 \pm 8.43	0.75 \pm 2.55	8.34 \pm 3.57	0.91	63
He I (7065 Å)	7065.0	7837.97 \pm 1.38	0.52 \pm 0.81	0.78 \pm 1.14	0.59 \pm 0.42	3.37	31
O II (3726 Å)	3726.0	4161.79 \pm 0.31	0.72 \pm 0.09	2.11 \pm 0.31	4.25 \pm 0.68	1.53	70
Ne III (3869 Å)	3869.0	4318.01 \pm 0.89	0.57 \pm 1.33	0.47 \pm 0.93	0.56 \pm 0.47	0.87	38
H β (4861 Å)	4861.0	5426.88 \pm 0.19	0.64 \pm 0.09	1.19 \pm 0.19	1.92 \pm 0.55	1.07	79

NOTE—Best-fit parameters for prominent emission lines in the optical spectrum of the host galaxy, derived using LIME. For each line, the table lists the rest-frame wavelength in vacuum, fitted line centre, amplitude, Gaussian width (σ), integrated line flux, and reduced χ^2 of the fit. Uncertainties represent 1σ errors from the fitting procedure. All fluxes are reported in units of 10^{-17} erg s $^{-1}$ cm $^{-2}$ Å $^{-1}$. These fits are used to determine line diagnostics and redshift.

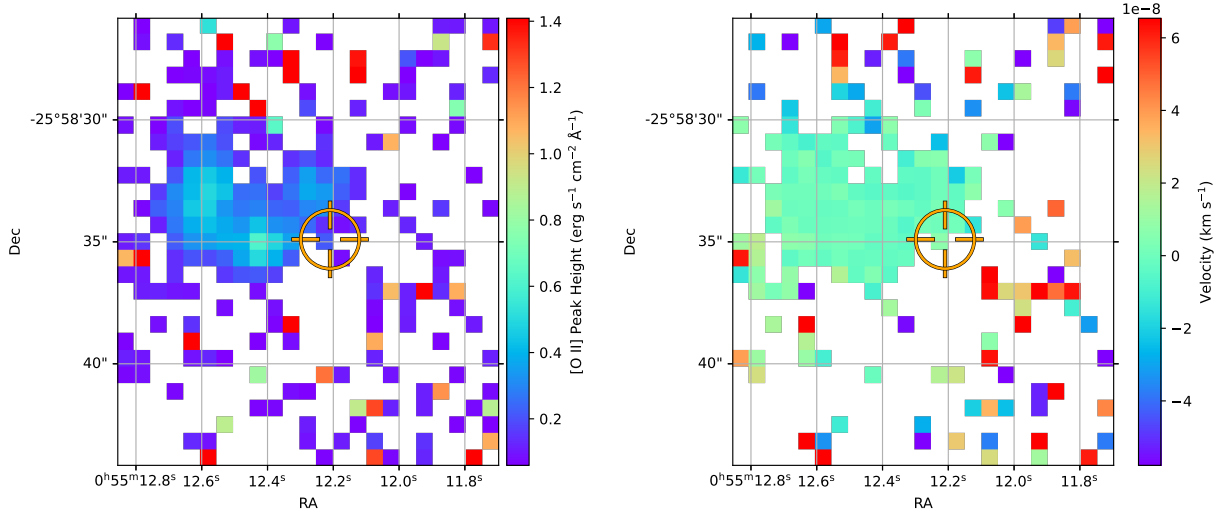


Figure 14. Velocity map of the ionized gas traced by the O II [3726] emission line. The plot on the left indicates the line intensity (height of the fitted emission line), while the plot on the right shows the relative line-of-sight velocity. Only spaxels with reliable O II detections are displayed. QFitsView and DPUserFunction (<https://github.com/MarkDurre/DPUserFunctions.git>) were used for making the map. The aggregate source position of the transient with uncertainty derived from ATCA and GMRT observations is also overlaid.

Table 6. The extracted parameters from the equipartition analysis. All errors are 1σ .

Geometry	Epoch	R (10^{17} cm)	E (10^{50} erg)	β	B (G)	n_o (10^{-4} cm^{-3})
Spherical	2023-05-04	$4.68^{+0.33}_{-0.41}$	$2.63^{+0.45}_{-0.36}$	$0.288^{+0.015}_{-0.017}$	$0.152^{+0.031}_{-0.026}$	$475.62^{+75.36}_{-72.11}$
	2023-07-07	$4.93^{+0.30}_{-0.39}$	$2.75^{+0.47}_{-0.37}$	$0.272^{+0.012}_{-0.015}$	$0.143^{+0.027}_{-0.024}$	$424.35^{+54.76}_{-56.29}$
	2023-08-27	$5.49^{+0.26}_{-0.35}$	$3.00^{+0.50}_{-0.40}$	$0.275^{+0.010}_{-0.013}$	$0.127^{+0.020}_{-0.019}$	$336.77^{+26.94}_{-32.55}$
	2023-11-29	$6.12^{+0.23}_{-0.31}$	$3.28^{+0.53}_{-0.43}$	$0.266^{+0.008}_{-0.010}$	$0.113^{+0.016}_{-0.015}$	$265.98^{+11.99}_{-17.09}$
	2024-05-05	$6.79^{+0.23}_{-0.26}$	$3.57^{+0.57}_{-0.49}$	$0.246^{+0.006}_{-0.007}$	$0.101^{+0.013}_{-0.012}$	$212.50^{+6.44}_{-7.29}$
	2024-06-24	$7.45^{+0.26}_{-0.25}$	$3.84^{+0.62}_{-0.56}$	$0.252^{+0.007}_{-0.006}$	$0.091^{+0.012}_{-0.010}$	$173.96^{+5.71}_{-5.03}$
	2024-09-28	$7.99^{+0.28}_{-0.27}$	$4.07^{+0.69}_{-0.61}$	$0.245^{+0.006}_{-0.006}$	$0.084^{+0.011}_{-0.010}$	$149.20^{+5.94}_{-5.37}$
	2024-12-26	$8.51^{+0.31}_{-0.35}$	$4.28^{+0.76}_{-0.65}$	$0.241^{+0.007}_{-0.007}$	$0.079^{+0.011}_{-0.010}$	$130.18^{+6.76}_{-7.19}$
	2025-03-20	$8.98^{+0.38}_{-0.41}$	$4.47^{+0.80}_{-0.69}$	$0.237^{+0.008}_{-0.008}$	$0.074^{+0.011}_{-0.010}$	$115.83^{+8.32}_{-8.31}$
Conical (5°)	2023-05-04	$84.58^{+5.73}_{-7.07}$	$13.98^{+2.76}_{-2.16}$	$0.880^{+0.008}_{-0.008}$	$0.062^{+0.013}_{-0.011}$	$36.52^{+5.20}_{-5.09}$
	2023-07-07	$89.16^{+5.29}_{-6.75}$	$14.59^{+2.87}_{-2.24}$	$0.871^{+0.007}_{-0.008}$	$0.058^{+0.011}_{-0.010}$	$32.59^{+3.70}_{-3.92}$
	2023-08-27	$99.21^{+4.52}_{-6.08}$	$15.91^{+3.07}_{-2.42}$	$0.873^{+0.005}_{-0.006}$	$0.052^{+0.009}_{-0.008}$	$25.86^{+1.68}_{-2.16}$
	2023-11-29	$110.66^{+3.95}_{-5.36}$	$17.40^{+3.27}_{-2.63}$	$0.868^{+0.004}_{-0.005}$	$0.046^{+0.007}_{-0.006}$	$20.43^{+0.63}_{-1.04}$
	2024-05-05	$122.76^{+3.87}_{-4.27}$	$18.93^{+3.51}_{-2.98}$	$0.855^{+0.004}_{-0.004}$	$0.041^{+0.006}_{-0.005}$	$16.32^{+0.26}_{-0.33}$
	2024-06-24	$134.63^{+4.28}_{-4.10}$	$20.39^{+3.83}_{-3.33}$	$0.859^{+0.004}_{-0.004}$	$0.037^{+0.005}_{-0.005}$	$13.36^{+0.25}_{-0.20}$
	2024-09-28	$144.50^{+4.63}_{-4.50}$	$21.59^{+4.23}_{-3.64}$	$0.855^{+0.004}_{-0.004}$	$0.034^{+0.005}_{-0.004}$	$11.46^{+0.29}_{-0.25}$
	2024-12-26	$153.85^{+5.25}_{-5.79}$	$22.70^{+4.62}_{-3.87}$	$0.852^{+0.004}_{-0.005}$	$0.032^{+0.005}_{-0.004}$	$10.00^{+0.37}_{-0.42}$
	2025-03-20	$162.37^{+6.47}_{-6.98}$	$23.71^{+4.87}_{-4.11}$	$0.849^{+0.005}_{-0.005}$	$0.030^{+0.005}_{-0.004}$	$8.89^{+0.51}_{-0.52}$
Conical (15°)	2023-05-04	$29.92^{+2.04}_{-2.52}$	$8.98^{+1.71}_{-1.34}$	$0.722^{+0.014}_{-0.016}$	$0.078^{+0.016}_{-0.014}$	$72.21^{+10.58}_{-10.29}$
	2023-07-07	$31.54^{+1.89}_{-2.40}$	$9.37^{+1.78}_{-1.39}$	$0.705^{+0.013}_{-0.015}$	$0.074^{+0.014}_{-0.013}$	$64.43^{+7.56}_{-7.95}$
	2023-08-27	$35.10^{+1.62}_{-2.17}$	$10.22^{+1.90}_{-1.50}$	$0.708^{+0.010}_{-0.012}$	$0.066^{+0.011}_{-0.010}$	$51.13^{+3.52}_{-4.45}$
	2023-11-29	$39.15^{+1.42}_{-1.92}$	$11.17^{+2.03}_{-1.64}$	$0.699^{+0.008}_{-0.010}$	$0.058^{+0.008}_{-0.008}$	$40.38^{+1.39}_{-2.19}$
	2024-05-05	$43.43^{+1.39}_{-1.53}$	$12.15^{+2.17}_{-1.85}$	$0.676^{+0.007}_{-0.008}$	$0.052^{+0.007}_{-0.006}$	$32.26^{+0.64}_{-0.77}$
	2024-06-24	$47.63^{+1.54}_{-1.48}$	$13.09^{+2.37}_{-2.08}$	$0.683^{+0.007}_{-0.007}$	$0.047^{+0.006}_{-0.006}$	$26.41^{+0.59}_{-0.49}$
	2024-09-28	$51.12^{+1.66}_{-1.62}$	$13.86^{+2.62}_{-2.27}$	$0.675^{+0.007}_{-0.007}$	$0.044^{+0.006}_{-0.005}$	$22.65^{+0.66}_{-0.58}$
	2024-12-26	$54.43^{+1.88}_{-2.08}$	$14.57^{+2.86}_{-2.42}$	$0.670^{+0.008}_{-0.008}$	$0.041^{+0.006}_{-0.005}$	$19.76^{+0.81}_{-0.89}$
	2025-03-20	$57.45^{+2.32}_{-2.50}$	$15.22^{+3.02}_{-2.56}$	$0.665^{+0.009}_{-0.009}$	$0.038^{+0.006}_{-0.005}$	$17.59^{+1.07}_{-1.09}$
Conical (30°)	2023-05-04	$18.22^{+1.23}_{-1.52}$	$30.71^{+6.41}_{-5.00}$	$0.612^{+0.017}_{-0.019}$	$0.040^{+0.009}_{-0.007}$	$10.90^{+1.48}_{-1.46}$
	2023-07-07	$19.21^{+1.14}_{-1.45}$	$32.05^{+6.68}_{-5.19}$	$0.593^{+0.015}_{-0.017}$	$0.038^{+0.008}_{-0.007}$	$9.72^{+1.04}_{-1.12}$
	2023-08-27	$21.37^{+0.97}_{-1.31}$	$34.95^{+7.15}_{-5.59}$	$0.596^{+0.011}_{-0.014}$	$0.034^{+0.006}_{-0.005}$	$7.71^{+0.45}_{-0.60}$
	2023-11-29	$23.84^{+0.85}_{-1.15}$	$38.21^{+7.63}_{-6.10}$	$0.586^{+0.009}_{-0.011}$	$0.030^{+0.005}_{-0.004}$	$6.09^{+0.15}_{-0.28}$
	2024-05-05	$26.44^{+0.83}_{-0.92}$	$41.57^{+8.19}_{-6.89}$	$0.559^{+0.008}_{-0.008}$	$0.027^{+0.004}_{-0.003}$	$4.87^{+0.05}_{-0.07}$
	2024-06-24	$29.00^{+0.92}_{-0.88}$	$44.79^{+8.93}_{-7.69}$	$0.567^{+0.008}_{-0.007}$	$0.024^{+0.003}_{-0.003}$	$3.99^{+0.05}_{-0.04}$
	2024-09-28	$31.13^{+0.99}_{-0.97}$	$47.41^{+9.83}_{-8.38}$	$0.559^{+0.008}_{-0.008}$	$0.023^{+0.003}_{-0.003}$	$3.42^{+0.07}_{-0.06}$
	2024-12-26	$33.14^{+1.12}_{-1.24}$	$49.84^{+10.72}_{-8.91}$	$0.553^{+0.009}_{-0.009}$	$0.021^{+0.003}_{-0.003}$	$2.98^{+0.09}_{-0.11}$
	2025-03-20	$34.98^{+1.39}_{-1.50}$	$52.07^{+11.31}_{-9.44}$	$0.547^{+0.010}_{-0.010}$	$0.020^{+0.003}_{-0.003}$	$2.65^{+0.13}_{-0.14}$

REFERENCES

- Agarwal, D., Aggarwal, K., Burke-Spolaor, S., Lorimer, D. R., & Garver-Daniels, N. 2020, *Monthly Notices of the Royal Astronomical Society*, 497, 1661, doi: [10.1093/mnras/staa1856](https://doi.org/10.1093/mnras/staa1856)
- Aggarwal, K., Budavári, T., Deller, A. T., et al. 2021, *ApJ*, 911, 95, doi: [10.3847/1538-4357/abe8d2](https://doi.org/10.3847/1538-4357/abe8d2)
- Ahn, C. P., Seth, A. C., Cappellari, M., et al. 2018, *ApJ*, 858, 102, doi: [10.3847/1538-4357/aabc57](https://doi.org/10.3847/1538-4357/aabc57)
- Alexander, K. D., Berger, E., Guillochon, J., Zauderer, B. A., & Williams, P. K. G. 2016, *The Astrophysical Journal*, 819, L25, doi: [10.3847/2041-8205/819/2/L25](https://doi.org/10.3847/2041-8205/819/2/L25)
- Alexander, K. D., Berger, E., Guillochon, J., Zauderer, B. A., & Williams, P. K. G. 2016, *ApJL*, 819, L25, doi: [10.3847/2041-8205/819/2/L25](https://doi.org/10.3847/2041-8205/819/2/L25)
- Alexander, K. D., van Velzen, S., Horesh, A., & Zauderer, B. A. 2020, *SSRv*, 216, 81, doi: [10.1007/s11214-020-00702-w](https://doi.org/10.1007/s11214-020-00702-w)
- Alexander, K. D., Wieringa, M. H., Berger, E., Saxton, R. D., & Komossa, S. 2017, *The Astrophysical Journal*, 837, 153, doi: [10.3847/1538-4357/aa6192](https://doi.org/10.3847/1538-4357/aa6192)
- Alexander, K. D., Wieringa, M. H., Berger, E., Saxton, R. D., & Komossa, S. 2017, *ApJ*, 837, 153, doi: [10.3847/1538-4357/aa6192](https://doi.org/10.3847/1538-4357/aa6192)
- Anderson, G. E., Leung, J. K., Murphy, T., et al. 2023, *GRB Coordinates Network*, 33475, 1
- Anderson, G. E., Miller-Jones, J. C. A., Middleton, M. J., et al. 2019, *MNRAS*, 489, 1181, doi: [10.1093/mnras/stz1303](https://doi.org/10.1093/mnras/stz1303)
- Anderson, G. E., Schroeder, G., van der Horst, A. J., et al. 2024, *ApJL*, 975, L13, doi: [10.3847/2041-8213/ad85e9](https://doi.org/10.3847/2041-8213/ad85e9)
- Anderson, G. E., Lamb, G. P., Gompertz, B. P., et al. 2025, *ApJ*, 994, 5, doi: [10.3847/1538-4357/adfed7](https://doi.org/10.3847/1538-4357/adfed7)
- Andreoni, I., Coughlin, M. W., Perley, D. A., et al. 2022, *Nature*, 612, 430, doi: [10.1038/s41586-022-05465-8](https://doi.org/10.1038/s41586-022-05465-8)
- Angus, C. R., Baldassare, V. F., Mockler, B., et al. 2022, *Nature Astronomy*, 6, 1452, doi: [10.1038/s41550-022-01811-y](https://doi.org/10.1038/s41550-022-01811-y)
- Bailes, M., Jameson, A., Abbate, F., et al. 2020, *PASA*, 37, e028, doi: [10.1017/pasa.2020.19](https://doi.org/10.1017/pasa.2020.19)
- Balasubramanian, A., Corsi, A., Mooley, K. P., et al. 2022, *ApJ*, 938, 12, doi: [10.3847/1538-4357/ac9133](https://doi.org/10.3847/1538-4357/ac9133)
- Baldwin, J. A., Phillips, M. M., & Terlevich, R. 1981, *PASP*, 93, 5, doi: [10.1086/130766](https://doi.org/10.1086/130766)
- Bannister, K. W., Murphy, T., Gaensler, B. M., Hunstead, R. W., & Chatterjee, S. 2011, *MNRAS*, 418, 2813, doi: [10.1111/j.1365-2966.2011.19739.x](https://doi.org/10.1111/j.1365-2966.2011.19739.x)
- Bannister, K. W., Murphy, T., Gaensler, B. M., Hunstead, R. W., & Chatterjee, S. 2011, *Monthly Notices of the Royal Astronomical Society*, 412, 634, doi: [10.1111/j.1365-2966.2010.17938.x](https://doi.org/10.1111/j.1365-2966.2010.17938.x)
- Bannister, K. W., Stevens, J., Tuntsov, A. V., et al. 2016, *Science*, 351, 354, doi: [10.1126/science.aac7673](https://doi.org/10.1126/science.aac7673)
- Barniol Duran, R., Nakar, E., & Piran, T. 2013, *ApJ*, 772, 78, doi: [10.1088/0004-637X/772/1/78](https://doi.org/10.1088/0004-637X/772/1/78)
- Barniol Duran, R., Nakar, E., Piran, T., & Sari, R. 2015, *MNRAS*, 448, 417, doi: [10.1093/mnras/stv011](https://doi.org/10.1093/mnras/stv011)
- Barsdell, B. R. 2012, PhD thesis, Swinburne University of Technology, Australia
- Bell, M. E., Fender, R. P., Swinbank, J., et al. 2011, *MNRAS*, 415, 2, doi: [10.1111/j.1365-2966.2011.18631.x](https://doi.org/10.1111/j.1365-2966.2011.18631.x)
- Bellm, E. C., Kulkarni, S. R., Graham, M. J., et al. 2019, *PASP*, 131, 018002, doi: [10.1088/1538-3873/aaecbe](https://doi.org/10.1088/1538-3873/aaecbe)
- Berger, E., Kulkarni, S. R., & Chevalier, R. A. 2002, *ApJL*, 577, L5, doi: [10.1086/344045](https://doi.org/10.1086/344045)
- Berger, E., Kulkarni, S. R., & Frail, D. A. 2001a, *The Astrophysical Journal*, 560, 652, doi: [10.1086/322247](https://doi.org/10.1086/322247)
- Berger, E., Soderberg, A. M., Frail, D. A., & Kulkarni, S. R. 2003, *The Astrophysical Journal*, 587, L5, doi: [10.1086/375158](https://doi.org/10.1086/375158)
- Berger, E., Sari, R., Frail, D. A., et al. 2000, *The Astrophysical Journal*, 545, 56, doi: [10.1086/317814](https://doi.org/10.1086/317814)
- Berger, E., Sari, R., Frail, D. A., et al. 2000, *ApJ*, 545, 56, doi: [10.1086/317814](https://doi.org/10.1086/317814)
- Berger, E., Diercks, A., Frail, D. A., et al. 2001b, *The Astrophysical Journal*, 556, 556, doi: [10.1086/321612](https://doi.org/10.1086/321612)
- Berger, E., Kulkarni, S. R., Pooley, G., et al. 2003, *Nature*, 426, 154, doi: [10.1038/nature01998](https://doi.org/10.1038/nature01998)
- Berger, E., Price, P. A., Cenko, S. B., et al. 2005, *Nature*, 438, 988, doi: [10.1038/nature04238](https://doi.org/10.1038/nature04238)
- Berghea, C. T., Johnson, M. C., Secretst, N. J., et al. 2020, *ApJ*, 896, 117, doi: [10.3847/1538-4357/ab9108](https://doi.org/10.3847/1538-4357/ab9108)
- Bertin, E., & Arnouts, S. 1996, *A&AS*, 117, 393, doi: [10.1051/aas:1996164](https://doi.org/10.1051/aas:1996164)
- Bertin, E., Delorme, P., & Bouy, H. 2012, in *Astrophysics and Space Science Proceedings*, Vol. 29, *Star Clusters in the Era of Large Surveys*, ed. A. Moitinho & J. Alves, 71, doi: [10.1007/978-3-642-22113-2_9](https://doi.org/10.1007/978-3-642-22113-2_9)
- Bertin, E., Mellier, Y., Radovich, M., et al. 2002, in *Astronomical Society of the Pacific Conference Series*, Vol. 281, *Astronomical Data Analysis Software and Systems XI*, ed. D. A. Bohlender, D. Durand, & T. H. Handley, 228
- Bhandari, S., Sadler, E. M., Prochaska, J. X., et al. 2020, *ApJL*, 895, L37, doi: [10.3847/2041-8213/ab672e](https://doi.org/10.3847/2041-8213/ab672e)

- Bietenholz, M. F., Bartel, N., Argo, M., et al. 2021, *ApJ*, 908, 75, doi: [10.3847/1538-4357/abccd9](https://doi.org/10.3847/1538-4357/abccd9)
- Bietenholz, M. F., Bartel, N., Argo, M., et al. 2021, *The Astrophysical Journal*, 908, 75, doi: [10.3847/1538-4357/abccd9](https://doi.org/10.3847/1538-4357/abccd9)
- Birmingham, S., & Ward, C. 2025, in *American Astronomical Society Meeting Abstracts*, Vol. 246, American Astronomical Society Meeting Abstracts, 142.16
- Bloom, J. S., Kulkarni, S. R., & Djorgovski, S. G. 2002, *AJ*, 123, 1111, doi: [10.1086/338893](https://doi.org/10.1086/338893)
- Bright, J. S., Margutti, R., Matthews, D., et al. 2022, *The Astrophysical Journal*, 926, 112, doi: [10.3847/1538-4357/ac4506](https://doi.org/10.3847/1538-4357/ac4506)
- Brown, G. C., Levan, A. J., Stanway, E. R., et al. 2017, *Monthly Notices of the Royal Astronomical Society*, 472, 4469, doi: [10.1093/mnras/stx2193](https://doi.org/10.1093/mnras/stx2193)
- Burn, M., Goodwin, A. J., Anderson, G. E., et al. 2025, *ApJ*, 993, 207, doi: [10.3847/1538-4357/ae0a16](https://doi.org/10.3847/1538-4357/ae0a16)
- Burrows, D. N., Hill, J. E., Nousek, J. A., et al. 2005, *SSRv*, 120, 165, doi: [10.1007/s11214-005-5097-2](https://doi.org/10.1007/s11214-005-5097-2)
- Calzetti, D. 1997, in *American Institute of Physics Conference Series*, Vol. 408, *The ultraviolet universe at low and High redshift*, ed. W. H. Waller (AIP), 403–412, doi: [10.1063/1.53764](https://doi.org/10.1063/1.53764)
- Calzetti, D., Armus, L., Bohlin, R. C., et al. 2000, *ApJ*, 533, 682, doi: [10.1086/308692](https://doi.org/10.1086/308692)
- Calzetti, D., Kinney, A. L., & Storchi-Bergmann, T. 1994, *ApJ*, 429, 582, doi: [10.1086/174346](https://doi.org/10.1086/174346)
- Carnall, A. C., McLure, R. J., Dunlop, J. S., & Davé, R. 2018, *MNRAS*, 480, 4379, doi: [10.1093/mnras/sty2169](https://doi.org/10.1093/mnras/sty2169)
- Cendes, Y., Alexander, K. D., Berger, E., et al. 2021, *The Astrophysical Journal*, 919, 127, doi: [10.3847/1538-4357/ac110a](https://doi.org/10.3847/1538-4357/ac110a)
- Cendes, Y., Eftekhari, T., Berger, E., & Polisensky, E. 2021, *ApJ*, 908, 125, doi: [10.3847/1538-4357/abd323](https://doi.org/10.3847/1538-4357/abd323)
- Cendes, Y., Berger, E., Alexander, K. D., et al. 2022, *The Astrophysical Journal*, 938, 28, doi: [10.3847/1538-4357/ac88d0](https://doi.org/10.3847/1538-4357/ac88d0)
- Cendes, Y., Berger, E., Alexander, K. D., et al. 2022, *ApJ*, 938, 28, doi: [10.3847/1538-4357/ac88d0](https://doi.org/10.3847/1538-4357/ac88d0)
- Cendes, Y., Berger, E., Alexander, K. D., et al. 2024, *The Astrophysical Journal*, 971, 185, doi: [10.3847/1538-4357/ad5541](https://doi.org/10.3847/1538-4357/ad5541)
- Cenko, S. B., Kasliwal, M., Harrison, F. A., et al. 2006, *The Astrophysical Journal*, 652, 490, doi: [10.1086/508149](https://doi.org/10.1086/508149)
- Cenko, S. B., Frail, D. A., Harrison, F. A., et al. 2010, *ApJ*, 711, 641, doi: [10.1088/0004-637X/711/2/641](https://doi.org/10.1088/0004-637X/711/2/641)
- Cenko, S. B., Frail, D. A., Harrison, F. A., et al. 2011, *The Astrophysical Journal*, 732, 29, doi: [10.1088/0004-637X/732/1/29](https://doi.org/10.1088/0004-637X/732/1/29)
- Cenko, S. B., Frail, D. A., Harrison, F. A., et al. 2011, *ApJ*, 732, 29, doi: [10.1088/0004-637X/732/1/29](https://doi.org/10.1088/0004-637X/732/1/29)
- Cenko, S. B., Krimm, H. A., Horesh, A., et al. 2012, *The Astrophysical Journal*, 753, 77, doi: [10.1088/0004-637X/753/1/77](https://doi.org/10.1088/0004-637X/753/1/77)
- Cenko, S. B., Krimm, H. A., Horesh, A., et al. 2012, *ApJ*, 753, 77, doi: [10.1088/0004-637X/753/1/77](https://doi.org/10.1088/0004-637X/753/1/77)
- Cenko, S. B., Urban, A. L., Perley, D. A., et al. 2015, *ApJL*, 803, L24, doi: [10.1088/2041-8205/803/2/L24](https://doi.org/10.1088/2041-8205/803/2/L24)
- Chakraborti, S., Soderberg, A., Chomiuk, L., et al. 2015, *ApJ*, 805, 187, doi: [10.1088/0004-637X/805/2/187](https://doi.org/10.1088/0004-637X/805/2/187)
- Chambers, K. C., Magnier, E. A., Metcalfe, N., et al. 2016, *arXiv e-prints*, arXiv:1612.05560, doi: [10.48550/arXiv.1612.05560](https://doi.org/10.48550/arXiv.1612.05560)
- Chandra, P., Chevalier, R. A., Chugai, N., et al. 2012, *ApJ*, 755, 110, doi: [10.1088/0004-637X/755/2/110](https://doi.org/10.1088/0004-637X/755/2/110)
- Chandra, P., & Frail, D. A. 2012, *ApJ*, 746, 156, doi: [10.1088/0004-637X/746/2/156](https://doi.org/10.1088/0004-637X/746/2/156)
- Chandra, P., Cenko, S. B., Frail, D. A., et al. 2008, *The Astrophysical Journal*, 683, 924, doi: [10.1086/589807](https://doi.org/10.1086/589807)
- Chandra, P., Cenko, S. B., Frail, D. A., et al. 2008, *ApJ*, 683, 924, doi: [10.1086/589807](https://doi.org/10.1086/589807)
- Chandra, P., Frail, D. A., Fox, D., et al. 2010, *The Astrophysical Journal*, 712, L31, doi: [10.1088/2041-8205/712/1/L31](https://doi.org/10.1088/2041-8205/712/1/L31)
- Chevalier, R. A. 1982, *ApJ*, 259, 302, doi: [10.1086/160167](https://doi.org/10.1086/160167)
- Chevalier, R. A. 1998, *The Astrophysical Journal*, 499, 810, doi: [10.1086/305676](https://doi.org/10.1086/305676)
- Chevalier, R. A., & Li, Z.-Y. 2000, *ApJ*, 536, 195, doi: [10.1086/308914](https://doi.org/10.1086/308914)
- Chilingarian, I. V., Mieske, S., Hilker, M., & Infante, L. 2011, *MNRAS*, 412, 1627, doi: [10.1111/j.1365-2966.2010.18000.x](https://doi.org/10.1111/j.1365-2966.2010.18000.x)
- Chrimes, A. A., Coppejans, D. L., Jonker, P. G., et al. 2024, *Astronomy and Astrophysics*, 691, A329, doi: [10.1051/0004-6361/202451172](https://doi.org/10.1051/0004-6361/202451172)
- Chrimes, A. A., Coppejans, D. L., Jonker, P. G., et al. 2024, *A&A*, 691, A329, doi: [10.1051/0004-6361/202451172](https://doi.org/10.1051/0004-6361/202451172)
- Clark, B. G. 1980, *A&A*, 89, 377
- Colless, M., Dalton, G., Maddox, S., et al. 2001, *MNRAS*, 328, 1039, doi: [10.1046/j.1365-8711.2001.04902.x](https://doi.org/10.1046/j.1365-8711.2001.04902.x)
- Conroy, C. 2013, *ARA&A*, 51, 393, doi: [10.1146/annurev-astro-082812-141017](https://doi.org/10.1146/annurev-astro-082812-141017)
- Coppejans, D. L., Margutti, R., Terreran, G., et al. 2020, *The Astrophysical Journal*, 895, L23, doi: [10.3847/2041-8213/ab8cc7](https://doi.org/10.3847/2041-8213/ab8cc7)

- Coppejans, D. L., Margutti, R., Terreran, G., et al. 2020, *ApJL*, 895, L23, doi: [10.3847/2041-8213/ab8cc7](https://doi.org/10.3847/2041-8213/ab8cc7)
- Coppin, P., de Vries, K. D., & van Eijndhoven, N. 2020, *Phys. Rev. D*, 102, 103014, doi: [10.1103/PhysRevD.102.103014](https://doi.org/10.1103/PhysRevD.102.103014)
- Cordes, J. M., & Lazio, T. J. W. 2002, arXiv e-prints, astro, doi: [10.48550/arXiv.astro-ph/0207156](https://doi.org/10.48550/arXiv.astro-ph/0207156)
- Cornwell, T. J., Golap, K., & Bhatnagar, S. 2008, *IEEE Journal of Selected Topics in Signal Processing*, 2, 647, doi: [10.1109/JSTSP.2008.2005290](https://doi.org/10.1109/JSTSP.2008.2005290)
- Craig, M., Crawford, S., Seifert, M., et al. 2017, *astropy/ccdproc*: v1.3.0.post1, doi: [10.5281/zenodo.1069648](https://doi.org/10.5281/zenodo.1069648)
- Croft, S., Bower, G. C., Ackermann, R., et al. 2010, *ApJ*, 719, 45, doi: [10.1088/0004-637X/719/1/45](https://doi.org/10.1088/0004-637X/719/1/45)
- de Vries, M. N., Wise, M. W., Nulsen, P. E. J., et al. 2019, *MNRAS*, 486, 3388, doi: [10.1093/mnras/stz1078](https://doi.org/10.1093/mnras/stz1078)
- Dermer, C. D., Chiang, J., & Böttcher, M. 1999, *ApJ*, 513, 656, doi: [10.1086/306871](https://doi.org/10.1086/306871)
- Dey, A., Schlegel, D. J., Lang, D., et al. 2019, *AJ*, 157, 168, doi: [10.3847/1538-3881/ab089d](https://doi.org/10.3847/1538-3881/ab089d)
- Dimitrijević, M. S., Popović, L. Č., Kovačević, J., Dačić, M., & Ilić, D. 2007, *MNRAS*, 374, 1181, doi: [10.1111/j.1365-2966.2006.11238.x](https://doi.org/10.1111/j.1365-2966.2006.11238.x)
- Djorgovski, S. G., Frail, D. A., Kulkarni, S. R., et al. 2001, *The Astrophysical Journal*, 562, 654, doi: [10.1086/323845](https://doi.org/10.1086/323845)
- Dopita, M., Hart, J., McGregor, P., et al. 2007, *A&AS*, 310, 255, doi: [10.1007/s10509-007-9510-z](https://doi.org/10.1007/s10509-007-9510-z)
- Dykaar, H., Drout, M. R., Gaensler, B. M., et al. 2024, *ApJ*, 973, 104, doi: [10.3847/1538-4357/ad5a98](https://doi.org/10.3847/1538-4357/ad5a98)
- Eftekhari, T., Berger, E., Williams, P. K. G., & Blanchard, P. K. 2018, *The Astrophysical Journal*, 860, 73, doi: [10.3847/1538-4357/aac270](https://doi.org/10.3847/1538-4357/aac270)
- Eftekhari, T., Berger, E., Zauderer, B. A., Margutti, R., & Alexander, K. D. 2018, *ApJ*, 854, 86, doi: [10.3847/1538-4357/aaa8e0](https://doi.org/10.3847/1538-4357/aaa8e0)
- Eftekhari, T., Berger, E., Zauderer, B. A., Margutti, R., & Alexander, K. D. 2018, *The Astrophysical Journal*, 854, 86, doi: [10.3847/1538-4357/aaa8e0](https://doi.org/10.3847/1538-4357/aaa8e0)
- Evans, P. A., Beardmore, A. P., Page, K. L., et al. 2009, *MNRAS*, 397, 1177, doi: [10.1111/j.1365-2966.2009.14913.x](https://doi.org/10.1111/j.1365-2966.2009.14913.x)
- Eyles-Ferris, R. A., King, A., Starling, R. L., et al. 2025, arXiv e-prints, arXiv:2509.22843, doi: [10.48550/arXiv.2509.22843](https://doi.org/10.48550/arXiv.2509.22843)
- Fernández, V., Amorín, R., Firpo, V., & Morisset, C. 2024, *A&A*, 688, A69, doi: [10.1051/0004-6361/202449224](https://doi.org/10.1051/0004-6361/202449224)
- Feuillet, L. M., Meléndez, M., Kraemer, S., et al. 2024, *ApJ*, 962, 104, doi: [10.3847/1538-4357/ad1a09](https://doi.org/10.3847/1538-4357/ad1a09)
- Fiedler, R. L., Dennison, B., Johnston, K. J., & Hewish, A. 1987, *Nature*, 326, 675, doi: [10.1038/326675a0](https://doi.org/10.1038/326675a0)
- Flesch, E. W. 2023, *The Open Journal of Astrophysics*, 6, 49, doi: [10.21105/astro.2308.01505](https://doi.org/10.21105/astro.2308.01505)
- Fong, W., Berger, E., Metzger, B. D., et al. 2014, *ApJ*, 780, 118, doi: [10.1088/0004-637X/780/2/118](https://doi.org/10.1088/0004-637X/780/2/118)
- Fong, W., Laskar, T., Rastinejad, J., et al. 2021, *ApJ*, 906, 127, doi: [10.3847/1538-4357/abc74a](https://doi.org/10.3847/1538-4357/abc74a)
- Foreman-Mackey, D., Hogg, D. W., Lang, D., & Goodman, J. 2013, *PASP*, 125, 306, doi: [10.1086/670067](https://doi.org/10.1086/670067)
- Fox, D. B., Frail, D. A., Price, P. A., et al. 2005, *Nature*, 437, 845, doi: [10.1038/nature04189](https://doi.org/10.1038/nature04189)
- Frail, D. A., Kulkarni, S. R., Nicastro, L., Feroci, M., & Taylor, G. B. 1997, *Nature*, 389, 261, doi: [10.1038/38451](https://doi.org/10.1038/38451)
- Frail, D. A., Soderberg, A. M., Kulkarni, S. R., et al. 2005, *The Astrophysical Journal*, 619, 994, doi: [10.1086/426680](https://doi.org/10.1086/426680)
- Frail, D. A., Soderberg, A. M., Kulkarni, S. R., et al. 2005, *ApJ*, 619, 994, doi: [10.1086/426680](https://doi.org/10.1086/426680)
- Frail, D. A., Waxman, E., & Kulkarni, S. R. 2000, *ApJ*, 537, 191, doi: [10.1086/309024](https://doi.org/10.1086/309024)
- Frail, D. A., Kulkarni, S. R., Bloom, J. S., et al. 1999, *The Astrophysical Journal*, 525, L81, doi: [10.1086/312347](https://doi.org/10.1086/312347)
- Frail, D. A., Berger, E., Galama, T., et al. 2000, *The Astrophysical Journal*, 538, L129, doi: [10.1086/312807](https://doi.org/10.1086/312807)
- Frail, D. A., Kulkarni, S. R., Sari, R., et al. 2001, *ApJL*, 562, L55, doi: [10.1086/338119](https://doi.org/10.1086/338119)
- Frail, D. A., Cameron, P. B., Kasliwal, M., et al. 2006, *The Astrophysical Journal*, 646, L99, doi: [10.1086/506934](https://doi.org/10.1086/506934)
- Frail, D. A., Cameron, P. B., Kasliwal, M., et al. 2006, *ApJL*, 646, L99, doi: [10.1086/506934](https://doi.org/10.1086/506934)
- Fransson, C., Lundqvist, P., & Chevalier, R. A. 1996, *ApJ*, 461, 993, doi: [10.1086/177119](https://doi.org/10.1086/177119)
- Freire, P. C., Kramer, M., Lyne, A. G., et al. 2001, *ApJL*, 557, L105, doi: [10.1086/323248](https://doi.org/10.1086/323248)
- Gal-Yam, A., Ofek, E. O., Poznanski, D., et al. 2006, *ApJ*, 639, 331, doi: [10.1086/499157](https://doi.org/10.1086/499157)
- Galama, T. J., Frail, D. A., Sari, R., et al. 2003, *The Astrophysical Journal*, 585, 899, doi: [10.1086/346083](https://doi.org/10.1086/346083)
- Galama, T. J., Bremer, M., Bertoldi, F., et al. 2000, *The Astrophysical Journal*, 541, L45, doi: [10.1086/312904](https://doi.org/10.1086/312904)
- Gao, H., Lei, W.-H., Zou, Y.-C., Wu, X.-F., & Zhang, B. 2013, *NewAR*, 57, 141, doi: [10.1016/j.newar.2013.10.001](https://doi.org/10.1016/j.newar.2013.10.001)
- Gehrels, N., Chincarini, G., Giommi, P., et al. 2004, *ApJ*, 611, 1005, doi: [10.1086/422091](https://doi.org/10.1086/422091)
- Geldzahler, B. J., Johnston, K. J., Spencer, J. H., et al. 1983, *ApJL*, 273, L65, doi: [10.1086/184131](https://doi.org/10.1086/184131)
- Gezari, S. 2021, *Annual Review of Astronomy and Astrophysics*, 59, 21, doi: [10.1146/annurev-astro-111720-030029](https://doi.org/10.1146/annurev-astro-111720-030029)

- Ghirlanda, G., Salvaterra, R., Campana, S., et al. 2015, *A&A*, 578, A71, doi: [10.1051/0004-6361/201526112](https://doi.org/10.1051/0004-6361/201526112)
- Goodwin, A. J., van Velzen, S., Miller-Jones, J. C. A., et al. 2022, *MNRAS*, 511, 5328, doi: [10.1093/mnras/stac333](https://doi.org/10.1093/mnras/stac333)
- Goodwin, A. J., van Velzen, S., Miller-Jones, J. C. A., et al. 2022, *Monthly Notices of the Royal Astronomical Society*, 511, 5328, doi: [10.1093/mnras/stac333](https://doi.org/10.1093/mnras/stac333)
- Goodwin, A. J., Miller-Jones, J. C. A., van Velzen, S., et al. 2023, *Monthly Notices of the Royal Astronomical Society*, 518, 847, doi: [10.1093/mnras/stac3127](https://doi.org/10.1093/mnras/stac3127)
- Goodwin, A. J., Miller-Jones, J. C. A., van Velzen, S., et al. 2023, *MNRAS*, 518, 847, doi: [10.1093/mnras/stac3127](https://doi.org/10.1093/mnras/stac3127)
- Goodwin, A. J., Anderson, G. E., Miller-Jones, J. C. A., et al. 2024, *MNRAS*, 528, 7123, doi: [10.1093/mnras/stae362](https://doi.org/10.1093/mnras/stae362)
- Goodwin, A. J., Mummery, A., Laskar, T., et al. 2024, A second radio flare from the tidal disruption event AT2020vwl: a delayed outflow ejection?, doi: [10.48550/arXiv.2410.18665](https://doi.org/10.48550/arXiv.2410.18665)
- Goodwin, A. J., Burn, M., Anderson, G. E., et al. 2025, A systematic analysis of the radio properties of 22 X-ray selected tidal disruption event candidates with the Australia Telescope Compact Array, arXiv, doi: [10.48550/arXiv.2504.08426](https://doi.org/10.48550/arXiv.2504.08426)
- Goodwin, A. J., Mummery, A., Laskar, T., et al. 2025a, *ApJ*, 981, 122, doi: [10.3847/1538-4357/adb0b1](https://doi.org/10.3847/1538-4357/adb0b1)
- Goodwin, A. J., Burn, M., Anderson, G. E., et al. 2025b, *ApJS*, 278, 36, doi: [10.3847/1538-4365/adbe80](https://doi.org/10.3847/1538-4365/adbe80)
- Graham, A. W. 2020, *MNRAS*, 492, 3263, doi: [10.1093/mnras/stz3547](https://doi.org/10.1093/mnras/stz3547)
- Granot, J., & Sari, R. 2002, *ApJ*, 568, 820, doi: [10.1086/338966](https://doi.org/10.1086/338966)
- Greiner, J., Krühler, T., Nardini, M., et al. 2013, *Astronomy and Astrophysics*, 560, A70, doi: [10.1051/0004-6361/201321284](https://doi.org/10.1051/0004-6361/201321284)
- Gulati, A., Murphy, T., Dobie, D., et al. 2025, *MNRAS*, 538, 2676, doi: [10.1093/mnras/staf452](https://doi.org/10.1093/mnras/staf452)
- Hajela, A., Alexander, K. D., Margutti, R., et al. 2025, *ApJ*, 983, 29, doi: [10.3847/1538-4357/adb620](https://doi.org/10.3847/1538-4357/adb620)
- Hancock, P. J., Murphy, T., Gaensler, B., & Zauderer, A. 2012, *GRB Coordinates Network*, 12804, 1
- Harrison, F. A., Bloom, J. S., Frail, D. A., et al. 1999, *The Astrophysical Journal*, 523, L121, doi: [10.1086/312282](https://doi.org/10.1086/312282)
- Harrison, F. A., Yost, S. A., Sari, R., et al. 2001, *The Astrophysical Journal*, 559, 123, doi: [10.1086/322368](https://doi.org/10.1086/322368)
- Hilker, M., Baumgardt, H., Infante, L., et al. 2007, *A&A*, 463, 119, doi: [10.1051/0004-6361:20066429](https://doi.org/10.1051/0004-6361:20066429)
- Hills, J. G. 1975, *Nature*, 254, 295, doi: [10.1038/254295a0](https://doi.org/10.1038/254295a0)
- Hinshaw, G., Larson, D., Komatsu, E., et al. 2013, *ApJS*, 208, 19, doi: [10.1088/0067-0049/208/2/19](https://doi.org/10.1088/0067-0049/208/2/19)
- Hinton, S. R., Davis, T. M., Lidman, C., Glazebrook, K., & Lewis, G. F. 2016, *Astronomy and Computing*, 15, 61, doi: [10.1016/j.ascom.2016.03.001](https://doi.org/10.1016/j.ascom.2016.03.001)
- Ho, A. Y. Q., Phinney, E. S., Ravi, V., et al. 2019, *The Astrophysical Journal*, 871, 73, doi: [10.3847/1538-4357/aaf473](https://doi.org/10.3847/1538-4357/aaf473)
- Ho, A. Y. Q., Phinney, E. S., Ravi, V., et al. 2019, *ApJ*, 871, 73, doi: [10.3847/1538-4357/aaf473](https://doi.org/10.3847/1538-4357/aaf473)
- Ho, A. Y. Q., Perley, D. A., Kulkarni, S. R., et al. 2020, *The Astrophysical Journal*, 895, 49, doi: [10.3847/1538-4357/ab8bcf](https://doi.org/10.3847/1538-4357/ab8bcf)
- Ho, A. Y. Q., Perley, D. A., Kulkarni, S. R., et al. 2020a, *ApJ*, 895, 49, doi: [10.3847/1538-4357/ab8bcf](https://doi.org/10.3847/1538-4357/ab8bcf)
- Ho, A. Y. Q., Perley, D. A., Beniamini, P., et al. 2020b, *ApJ*, 905, 98, doi: [10.3847/1538-4357/abc34d](https://doi.org/10.3847/1538-4357/abc34d)
- Hobbs, G., Manchester, R. N., Dunning, A., et al. 2020, *PASA*, 37, e012, doi: [10.1017/pasa.2020.2](https://doi.org/10.1017/pasa.2020.2)
- Horesh, A., Cenko, S. B., & Arcavi, I. 2021a, *Nature Astronomy*, 5, 491, doi: [10.1038/s41550-021-01300-8](https://doi.org/10.1038/s41550-021-01300-8)
- Horesh, A., Cenko, S. B., Perley, D. A., et al. 2015, *The Astrophysical Journal*, 812, 86, doi: [10.1088/0004-637X/812/1/86](https://doi.org/10.1088/0004-637X/812/1/86)
- Horesh, A., Sfaradi, I., Fender, R., et al. 2021b, *The Astrophysical Journal*, 920, L5, doi: [10.3847/2041-8213/ac25fe](https://doi.org/10.3847/2041-8213/ac25fe)
- Horesh, A., Stockdale, C., Fox, D. B., et al. 2013, *MNRAS*, 436, 1258, doi: [10.1093/mnras/stt1645](https://doi.org/10.1093/mnras/stt1645)
- Hotan, A. W., van Straten, W., & Manchester, R. N. 2004, *PASA*, 21, 302, doi: [10.1071/AS04022](https://doi.org/10.1071/AS04022)
- Hotan, A. W., et al. 2021, *PASA*, 38, e009, doi: [10.1017/pasa.2021.1](https://doi.org/10.1017/pasa.2021.1)
- Huang, Y. F., Dai, Z. G., & Lu, T. 2002, *MNRAS*, 332, 735, doi: [10.1046/j.1365-8711.2002.05334.x](https://doi.org/10.1046/j.1365-8711.2002.05334.x)
- Jin, C. C., Li, D. Y., Jiang, N., et al. 2025, arXiv e-prints, arXiv:2501.09580, doi: [10.48550/arXiv.2501.09580](https://doi.org/10.48550/arXiv.2501.09580)
- Johnston, S., Bailes, M., Bartel, N., et al. 2007, *PASA*, 24, 174, doi: [10.1071/AS07033](https://doi.org/10.1071/AS07033)
- Jonas, J., & MeerKAT Team. 2016, in *MeerKAT Science: On the Pathway to the SKA*, 1
- Joseph, T. D., Maccarone, T. J., & Fender, R. P. 2011, *MNRAS*, 415, L59, doi: [10.1111/j.1745-3933.2011.01078.x](https://doi.org/10.1111/j.1745-3933.2011.01078.x)
- Kamble, A., Soderberg, A. M., Chomiuk, L., et al. 2013, arXiv e-prints, arXiv:1309.3573, doi: [10.48550/arXiv.1309.3573](https://doi.org/10.48550/arXiv.1309.3573)
- Katira, A., Mooley, K. P., & Hotokezaka, K. 2025, *MNRAS*, 539, 2654, doi: [10.1093/mnras/staf579](https://doi.org/10.1093/mnras/staf579)
- Kauffmann, G., Heckman, T. M., White, S. D. M., et al. 2003, *MNRAS*, 341, 54, doi: [10.1046/j.1365-8711.2003.06292.x](https://doi.org/10.1046/j.1365-8711.2003.06292.x)

- Kennicutt, R. C., & Evans, N. J. 2012, *ARA&A*, 50, 531, doi: [10.1146/annurev-astro-081811-125610](https://doi.org/10.1146/annurev-astro-081811-125610)
- Kennicutt, Jr., R. C. 1998, *ApJ*, 498, 541, doi: [10.1086/305588](https://doi.org/10.1086/305588)
- Kewley, L. J., & Dopita, M. A. 2002, *ApJS*, 142, 35, doi: [10.1086/341326](https://doi.org/10.1086/341326)
- Kewley, L. J., Groves, B., Kauffmann, G., & Heckman, T. 2006, *MNRAS*, 372, 961, doi: [10.1111/j.1365-2966.2006.10859.x](https://doi.org/10.1111/j.1365-2966.2006.10859.x)
- Kulkarni, S. R., Frail, D. A., Wieringa, M. H., et al. 1998, *Nature*, 395, 663, doi: [10.1038/27139](https://doi.org/10.1038/27139)
- Kumar, P., Shannon, R. M., Lower, M. E., et al. 2022, *MNRAS*, 512, 3400, doi: [10.1093/mnras/stac683](https://doi.org/10.1093/mnras/stac683)
- Lacy, M., Baum, S. A., Chandler, C. J., et al. 2020, *PASP*, 132, 035001, doi: [10.1088/1538-3873/ab63eb](https://doi.org/10.1088/1538-3873/ab63eb)
- Lamb, G. P., Mandel, I., & Resmi, L. 2018, *MNRAS*, 481, 2581, doi: [10.1093/mnras/sty2196](https://doi.org/10.1093/mnras/sty2196)
- Lamb, G. P., Tanvir, N. R., Levan, A. J., et al. 2019, *ApJ*, 883, 48, doi: [10.3847/1538-4357/ab38bb](https://doi.org/10.3847/1538-4357/ab38bb)
- Laskar, T., Berger, E., Zauderer, B. A., et al. 2013, *ApJ*, 776, 119, doi: [10.1088/0004-637X/776/2/119](https://doi.org/10.1088/0004-637X/776/2/119)
- Laskar, T., Berger, E., Tanvir, N., et al. 2014, *ApJ*, 781, 1, doi: [10.1088/0004-637X/781/1/1](https://doi.org/10.1088/0004-637X/781/1/1)
- Laskar, T., Alexander, K. D., Berger, E., et al. 2016, *The Astrophysical Journal*, 833, 88, doi: [10.3847/1538-4357/833/1/88](https://doi.org/10.3847/1538-4357/833/1/88)
- Laskar, T., Berger, E., Margutti, R., et al. 2018, *The Astrophysical Journal*, 859, 134, doi: [10.3847/1538-4357/aabfd8](https://doi.org/10.3847/1538-4357/aabfd8)
- Laskar, T., Escorial, A. R., Schroeder, G., et al. 2022, *ApJL*, 935, L11, doi: [10.3847/2041-8213/ac8421](https://doi.org/10.3847/2041-8213/ac8421)
- Laskar, T., Alexander, K. D., Margutti, R., et al. 2023, *The Astrophysical Journal*, 946, L23, doi: [10.3847/2041-8213/acbfad](https://doi.org/10.3847/2041-8213/acbfad)
- Law, C. J., Gaensler, B. M., Metzger, B. D., Ofek, E. O., & Sironi, L. 2018, *The Astrophysical Journal*, 866, L22, doi: [10.3847/2041-8213/aae5f3](https://doi.org/10.3847/2041-8213/aae5f3)
- Law, C. J., Gaensler, B. M., Metzger, B. D., Ofek, E. O., & Sironi, L. 2018, *ApJL*, 866, L22, doi: [10.3847/2041-8213/aae5f3](https://doi.org/10.3847/2041-8213/aae5f3)
- Leung, J. K., Murphy, T., Lenc, E., et al. 2023, *MNRAS*, 523, 4029, doi: [10.1093/mnras/stad1670](https://doi.org/10.1093/mnras/stad1670)
- Leung, J. K., Murphy, T., Ghirlanda, G., et al. 2021, *Monthly Notices of the Royal Astronomical Society*, 503, 1847, doi: [10.1093/mnras/stab326](https://doi.org/10.1093/mnras/stab326)
- Levan, A. J., Tanvir, N. R., Cenko, S. B., et al. 2011, *Science*, 333, 199, doi: [10.1126/science.1207143](https://doi.org/10.1126/science.1207143)
- Levan, A. J., Gompertz, B. P., Salafia, O. S., et al. 2024, *Nature*, 626, 737, doi: [10.1038/s41586-023-06759-1](https://doi.org/10.1038/s41586-023-06759-1)
- Levan, A. J., Martin-Carrillo, A., Laskar, T., et al. 2025, arXiv e-prints, arXiv:2507.14286, doi: [10.48550/arXiv.2507.14286](https://doi.org/10.48550/arXiv.2507.14286)
- Levinson, A., Ofek, E. O., Waxman, E., & Gal-Yam, A. 2002, *ApJ*, 576, 923, doi: [10.1086/341866](https://doi.org/10.1086/341866)
- Li, D. Y., Yang, J., Zhang, W. D., & the Einstein Probe collaborations. 2025, arXiv e-prints, arXiv:2509.25877, doi: [10.48550/arXiv.2509.25877](https://doi.org/10.48550/arXiv.2509.25877)
- Lin, D., Strader, J., Carrasco, E. R., et al. 2018, *Nature Astronomy*, 2, 656, doi: [10.1038/s41550-018-0493-1](https://doi.org/10.1038/s41550-018-0493-1)
- Liu, C., Peng, E. W., Toloba, E., et al. 2015, *ApJL*, 812, L2, doi: [10.1088/2041-8205/812/1/L2](https://doi.org/10.1088/2041-8205/812/1/L2)
- Lu, W., & Bonnerot, C. 2020, *MNRAS*, 492, 686, doi: [10.1093/mnras/stz3405](https://doi.org/10.1093/mnras/stz3405)
- Ma, R., Xie, F.-G., & Hou, S. 2014, *ApJL*, 780, L14, doi: [10.1088/2041-8205/780/1/L14](https://doi.org/10.1088/2041-8205/780/1/L14)
- Maity, B., & Chandra, P. 2021, *ApJ*, 907, 60, doi: [10.3847/1538-4357/abd2be](https://doi.org/10.3847/1538-4357/abd2be)
- Marcote, B., Nimmo, K., Salafia, O. S., et al. 2019, *ApJL*, 876, L14, doi: [10.3847/2041-8213/ab1aad](https://doi.org/10.3847/2041-8213/ab1aad)
- Margutti, R., Soderberg, A. M., Wieringa, M. H., et al. 2013, *The Astrophysical Journal*, 778, 18, doi: [10.1088/0004-637X/778/1/18](https://doi.org/10.1088/0004-637X/778/1/18)
- Margutti, R., Soderberg, A. M., Wieringa, M. H., et al. 2013, *ApJ*, 778, 18, doi: [10.1088/0004-637X/778/1/18](https://doi.org/10.1088/0004-637X/778/1/18)
- Margutti, R., Alexander, K. D., Xie, X., et al. 2018, *ApJL*, 856, L18, doi: [10.3847/2041-8213/aab2ad](https://doi.org/10.3847/2041-8213/aab2ad)
- Margutti, R., Metzger, B. D., Chornock, R., et al. 2019, *The Astrophysical Journal*, 872, 18, doi: [10.3847/1538-4357/aafa01](https://doi.org/10.3847/1538-4357/aafa01)
- Margutti, R., Metzger, B. D., Chornock, R., et al. 2019, *ApJ*, 872, 18, doi: [10.3847/1538-4357/aafa01](https://doi.org/10.3847/1538-4357/aafa01)
- Martin, D. C., Fanson, J., Schiminovich, D., et al. 2005, *ApJL*, 619, L1, doi: [10.1086/426387](https://doi.org/10.1086/426387)
- Masqué, J. M., Jeyakumar, S., Trinidad, M. A., Rodríguez-Esnard, T., & Ishwara-Chandra, C. H. 2019, *MNRAS*, 483, 1184, doi: [10.1093/mnras/sty3179](https://doi.org/10.1093/mnras/sty3179)
- Mathewson, D. S., Hart, J., Wehner, H. P., Hovey, G. R., & van Harmelen, J. 2013, *Journal of Astronomical History and Heritage*, 16, 2
- Matsumoto, T., & Piran, T. 2023, *MNRAS*, 522, 4565, doi: [10.1093/mnras/stad1269](https://doi.org/10.1093/mnras/stad1269)
- Mattila, S., Dahlen, T., Efstathiou, A., et al. 2012, *ApJ*, 756, 111, doi: [10.1088/0004-637X/756/2/111](https://doi.org/10.1088/0004-637X/756/2/111)
- Mattila, S., Pérez-Torres, M., Efstathiou, A., et al. 2018, *Science*, 361, 482, doi: [10.1126/science.aao4669](https://doi.org/10.1126/science.aao4669)
- Mattila, S., Pérez-Torres, M., Efstathiou, A., et al. 2018, *Science*, 361, 482, doi: [10.1126/science.aao4669](https://doi.org/10.1126/science.aao4669)
- McConnell, D., Hale, C. L., Lenc, E., et al. 2020, *PASA*, 37, e048, doi: [10.1017/pasa.2020.41](https://doi.org/10.1017/pasa.2020.41)

- McCrary, N., & Graham, J. R. 2007, *ApJ*, 663, 844, doi: [10.1086/518357](https://doi.org/10.1086/518357)
- McCully, C., Crawford, S., Kovacs, G., et al. 2018, *astropy/astrocrappy: v1.0.5 Zenodo Release, v1.0.5, Zenodo*, doi: [10.5281/zenodo.1482019](https://doi.org/10.5281/zenodo.1482019)
- McLean, I. S., Steidel, C. C., Epps, H., et al. 2010, in *Society of Photo-Optical Instrumentation Engineers (SPIE) Conference Series*, Vol. 7735, *Ground-based and Airborne Instrumentation for Astronomy III*, ed. I. S. McLean, S. K. Ramsay, & H. Takami, 77351E, doi: [10.1117/12.856715](https://doi.org/10.1117/12.856715)
- McLean, I. S., Steidel, C. C., Epps, H. W., et al. 2012, in *Society of Photo-Optical Instrumentation Engineers (SPIE) Conference Series*, Vol. 8446, *Ground-based and Airborne Instrumentation for Astronomy IV*, ed. I. S. McLean, S. K. Ramsay, & H. Takami, 84460J, doi: [10.1117/12.924794](https://doi.org/10.1117/12.924794)
- McMullin, J. P., Waters, B., Schiebel, D., Young, W., & Golap, K. 2007, in *Astronomical Society of the Pacific Conference Series*, Vol. 376, *Astronomical Data Analysis Software and Systems XVI*, ed. R. A. Shaw, F. Hill, & D. J. Bell, 127
- Meegan, C., Lichti, G., Bhat, P. N., et al. 2009, *ApJ*, 702, 791, doi: [10.1088/0004-637X/702/1/791](https://doi.org/10.1088/0004-637X/702/1/791)
- Melchior, P., Moolekamp, F., Jerdee, M., et al. 2018, *Astronomy and Computing*, 24, 129, doi: [10.1016/j.ascom.2018.07.001](https://doi.org/10.1016/j.ascom.2018.07.001)
- Mészáros, P., & Rees, M. J. 1997a, *ApJ*, 476, 232, doi: [10.1086/303625](https://doi.org/10.1086/303625)
- . 1997b, *ApJL*, 482, L29, doi: [10.1086/310692](https://doi.org/10.1086/310692)
- Metzger, B. D., & Stone, N. C. 2016, *MNRAS*, 461, 948, doi: [10.1093/mnras/stw1394](https://doi.org/10.1093/mnras/stw1394)
- Meyer, E. T., Laha, S., Shuvo, O. I., et al. 2025, *The Astrophysical Journal*, 979, L2, doi: [10.3847/2041-8213/ad8651](https://doi.org/10.3847/2041-8213/ad8651)
- Mieske, S., Hilker, M., Jordán, A., et al. 2008, *A&A*, 487, 921, doi: [10.1051/0004-6361:200810077](https://doi.org/10.1051/0004-6361:200810077)
- Moin, A., Chandra, P., Miller-Jones, J. C. A., et al. 2013, *The Astrophysical Journal*, 779, 105, doi: [10.1088/0004-637X/779/2/105](https://doi.org/10.1088/0004-637X/779/2/105)
- Möller, A., Ishida, E., Peloton, J., et al. 2025, *PASA*, 42, e057, doi: [10.1017/pasa.2025.20](https://doi.org/10.1017/pasa.2025.20)
- Mooley, K. P., Margalit, B., Law, C. J., et al. 2022, *The Astrophysical Journal*, 924, 16, doi: [10.3847/1538-4357/ac3330](https://doi.org/10.3847/1538-4357/ac3330)
- Mooley, K. P., Margalit, B., Law, C. J., et al. 2022, *ApJ*, 924, 16, doi: [10.3847/1538-4357/ac3330](https://doi.org/10.3847/1538-4357/ac3330)
- Murphy, T., Kaplan, D. L., Croft, S., et al. 2017, *MNRAS*, 466, 1944, doi: [10.1093/mnras/stw3087](https://doi.org/10.1093/mnras/stw3087)
- Murphy, T., Kaplan, D. L., Stewart, A. J., et al. 2021, *PASA*, 38, e054, doi: [10.1017/pasa.2021.44](https://doi.org/10.1017/pasa.2021.44)
- Muxlow, T. W. B., Beswick, R. J., Garrington, S. T., et al. 2010, *MNRAS*, 404, L109, doi: [10.1111/j.1745-3933.2010.00845.x](https://doi.org/10.1111/j.1745-3933.2010.00845.x)
- O'Connor, B., Troja, E., Ryan, G., et al. 2023, *Science Advances*, 9, eadi1405, doi: [10.1126/sciadv.adi1405](https://doi.org/10.1126/sciadv.adi1405)
- O'Dea, C. P., & Baum, S. A. 1997, *AJ*, 113, 148, doi: [10.1086/118241](https://doi.org/10.1086/118241)
- Orienti, M. 2016, *Astronomische Nachrichten*, 337, 9, doi: [10.1002/asna.201512257](https://doi.org/10.1002/asna.201512257)
- Osip, D. J., Floyd, D., & Covarrubias, R. 2008, in *Society of Photo-Optical Instrumentation Engineers (SPIE) Conference Series*, Vol. 7014, *Ground-based and Airborne Instrumentation for Astronomy II*, ed. I. S. McLean & M. M. Casali, 70140A, doi: [10.1117/12.790011](https://doi.org/10.1117/12.790011)
- Osterbrock, D. E. 1989, *Astrophysics of gaseous nebulae and active galactic nuclei*
- Osterbrock, D. E., & Ferland, G. J. 2006, *Astrophysics of gaseous nebulae and active galactic nuclei*. <https://ui.adsabs.harvard.edu/abs/2006agna.book.....O>
- Owsianik, I., & Conway, J. E. 1998, *A&A*, 337, 69, doi: [10.48550/arXiv.astro-ph/9712062](https://doi.org/10.48550/arXiv.astro-ph/9712062)
- Panaitescu, A., & Kumar, P. 2000, *ApJ*, 543, 66, doi: [10.1086/317090](https://doi.org/10.1086/317090)
- . 2001, *ApJ*, 554, 667, doi: [10.1086/321388](https://doi.org/10.1086/321388)
- . 2002, *ApJ*, 571, 779, doi: [10.1086/340094](https://doi.org/10.1086/340094)
- Pasham, D. R., Cenko, S. B., Levan, A. J., et al. 2015, *The Astrophysical Journal*, 805, 68, doi: [10.1088/0004-637X/805/1/68](https://doi.org/10.1088/0004-637X/805/1/68)
- Pearson, T. J., & Readhead, A. C. S. 1984, *ARA&A*, 22, 97, doi: [10.1146/annurev.aa.22.090184.000525](https://doi.org/10.1146/annurev.aa.22.090184.000525)
- Perley, D. A., Perley, R. A., Dhawan, V., & Carilli, C. L. 2017, *ApJ*, 841, 117, doi: [10.3847/1538-4357/aa725b](https://doi.org/10.3847/1538-4357/aa725b)
- Perley, D. A., Li, W., Chornock, R., et al. 2008, *The Astrophysical Journal*, 688, 470, doi: [10.1086/591961](https://doi.org/10.1086/591961)
- Perley, D. A., Li, W., Chornock, R., et al. 2008, *ApJ*, 688, 470, doi: [10.1086/591961](https://doi.org/10.1086/591961)
- Perley, D. A., Cenko, S. B., Corsi, A., et al. 2014, *The Astrophysical Journal*, 781, 37, doi: [10.1088/0004-637X/781/1/37](https://doi.org/10.1088/0004-637X/781/1/37)
- Perley, R. A., & Butler, B. J. 2017, *ApJS*, 230, 7, doi: [10.3847/1538-4365/aa6df9](https://doi.org/10.3847/1538-4365/aa6df9)
- Perley, R. A., Chandler, C. J., Butler, B. J., & Wrobel, J. M. 2011, *ApJL*, 739, L1, doi: [10.1088/2041-8205/739/1/L1](https://doi.org/10.1088/2041-8205/739/1/L1)
- Portegies Zwart, S. F., McMillan, S. L. W., & Gieles, M. 2010, *ARA&A*, 48, 431, doi: [10.1146/annurev-astro-081309-130834](https://doi.org/10.1146/annurev-astro-081309-130834)

- Price, P. A., Berger, E., Reichart, D. E., et al. 2002, *ApJL*, 572, L51, doi: [10.1086/341552](https://doi.org/10.1086/341552)
- Pritchard, J. 2025, *askap-vast/dstools: v2.0.0, v2.0.0*, Zenodo, doi: [10.5281/zenodo.15232974](https://doi.org/10.5281/zenodo.15232974)
- Prochaska, J., Hennawi, J., Westfall, K., et al. 2020, *The Journal of Open Source Software*, 5, 2308, doi: [10.21105/joss.02308](https://doi.org/10.21105/joss.02308)
- Ransom, S. 2011, *PRESTO: Pulsar Exploration and Search TOolkit*, Astrophysics Source Code Library, record ascl:1107.017. <http://ascl.net/1107.017>
- Rees, M. J. 1988, *Nature*, 333, 523, doi: [10.1038/333523a0](https://doi.org/10.1038/333523a0)
- Rhoads, J. E. 2003, *ApJ*, 591, 1097, doi: [10.1086/368125](https://doi.org/10.1086/368125)
- Rhodes, L., van der Horst, A. J., Bright, J. S., et al. 2024, *Monthly Notices of the Royal Astronomical Society*, 533, 4435, doi: [10.1093/mnras/stae2050](https://doi.org/10.1093/mnras/stae2050)
- Rhodes, L., Margalit, B., Bright, J. S., et al. 2025, *arXiv e-prints*, arXiv:2506.13618, doi: [10.48550/arXiv.2506.13618](https://doi.org/10.48550/arXiv.2506.13618)
- Ridolfi, A., Gautam, T., Freire, P. C. C., et al. 2021, *MNRAS*, 504, 1407, doi: [10.1093/mnras/stab790](https://doi.org/10.1093/mnras/stab790)
- Rol, E., van der Horst, A., Wiersema, K., et al. 2007, *The Astrophysical Journal*, 669, 1098, doi: [10.1086/521336](https://doi.org/10.1086/521336)
- Rola, C., & Pelat, D. 1994, *A&A*, 287, 676
- Rose, K., Horesh, A., Murphy, T., et al. 2024, *Monthly Notices of the Royal Astronomical Society*, 534, 3853, doi: [10.1093/mnras/stae2289](https://doi.org/10.1093/mnras/stae2289)
- Ross, K., Hurley-Walker, N., Seymour, N., et al. 2022, *MNRAS*, 512, 5358, doi: [10.1093/mnras/stac819](https://doi.org/10.1093/mnras/stac819)
- Roth, N., Kasen, D., Guillochon, J., & Ramirez-Ruiz, E. 2016, *ApJ*, 827, 3, doi: [10.3847/0004-637X/827/1/3](https://doi.org/10.3847/0004-637X/827/1/3)
- Rowlinson, A., Bell, M. E., Murphy, T., et al. 2016, *MNRAS*, 458, 3506, doi: [10.1093/mnras/stw451](https://doi.org/10.1093/mnras/stw451)
- Ryan, G., van Eerten, H., Piro, L., & Troja, E. 2020, *ApJ*, 896, 166, doi: [10.3847/1538-4357/ab93cf](https://doi.org/10.3847/1538-4357/ab93cf)
- Salafia, O. S., & Ghirlanda, G. 2022, *Galaxies*, 10, 93, doi: [10.3390/galaxies10050093](https://doi.org/10.3390/galaxies10050093)
- Salas, P., Bauer, F. E., Stockdale, C., & Prieto, J. L. 2013, *MNRAS*, 428, 1207, doi: [10.1093/mnras/sts104](https://doi.org/10.1093/mnras/sts104)
- Sault, R. J., Teuben, P. J., & Wright, M. C. H. 1995, in *Astronomical Society of the Pacific Conference Series*, Vol. 77, *Astronomical Data Analysis Software and Systems IV*, ed. R. A. Shaw, H. E. Payne, & J. J. E. Hayes, 433. <https://arxiv.org/abs/astro-ph/0612759>
- Schroeder, G., Rhodes, L., Laskar, T., et al. 2024, *The Astrophysical Journal*, 970, 139, doi: [10.3847/1538-4357/ad49ab](https://doi.org/10.3847/1538-4357/ad49ab)
- Schroeder, G., Fong, W.-f., Kilpatrick, C. D., et al. 2025, *The Astrophysical Journal*, 982, 42, doi: [10.3847/1538-4357/ada9e5](https://doi.org/10.3847/1538-4357/ada9e5)
- Seth, A. C., van den Bosch, R., Mieske, S., et al. 2014, *Nature*, 513, 398, doi: [10.1038/nature13762](https://doi.org/10.1038/nature13762)
- Sfaradi, I., Beniamini, P., Horesh, A., et al. 2024, *Monthly Notices of the Royal Astronomical Society*, 527, 7672, doi: [10.1093/mnras/stad3717](https://doi.org/10.1093/mnras/stad3717)
- Sfaradi, I., Margutti, R., Chornock, R., et al. 2025, *arXiv e-prints*, arXiv:2508.03807, doi: [10.48550/arXiv.2508.03807](https://doi.org/10.48550/arXiv.2508.03807)
- Sironi, L., & Giannios, D. 2013, *ApJ*, 778, 107, doi: [10.1088/0004-637X/778/2/107](https://doi.org/10.1088/0004-637X/778/2/107)
- Soderberg, A. M., Brunthaler, A., Nakar, E., Chevalier, R. A., & Bietenholz, M. F. 2010, *ApJ*, 725, 922, doi: [10.1088/0004-637X/725/1/922](https://doi.org/10.1088/0004-637X/725/1/922)
- Soderberg, A. M., Chevalier, R. A., Kulkarni, S. R., & Frail, D. A. 2006a, *ApJ*, 651, 1005, doi: [10.1086/507571](https://doi.org/10.1086/507571)
- Soderberg, A. M., Frail, D. A., & Wieringa, M. H. 2004a, *The Astrophysical Journal*, 607, L13, doi: [10.1086/421722](https://doi.org/10.1086/421722)
- Soderberg, A. M., Kulkarni, S. R., Berger, E., et al. 2005, *ApJ*, 621, 908, doi: [10.1086/427649](https://doi.org/10.1086/427649)
- Soderberg, A. M., Kulkarni, S. R., Berger, E., et al. 2004b, *The Astrophysical Journal*, 606, 994, doi: [10.1086/383082](https://doi.org/10.1086/383082)
- Soderberg, A. M., Berger, E., Kasliwal, M., et al. 2006b, *ApJ*, 650, 261, doi: [10.1086/506429](https://doi.org/10.1086/506429)
- Soderberg, A. M., Kulkarni, S. R., Nakar, E., et al. 2006, *Nature*, 442, 1014, doi: [10.1038/nature05087](https://doi.org/10.1038/nature05087)
- Soderberg, A. M., Kulkarni, S. R., Nakar, E., et al. 2006, *Nature*, 442, 1014, doi: [10.1038/nature05087](https://doi.org/10.1038/nature05087)
- Soderberg, A. M., Berger, E., Page, K. L., et al. 2008, *Nature*, 453, 469, doi: [10.1038/nature06997](https://doi.org/10.1038/nature06997)
- Soderberg, A. M., Margutti, R., Zauderer, B. A., et al. 2012, *ApJ*, 752, 78, doi: [10.1088/0004-637X/752/2/78](https://doi.org/10.1088/0004-637X/752/2/78)
- Spencer, R. E. 1996, in *Astronomical Society of the Pacific Conference Series*, Vol. 93, *Radio Emission from the Stars and the Sun*, ed. A. R. Taylor & J. M. Paredes, 252
- Stein, R., van Velzen, S., Kowalski, M., et al. 2021, *Nature Astronomy*, 5, 510, doi: [10.1038/s41550-020-01295-8](https://doi.org/10.1038/s41550-020-01295-8)
- Stewart, A., Dobie, D., O'Brien, A., & Kaplan, D. 2023, *vast-tools, v3.0.1*, Zenodo, doi: [10.5281/zenodo.8373330](https://doi.org/10.5281/zenodo.8373330)
- Suzuki, A., Maeda, K., & Shigezuma, T. 2019, *ApJ*, 870, 38, doi: [10.3847/1538-4357/aaf85](https://doi.org/10.3847/1538-4357/aaf85)
- Taylor, G. B., Frail, D. A., Kulkarni, S. R., et al. 1998, *The Astrophysical Journal*, 502, L115, doi: [10.1086/311513](https://doi.org/10.1086/311513)
- Tingay, S. J., Miller-Jones, J. C. A., & Lenc, E. 2020, *ApJL*, 901, L17, doi: [10.3847/2041-8213/abb60d](https://doi.org/10.3847/2041-8213/abb60d)
- Tody, D. 1986, in *Society of Photo-Optical Instrumentation Engineers (SPIE) Conference Series*, Vol. 627, *Instrumentation in astronomy VI*, ed. D. L. Crawford, 733, doi: [10.1117/12.968154](https://doi.org/10.1117/12.968154)
- Tonry, J. L., Stubbs, C. W., Lykke, K. R., et al. 2012, *ApJ*, 750, 99, doi: [10.1088/0004-637X/750/2/99](https://doi.org/10.1088/0004-637X/750/2/99)

- Tuntsov, A. V., Walker, M. A., Koopmans, L. V. E., et al. 2016, *ApJ*, 817, 176, doi: [10.3847/0004-637X/817/2/176](https://doi.org/10.3847/0004-637X/817/2/176)
- Urquhart, R., Soria, R., Pakull, M. W., et al. 2019, *MNRAS*, 482, 2389, doi: [10.1093/mnras/sty2771](https://doi.org/10.1093/mnras/sty2771)
- van Breugel, W., Miley, G., & Heckman, T. 1984, *AJ*, 89, 5, doi: [10.1086/113480](https://doi.org/10.1086/113480)
- Van Der Horst, A. J. 2008, in *AAS/High Energy Astrophysics Division*, Vol. 10, AAS/High Energy Astrophysics Division #10, 5.06
- van der Horst, A. J., Kamble, A., Resmi, L., et al. 2008, *Astronomy and Astrophysics*, 480, 35, doi: [10.1051/0004-6361:20078051](https://doi.org/10.1051/0004-6361:20078051)
- van der Horst, A. J., Kamble, A., Resmi, L., et al. 2008, *A&A*, 480, 35, doi: [10.1051/0004-6361:20078051](https://doi.org/10.1051/0004-6361:20078051)
- van Dokkum, P. G. 2001, *PASP*, 113, 1420, doi: [10.1086/323894](https://doi.org/10.1086/323894)
- Walcher, C. J., van der Marel, R. P., McLaughlin, D., et al. 2005, *ApJ*, 618, 237, doi: [10.1086/425977](https://doi.org/10.1086/425977)
- Walker, M. A. 1998, *MNRAS*, 294, 307, doi: [10.1046/j.1365-8711.1998.01238.x](https://doi.org/10.1046/j.1365-8711.1998.01238.x)
- Weiler, K. W., Panagia, N., Montes, M. J., & Sramek, R. A. 2002, *Annual Review of Astronomy and Astrophysics*, 40, 387, doi: [10.1146/annurev.astro.40.060401.093744](https://doi.org/10.1146/annurev.astro.40.060401.093744)
- Yao, J. M., Manchester, R. N., & Wang, N. 2017, *ApJ*, 835, 29, doi: [10.3847/1538-4357/835/1/29](https://doi.org/10.3847/1538-4357/835/1/29)
- Yost, S. A., Harrison, F. A., Sari, R., & Frail, D. A. 2003, *ApJ*, 597, 459, doi: [10.1086/378288](https://doi.org/10.1086/378288)
- Zauderer, B. A., Berger, E., Margutti, R., et al. 2013, *The Astrophysical Journal*, 767, 152, doi: [10.1088/0004-637X/767/2/152](https://doi.org/10.1088/0004-637X/767/2/152)
- Zauderer, B. A., Berger, E., Soderberg, A. M., et al. 2011, *Nature*, 476, 425, doi: [10.1038/nature10366](https://doi.org/10.1038/nature10366)
- Zhang, W., Shu, X., Sun, L., et al. 2025, *Nature Astronomy*, 9, 702, doi: [10.1038/s41550-025-02502-0](https://doi.org/10.1038/s41550-025-02502-0)